

---

# Methods<sup>1</sup>

---

## Expedition 301 Scientists<sup>2</sup>

### Chapter contents

<b>Introduction</b> .....	<b>1</b>
<b>Lithostratigraphy</b> .....	<b>3</b>
<b>Igneous and metamorphic petrology</b> .....	<b>6</b>
<b>Paleomagnetism</b> .....	<b>10</b>
<b>Biogeochemistry</b> .....	<b>12</b>
<b>Microbiology</b> .....	<b>14</b>
<b>Physical properties</b> .....	<b>18</b>
<b>Thermal experiments</b> .....	<b>22</b>
<b>Packer experiments</b> .....	<b>22</b>
<b>Wireline logging</b> .....	<b>22</b>
<b>References</b> .....	<b>24</b>
<b>Figures</b> .....	<b>28</b>
<b>Tables</b> .....	<b>45</b>

### Introduction

This “Methods” chapter documents the primary procedures and methods employed by the various shipboard laboratories during Integrated Ocean Drilling Program (IODP) Expedition 301. This information concerns only shipboard methods described in the site report chapters. Methods for shore-based analysis of Expedition 301 samples and data will be described in individual scientific contributions to be published after the cruise. Detailed drilling and engineering operations are described in the “Operations” sections of the individual site report chapters.

### Shipboard scientific procedures

#### Numbering of sites, holes, cores, and samples

Expedition numbers for IODP expeditions are sequential starting with 301. Drilling sites are numbered consecutively, and for the U.S. Implementing Organization (USIO)-operated platform, numbering starts with Site U1301 (the U indicates the USIO-operated platform). Multiple holes may be drilled at a single site. For all IODP drill sites, a letter suffix distinguishes each hole drilled at one site. The first hole drilled is assigned the site number modified by the suffix “A,” the second hole takes the site number and the suffix “B,” and so forth.

The cored interval is measured in meters below seafloor (mbsf). The depth below seafloor is determined by subtracting the water depth estimated from the initial drill pipe measurement, which gives the length of pipe from the rig floor to the seafloor (meters below rig floor), from the total drill pipe measurement. Each cored interval is generally 9.5 m long, which is the length of a core barrel. Coring intervals may be shorter and may not necessarily be adjacent if they are separated by drilled intervals.

A recovered core is typically divided into 1.5 m sections that are numbered serially from the top. When full recovery is obtained, the sections are numbered from 1 to 7, with the last section generally being <1.5 m (Fig. F1); rarely, an unusually long core may require more than 7 sections. When less than full recovery is obtained, there will be as many sections as needed to accommodate the length of the core recovered. By convention, material recovered from the core catcher of a sedimentary core is treated as a separate section labeled “core catcher” (or “CC”) and placed below the last section recovered in the liner. The core catcher is as-

<sup>1</sup>Expedition 301 Scientists, 2005. Methods. *In* Fisher, A.T., Urabe, T., Klaus, A., and the Expedition 301 Scientists, *Proc. IODP, 301*: College Station TX (Integrated Ocean Drilling Program Management International, Inc.). doi:10.2204/iodp.proc.301.105.2005

<sup>2</sup>Expedition 301 Scientists’ addresses.



signed to the top of the cored interval in cases where material is recovered only in the core catcher.

When recovered core is shorter than the cored interval, the top of the core, by convention, is equated to the top of the cored interval to achieve consistency in reporting depth-in-core. Any sample removed from a core is designated by distance measured in centimeters from the top of the section to the top and bottom of the sample removed. A full identification number for a sample consists of the following information: expedition, site, hole, core number, core type, section number, piece number (for hard rock), and interval in centimeters measured from the top of section. For example, a sample identification of “301-U1301A-3H-3, 80–85 cm,” represents a sample removed from the interval 80–85 cm below the top of Section 3, Core 3H (H designates that this core was taken using the advanced piston corer [APC]), from Hole U1301A from Expedition 301 (Fig. F1).

All IODP core identifiers indicate core type. The following abbreviations are used:

- R = rotary core barrel (RCB)
- H = APC
- X = extended core barrel (XCB)

## Core handling

### Sedimentary cores

As soon as a core is retrieved on deck, it goes through a sequence of processing steps. Usually, a sample is first taken from the core catcher and given to the paleontological laboratory for initial age assessment, but no micropaleontologic analyses were conducted during Expedition 301. The core is placed on a long horizontal rack outside the laboratory. For safety monitoring, small (~5 cm<sup>3</sup>) plugs of sediment are usually taken from the end of a few sections per core for headspace gas analysis. Gas samples may also be taken by piercing the core liner, typically at voids, and withdrawing gas into a syringe (referred to as vacuum-seal tube samples). Next, the core is marked into section lengths, each section is labeled, and the core is cut into sections. Whole-round samples for interstitial water (IW) and microbiological analyses are taken. Each section is sealed at the top and bottom by attaching color-coded plastic caps—blue to identify the top of a section and clear at the bottom. A yellow cap is placed on section ends where a whole-round sample has been removed, and the sample code is written on the yellow cap. Caps are usually secured to liners by coating the liner ends and inside rims of caps with acetone before attaching the caps. The core sections are carried into the laboratory, where individual sections are permanently labeled with an engraver. The length of the

core in each section and the core catcher sample are measured to the nearest centimeter; this information is logged into the IODP database.

Once they are in the laboratory, labeled, and equilibrated to ambient laboratory temperature (~1–3 h), whole-round core sections are run through the multisensor track (MST) and thermal conductivity measurements are made on soft-sediment cores. Whole-round samples for shore-based studies (e.g., consolidation, shear strength, permeability, structure, etc.) may be taken at this stage.

Cores are split lengthwise into working and archive halves. Softer cores are split with a wire or saw, depending on the degree of induration. Harder cores are split with a band saw or diamond saw. Wire-cut cores are split from bottom to top, so investigators should be aware that older material could have been dragged up the core on the split face of each section.

### Igneous cores

Igneous rock cores are handled differently from sediment cores. Once on deck, the core catcher sample is placed at the bottom of the core liner and total core recovery is calculated by pushing the rock pieces together and measuring to the nearest centimeter. Small fractured samples for microbiological cultivation experiments are collected from the catwalk immediately after the core liner is cut into sections. The core is cut into 1.5 m long sections and transferred into the laboratory. Whole-round samples are collected at this point for microbiological studies; these are handled using latex gloves, photographed, and removed to an anaerobic chamber as quickly as possible. The contents of each section are transferred into 1.5 m long sections of split core liner, where the bottoms of oriented pieces (i.e., pieces that clearly could not have rotated top to bottom about a horizontal axis in the liner) are marked with red wax pencil. This is done to ensure that orientation is not lost during the splitting and labeling processes. Macroscopic description of the core surface can be performed at this time. Plastic spacers separate individual pieces and/or reconstruct contiguous groups of pieces in the core liner. These spacers may represent substantial intervals of no recovery. The length of each section is recorded and entered into the database as the curated length. The curated length will commonly differ by a few centimeters from that measured on the catwalk. Each piece of core is split into archive and working halves, with the positions of spacers maintained for both halves. Each piece is numbered sequentially from the top of each section, beginning with number 1; reconstructed groups of pieces are assigned the same number, but they are lettered consecutively. Pieces are labeled only on the

outer, cylindrical surfaces of the core. If the piece is oriented, an arrow pointing to the top of the section is added to the label.

### All cores

For both sedimentary and igneous cores, the archive half is described visually. Smear slides are made from small sediment samples taken from the archive half (all shipboard samples are analyzed on board and either archived at the IODP core repositories or made available to shipboard scientists for postcruise research). Digital images of the archive halves are made with a digital imaging system. Archive sections of sediment sections are run through the archive MST (AMST) for color reflectance spectroscopy measurements and susceptibility measurements with a point susceptibility meter. Both sedimentary and igneous sections are passed through the cryogenic magnetometer for magnetic remanence measurements. The archive half is then photographed using color film. Close-up color photographs are taken of particular features for illustrations in the summary of each site, as requested by individual scientists.

The working half of the core is sampled for both shipboard and shore-based laboratory studies. Each sample is logged into the sampling database program by location and by the name of the investigator receiving the sample. The IODP curator and database maintain information about all samples taken. Samples are sealed in plastic vials, cubes, or bags, labeled, and stored as appropriate. Samples are routinely taken for shipboard physical properties, paleomagnetism, thin section, and geochemistry analyses, which are described in the sections below.

Following initial shipboard scientific measurements and sampling, both halves of igneous cores are shrink-wrapped in plastic to prevent rock pieces from vibrating out of sequence during transit. Working and archive halves of both sedimentary and igneous cores are put into labeled plastic “D” tubes, sealed, and transferred to cold-storage space aboard the drilling vessel. During Expedition 301, the cores were shipped in refrigerated containers to cold storage at the IODP Gulf Coast Core Repository in College Station, Texas (USA).

## Lithostratigraphy

### Lithologic classification

Expedition 301 lithologic classification is based on three end-member grain components (biogenic silica, carbonate, and terrigenous or volcanic grains), the grain size of the terrigenous component (i.e., proportions of clay, silt, and sand), and the degree of

sediment induration (e.g., chalk versus limestone). Percentages of end-member grain components, as well as siliciclastic textures used to define lithologies reported on the visual core descriptions (VCDs) and barrel sheets, were determined with a hand lens, binocular microscope, or smear slide examination of disaggregated core material. Thin sections and carbonate analyses were used to refine or modify lithology designations made at the description table.

In detail, lithologic names consist of a principal name based on composition, degree of lithification, and/or texture as determined from visual description and smear slide observations. For a mixture of components, the principal name is preceded by major modifiers (in order of increasing abundance) that refer to components making up 25% or more of the sediment. Minor components that represent between 10% and 25% of the sediment follow the principal name after a “with” in order of increasing abundance. Thus, an unconsolidated sediment containing 30% nannofossils, 25% clay minerals, 20% foraminifers, 15% quartz silt, and 10% manganese nodules would be described as a clayey nannofossil ooze with manganese nodules, quartz silt, and foraminifers. These naming conventions follow the Ocean Drilling Program (ODP) sediment classification scheme (Mazzullo et al., 1988), with the exception that during Expedition 301 a separate “mixed sediment” category was not distinguished.

Sediment was classified on the basis of composition estimated by visual examination of the core and smear slides, by shipboard measurements of carbonate content, and by shipboard X-ray diffraction (XRD) analyses. Size divisions for grains are those of Wentworth (1922) (Fig. F2). Size-textural qualifiers were not used for pelagic sediment names (e.g., nannofossil clay implies that the dominant component is detrital clay rather than clay-sized nannofossils).

Terms that describe lithification vary depending upon the dominant composition:

- Sediment derived predominantly from calcareous pelagic organisms (e.g., calcareous nannofossils and foraminifers):
  - Ooze = sediment can be deformed with a finger.
  - Chalk = sediment can be scratched easily by a fingernail.
  - Limestone = sediment cannot be scratched easily.
- Sediment derived predominantly from siliceous microfossils (diatoms, radiolarians, and siliceous sponge spicules):
  - Ooze = sediment can be deformed with a finger.
  - Radiolarite/spiculite/diatomite = sediment cannot be easily deformed manually.

- Porcellanite = siliceous limestone/claystone that has a dull luster and is less hard and compact than chert (Keene, 1975). It may contain a mix of opal, quartz, clay minerals, and carbonate. Note that the terms porcellanite and chert do not imply crystallinity of the silica.
- Chert = sediment displays a glassy luster. It may contain a mix of opal, quartz, clay minerals, and carbonate.
- Sediment derived predominantly from siliciclastic material: If the sediment can be deformed easily with a finger, no lithification term is added and the sediment is named for the dominant grain size. For more consolidated material, the lithification suffix “-stone” is appended to the dominant size classification (e.g., clay versus claystone).
- Sediment composed of sand-sized volcanoclastic grains:
  - Ash = sediment can be deformed easily with a finger.
  - Tuff = more consolidated material.
  - Lapilli = coarse-grained material.

### Visual core description and barrel sheets

Shipboard scientists were responsible for visual core description and smear slide analysis. Detailed observations of each section were recorded initially by hand on a blank sediment VCD form. This information was subsequently entered into the AppleCORE software (version 9.4a), which generates a simplified, annotated graphical description (barrel sheet) for each core (Fig. F3). These barrel sheets are linked to corresponding core photographs in “Core Descriptions.”

Site, hole, and depth in mbsf are given at the top of the barrel sheet, with depth positions of core sections indicated along the left margin. Columns on the barrel sheets include Graphic Lithology, Bioturbation, Sedimentary Structures, Fossils (ichnofossils), Sediment Disturbance, Sample Types, Color, and Description. These columns are discussed below, followed by an outline of the lithostratigraphic classification used during Expedition 301.

### Graphic lithology

Lithologies of the core intervals recovered are represented on barrel sheets by graphic patterns in the Graphic Lithology column (Fig. F4). For intervals containing homogeneous mixtures of multiple lithologies, symbols are arranged within the column from left to right in order of their relative abundance. Graphic lithologies are used for components that compose 10% or more of the total sediment, with only the three most abundant components

shown. The width of each pattern in the column approximates the relative abundance of that component. Relative abundances reported in this column are useful for general characterization of the sediment, but they are not precise, quantitative data. No graphic lithology is shown for intervals from which whole round samples were taken.

### Sedimentary structures

Sedimentary structures formed by natural processes and not as a result of drilling disturbance are represented on the barrel sheet in the Structure column (Fig. F4). Structures formed by both biogenic and physical processes are included. These include varying degrees of bioturbation, types of trace fossils, parallel laminations, and soft-sediment deformation structures.

### Ichnofossils

Symbols are used to denote the location of clearly identifiable ichnofossils (Fig. F4).

### Bioturbation

The extent of general bioturbation is indicated in the Bioturbation column (Fig. F4). Bioturbation is shown by the shading of a vertical bar to the right of the Graphic Lithology column. Using a scheme similar to that proposed by Droser and Bottjer (1986), five levels of bioturbation were recognized. Bioturbation intensity is classified as follows:

- 5 = abundant (>75%)
- 4 = common (50%–75%)
- 3 = moderate (10%–50%)
- 2 = rare (<10%)
- 1 = barren (none)

### Color

Color is determined qualitatively using the Munsell rock color charts (Rock-Color Chart Committee, 1991) and is described immediately after the cores are split to avoid color changes associated with drying and oxidation. Color is generalized in the Color column with abbreviations (e.g., “dk mo Br,” which is dark mottled brown) (Table T1).

### Drilling disturbance

Symbols are used to denote sediment disturbance induced by the coring process (Fig. F4).

- Slightly fractured: Core pieces are in situ with cracks across the core each few centimeters. Some pieces may not be in stratigraphic continuity with the adjacent piece where core recovery was incomplete.

- Moderately fractured: Core pieces are probably in correct stratigraphic sequence but may not represent the entire section. The core is more fractured than in the preceding category.
- Highly fractured: Core pieces are probably in correct stratigraphic sequence but are strongly fractured and may be rotated. Such intervals are difficult to describe because the fracturing obscures primary features.

Symbols are positioned at the location in the section where that feature is observed. If the feature extends over an interval, the symbol appears centered on a vertical line to denote the stratigraphic extent of occurrence.

### Sample types

Sample material taken for shipboard analysis consisted of IW from whole-round samples; whole-round samples for microbiology (WRB), organic geochemistry (WRO), and physical property analyses (WRP); smear slide “toothpick” samples (SS); discrete samples for XRD; and carbonate analysis (CAR). The locations of other shipboard samples can be found by interrogation of the Janus database on the IODP Web site.

### Description

The written description for each core contains a brief overview of major and minor lithologies that are present, as well as notable features (e.g., sedimentary structures).

### Smear slide analyses

Smear slides can be prepared from moderately consolidated sedimentary rocks. For each smear slide, a small amount of archive-half sediment was gently crushed and dispersed in a dilute Calgon solution or deionized water on a 22 mm × 40 mm coverslip and then dried on a hot plate at a low setting. A drop of Norland optical adhesive was applied to a pre-labeled 25 mm × 75 mm glass microscope slide, after which the coverslip was transferred onto the slide and cured in an ultraviolet light box. This procedure is different from most preparations in that the sediment dispersion is prepared on the coverslip rather than on the glass slide. The advantage is that small particles like nanofossils and clay minerals adhere directly to the coverslip and can be viewed at high magnification because they are very close to the top of the prepared slide. Some of the scientific party preferred to prepare smear slides directly on the more robust glass slide, otherwise following the procedure outlined above.

Smear slides were examined with a transmitted-light petrographic microscope equipped with a standard eyepiece micrometer to assess the percentages of different sized grains (sand, silt, and clay) and the proportions and presence of biogenic and mineral components.

In these tables, components are assigned to one of the following categories:

- T = trace (0%–2%)
- R = rare (2%–10%)
- M = minor (10%–20%)
- C = common (20%–40%)
- A = abundant (40%–60%)
- D = dominant (>60%)

### Digital imaging

All archive core halves were scanned using a Geotek digital imaging system (DIS). The DIS uses an interference filter and three line-scan charge-coupled device arrays (1024 pixels each) to continuously record the three red-green-blue (RGB) color channels with 8 bit dynamic range. The standard DIS configuration produces 300 dpi on an 8 cm wide core with a zoom capability of up to 1200 dpi on a 2 cm wide core. Synchronization and track control is better than 0.02 mm, and a framestore card contains 48 MB of random access memory (RAM) for image acquisition. The camera aperture was set to maximize contrast within the lightest colored sediment of each core. Each archive section, along with a neutral gray color chip and identification bar-code label, was DIS scanned to produce a TIFF (no compression). Using the Geotek Image Tools utilities, these photos were resampled to produce a JPEG file with a resolution of ~300 dpi. The JPEG files were viewable via the Web browser as “photo table” composite images. Profiles for each RGB channel were produced by averaging pixels in 3 cm × 0.5 cm rectangles along the central axis of the core. The DIS system was calibrated for black and white whenever deemed necessary by IODP technical staff. This capability was essential for reviewing previous cores.

### X-ray diffraction analyses

Routine samples for shipboard XRD analysis were taken from approximately three sections per core, and most were located adjacent to samples for analysis of methane concentration. Samples were freeze-dried, crushed either by hand or with a ball mill, and mounted as random bulk powders. The X-ray laboratory aboard the *JOIDES Resolution* is equipped with a Philips PW-1729 X-ray generator and a Philips PW1710/00 diffraction control unit with a PW-1775

35 port automatic sample changer. Instrument settings for all standards were as follows:

- Generator = 40 kV and 35 mA
- Tube anode = Cu
- Wavelength = 1.54056 Å (CuK $\alpha$ )
- Intensity ratio = 0.5
- Focus = fine
- Irradiated length = 12 mm
- Divergence slit = automatic
- Receiving slit = 0.2 mm
- Step size = 0.02°2 $\theta$
- Count time per step = 1 s
- Scanning rate = 4°2 $\theta$ /min
- Rate-meter constant = 0.2 s
- Spinner = off
- Monochromator = on
- Scan = step
- Scanning from 2°2 $\theta$  to 70°2 $\theta$

The software used for XRD data reduction was MacDiff (version 4.2.5), a shareware application for Macintosh computers that supports routine measurement of peak intensity and peak area.

## Igneous and metamorphic petrology

### Core curation and shipboard sampling

To preserve important features and structures, core sections containing igneous rocks were examined before the core was split. Whole-round samples taken on the core receiving platform for microbiological studies were examined and photographed when possible. Contacts were examined for evidence of chilling, baking, and alteration. Each piece was numbered sequentially from the top of each core section and labeled on the outside surface. Broken core pieces that could be fitted together were assigned the same number and were lettered consecutively from the top down (e.g., 1A, 1B, and 1C). Composite pieces sometimes occupied more than one section. Plastic spacers were placed between pieces with different numbers. The presence of a spacer may represent a substantial interval without recovery. If it was evident that an individual piece had not rotated about a horizontal axis during drilling, an arrow was added to the label pointing toward the top of the section.

Nondestructive physical property measurements, such as magnetic susceptibility and natural gamma ray (NGR) emission, were made before the core was split (see “[Physical properties](#)”). The pieces were split with a diamond-impregnated saw in such a way that important compositional and structural features were preserved in both the archive and working

halves. After splitting, the archive half was described on VCD forms and photographed. Digital images of the core were taken using the Geotek DIS before they were described. To minimize contamination of the core with platinum group elements and gold, the describers removed jewelry from their hands and wrists before handling. After the core was split and described, the working half was sampled for shipboard analysis of physical properties, paleomagnetic studies, thin sections, XRD, inductively coupled plasma-atomic emission spectroscopy (ICP-AES), and shore-based studies.

The depth interval and length of each piece were entered in a piece log (see Table T2 for an example). Lithologic units and subunits were then identified on the basis of the presence of contacts, chilled margins, changes in primary mineralogy (occurrence and abundance), color, grain size, and structural or textural variations (see Table T3 for an example). Unit boundaries were generally chosen to indicate different volcanic cooling units, although we were forced by limited recovery in some cases to arbitrarily decide the exact location of a unit boundary within an interval where the lithology above and below the interval was different. In order to preserve important information about the volcanology without defining an unreasonable number of units within a single core, subunits were designated in cases where there were frequent changes in texture without accompanying changes in mineralogy (for example, several pieces containing glass within 50 cm of core, all of which are mineralogically similar).

### Hard rock visual core descriptions

Hard rock VCD forms (HRVCDs) (Fig. F5) were used to describe each section of the igneous rock cores. A key to the symbols used on VCDs is given in Figure F6, and definitions of the terms used are provided in Table T4. From left to right on the HRVCD, the following are displayed:

1. Photograph of the archive half of the core
2. Scale from 0 to 150 cm
3. Piece number
4. Graphical representation of the rock with structural details
5. Piece orientation
6. Location of samples selected for shipboard studies
7. Boundaries of lithologic units
8. Structures
9. Presence of glass or altered glass
10. Phenocryst abundance and mineralogy
11. Groundmass grain size
12. Alteration intensity

In the graphical representation (column 4), chilled margins were indicated by using the symbol shown in Figure F6. A horizontal line across the entire width of column 4 denotes a plastic spacer, reflecting the curator's interpretation of the boundaries between different pieces of core. Vertically oriented pieces are indicated on the form by an upward-pointing arrow to the right of the appropriate piece (column 5). The locations of samples selected for shipboard studies are indicated in the column headed Shipboard Studies using the following notation:

XRD = X-ray diffraction analysis  
 ICP = ICP-AES analysis  
 TS = petrographic thin section  
 PP = physical property analysis  
 TC = thermal conductivity  
 PM = paleomagnetic analysis  
 MB = microbiological analysis

The Lithologic Unit column displays the location of the boundaries between units and subunits and the unit designator (e.g., 1, 2A, 2B, etc.). The Structure column displays the graphical representations of structural types from the key in Figure F6.

The boundaries of the lithologic units and subunits were drawn on the HRVCD across columns 4–12 (solid lines = unit boundaries; dotted lines = subunit boundaries) and numbered consecutively within each hole. HRVCDs also contain a text description of each unit in each section of core that includes the following:

1. Expedition, site, hole, core number, core type, and section number
2. Depth of the top of the section in meters below seafloor
3. Unit number (consecutive downhole; subunits are designated by letters after the unit number [e.g., 1, 2A, 2B, etc.]
4. Rock name
5. Summary description of the unit as it appears in the section, including a brief rock name and the rock type (e.g., pillow basalt or sheet flow)
6. Piece numbers included in the unit
7. Type of contacts
8. Munsell color
9. Phenocryst minerals, abundance, and size
10. Groundmass grain size
11. Vesicle abundance
12. Nature of the alteration
13. Information about abundance and mineralogy of veins
14. Description of structures in the rock
15. Additional comments

Units and subunits were named on the basis of the groundmass texture and the abundance of primary minerals. Basalts were described based on the identification of phenocrysts in hand sample:

- Aphyric = <1% phenocrysts
- Sparsely phyric = 1%–5% phenocrysts
- Moderately phyric = 5%–10% phenocrysts
- Highly phyric = >10% phenocrysts

Rock names were further classified by the types of phenocrysts, where present (e.g., sparsely plagioclase-olivine phyric, in which the amount of olivine exceeds the amount of plagioclase). Rock color was determined on a wet, cut surface of the rock using the Munsell color chart. Groundmass character was determined by measuring average groundmass grain size (width of elongated grains) with a binocular microscope. Grain size was identified as follows:

mg = medium grained (average groundmass grain size  $\geq 1$  mm)  
 fg = fine grained (grains = 0.2–1 mm)  
 $\mu$ x = microcrystalline (groundmass crystals = 0.1–0.2 mm)  
 cx = cryptocrystalline (crystals = <0.1 mm)  
 G = glassy

An estimate of the percentage of vesicles and their average sizes was made and included in the comments on the HRVCDs. Mineral abundance was used in determining the rock name. The igneous unit and contact logs are included (see Table T3).

Pillow basalts were identified by curved chilled margins oblique to the vertical axis of the core or, when these margins were absent, by variolitic texture, curved fractures, and microcrystalline or cryptocrystalline grain size. For glassy or chilled pieces lacking definitive indications of pillow structures (e.g., curved glassy margins), we designated these units as “basalt flows,” which could be interpreted as pillow basalts or sheet flows. Massive basalt flows were identified by sections of core bounded by planar sub-horizontal chilled margins, with the same lithology and grain size that increased toward the center of the unit. Other rock types distinguished were breccias and hyaloclastites.

### Igneous unit and contact logs

The first step in describing the core was the selection of unit boundaries, as described in “**Hard rock visual core descriptions**” in “Igneous and metamorphic petrology.” Subunits are designated on the HRVCD, and their descriptions are included within the overall written description of the unit. The igneous unit and contacts log (Table T3) provides information about the unit boundaries and a brief de-

scription of each unit. The table lists the following for each unit:

- Core number
- Section number
- Piece number(s)
- Location (in meters below seafloor) of the upper contact, calculated from the curated depth of the top of the core and the length of the pieces in the core above the upper contact
- Type of the upper contact (listed in Table T3)
- Minimum thickness of the unit, calculated from the piece lengths
- Rock type of each unit

### Thin sections

Thin sections of igneous rocks were studied to complete and refine the hand-specimen observations. This included textural features that were not identified in hand specimen; precise determination of grain size of phenocrysts and groundmass; the mineralogy, abundance, and type of glomerocrysts; the presence of inclusions within phenocrysts; and the presence of spinel, oxides, and sulfides. Crystal sizes of all primary phases were measured. In addition, mineral morphologies, grain sizes, and textural features were described. The terms heterogranular (different crystal sizes), seriate (continuous range in grain size), porphyritic (indicating presence of phenocrysts), glomeroporphyritic (containing clusters of phenocrysts), hypocrySTALLINE (100% crystals) to hypohyaline (100% glass), variolitic, intergranular (olivine and pyroxene grains between plagioclase laths), intersertal, subophitic, and ophitic were used to describe the textures of the mesostasis. The same terminology was used for thin section descriptions and the macroscopic descriptions. An example of the thin section description form is given in Table T5, with a key in Table T4. Thin section descriptions are included in “Core Descriptions” and are also available from the IODP database. Digital photomicrographs were taken during the cruise to document features described in the thin sections. A list of available images, any of which can be obtained from the IODP data librarian, is given in the Site U1301 chapter.

### Alteration

All igneous rocks recovered during Expedition 301 have undergone alteration and veining. On the HRVCD forms, rocks were graded according to whether they are fresh (<2% by volume alteration products) or have slight (2%–10%), moderate (10%–50%), high (50%–90%), or complete (90%–100%) alteration. Alteration and vein description logs on a piece-by-piece scale were tabulated to provide a con-

sistent characterization of the rocks and to quantify the different alteration types (see Tables T6, T7). Descriptions are based mostly on hand-specimen observations, and specific secondary minerals are not generally distinguished, except where crystal morphology allows unequivocal identification. Where additional mineralogical evidence is available from either thin section descriptions and/or X-ray diffractograms, these identifications were integrated into the alteration and vein logs and the HRVCDs. We recorded the following information in the logs:

- Alteration log (e.g., Table T6): This log records bulk rock alteration. Each entry records the igneous unit; identifiers for the core, section, piece, and subpiece; the locations of top and bottom of each piece; the length of each piece; and the depth below seafloor of the top of the core. The alteration type (as represented by rock color and calibrated by thin section observations), the abundance (in percent) and fill-mineralogy of vesicles, the abundance (in percent) of glass, and the percent alteration of glass are documented for each piece or group of pieces. A column for comments is included.
- Vein log (e.g., Table T7): This log records the presence, location, width, and mineral content of veins observed on the cut surface of the cores. Each entry records the igneous unit and the identifiers for the core, section, piece, and subpiece. For each vein, the location of the top and bottom of the feature is recorded, and the mineralogy, vein width (in millimeters), presence or absence of a related alteration halo, and the width (in millimeters) of the halo on one side of the vein are recorded. For breccia and vein nets, recorded data include the centimeter interval, the percentage of nonbasalt material (e.g., veins and cement), and the percentages of secondary minerals. A column for comments is included.

### Structures

This section outlines the techniques used for macroscopic and microscopic description of structural features observed in hard rock basement cores. Conventions for structural studies established during previous ODP hard rock drilling legs (Shipboard Scientific Party, 1989, 1991, 1992a, 1992c, 1992d, 1993a, 1993b, 1995, 1999, 2003a) were generally followed during Expedition 301.

### Graphical representation and terminology

All material from both working and archive halves was examined, although the sketches of the structures and orientation measurements were made on



the archive half. The most representative structural features in the cores recovered during Expedition 301 are summarized on the HRVCD form (see “Core Descriptions”). For each section, more detailed structural information is described and sketched on a separate Structural Geology Description form (Fig. F7). Structural data were tabulated in the structure log (Table T8).

To maintain consistency of core descriptions we used a set of structural feature “identifiers.” Brittle deformation identifiers include joint, vein, shear vein, fault, and breccia. Identification of these features is based on the presence of fractures, filling phases, and evidence of shear displacement. The terminology adopted generally follows that of Ramsay and Huber (1987), Twiss and Moores (1992), and Passchier and Trouw (1996) and is consistent with the terminology used during Leg 153 for brittle deformation (Shipboard Scientific Party, 1995). Some of the terms commonly used in the structural description are sketched in Figure F8:

- J = joints (fractures where the two sides show no differential displacement [relative to the naked eye or 10× pocket lens] and have no filling material)
- V = veins (extensional open fractures filled with epigenetic minerals)
- SV = shear veins (obliquely opening veins with minor shear displacement, filled with slickenfibers or overlapping fibers)
- F = faults (fractures with kinematic evidence for shear displacement across the discontinuity or with an associated cataclasis; we adopted the term microfault when the scale of the offset is millimetric)

This subdivision of the structures does not imply that all features fall into distinct and exclusive categories. We prefer to use the term veins for all the healed fractures, avoiding the usual subdivision based on fracture width (e.g., Ramsay and Huber [1987] defined veins as having >1 mm filling material), mainly to be consistent with the vein log (see “Alteration” in “Igneous and metamorphic petrology”). There are not rigid boundaries between the adopted structural categories; where necessary, details of specific structural features are illustrated with comments and sketches.

### Geometric reference frame

Structures are measured on the archive half relative to the core reference frame used by IODP. The plane normal to the axis of the borehole is referred to as the horizontal plane. On this plane, a 360° net is

used with a pseudo-south (180°) pointing into the archive half and a pseudo-north (0°) pointing out of the archive half and perpendicular to the cut surface of the core. The cut surface of the core, therefore, is a vertical plane striking 90°–270°. The strike of planar features across the cut face of the archive half was measured with 0° down the vertical axis of the core, and the dip was measured using the right-hand rule (Fig. F9). The orientations were then rotated into the IODP reference frame using the Stereonet (version 6.3.0X) Macintosh program by Rick Allmendinger.

### Hard rock geochemical analyses

Representative samples from selected igneous units were analyzed for major and trace elements during Expedition 301 using ICP-AES. Approximately 10 cm<sup>3</sup> samples were cut from the core with a diamond saw blade. All outer surfaces were ground on a diamond-impregnated disk to remove surface contamination and altered rinds resulting from drilling. Each cleaned sample was placed in a beaker containing trace metal-grade methanol and was ultrasonicated for 15 min. The methanol was decanted and the samples were ultrasonicated twice in deionized water for 10 min and then ultrasonicated 10 min in nanopure deionized water. The clean pieces were then dried for 10–12 h at 65°C.

The clean, dry whole-rock samples were fragmented to chips <1 cm by crushing them between two disks of Delrin plastic in a hydraulic press. They were then ground to a fine powder in a tungsten carbide (WC) mill by a SPEX 8510 shatterbox. A 1.0000 ± 0.0005 g aliquot of the sample powder was weighed on a Scientech balance and ignited to determine weight loss on ignition (LOI).

ODP *Technical Note 29* (Murray et al., 2000) describes in detail the shipboard procedure for dissolution of rocks and ICP-AES analysis of samples. The following protocol is an abbreviated form of this with minor changes and additions. After determination of LOI, 100.0 ± 0.2 mg aliquots of the ignited whole-rock powders were weighed and mixed with 400.0 ± 0.5 mg of LiBO<sub>2</sub> flux that had been preweighed on shore. Standard rock powders and full procedural blanks (400 mg LiBO<sub>2</sub>) were included with the unknowns in each ICP-AES run. During ODP Leg 206, a grinding blank of pure SiO<sub>2</sub> was analyzed as a check on grinding contamination contributed by the WC mills (Table T9), using a grinding blank that was processed using the shatterbox that appeared dirtiest and was therefore a “worst-case” scenario. The Leg 206 analysis gives an indication of the potential grinding contamination in Hole U1301B samples. All samples and standards were weighed to ±0.20 mg on the

Scientech balance, and weighing errors are estimated to be ~0.05 mg.

We added 10  $\mu\text{L}$  of 0.172 mM aqueous LiBr solution to the flux and rock powder mixture as an antiwetting agent to prevent the cooled bead from sticking to the crucible. Samples were then individually fused in Pt-Au (95%:5%) crucibles for ~3 min at a maximum temperature of 1050°C in a Bead Sampler NT-2100. After cooling, beads were transferred to 125 mL high-density (HD) polypropylene bottles and dissolved in 50 mL of 10%  $\text{HNO}_3$ , aided by shaking with a Burrell reciprocal bottle shaker for 1 h. From Run 2 onward, the samples were ultrasonicated for ~1 h after shaking to ensure complete dissolution of the glass bead. After digestion of the glass bead, all of the solution was passed through a 0.45  $\mu\text{m}$  filter into a clean 60 mL wide-mouth HD polypropylene bottle. Next, 2.5 mL of this solution was transferred to a plastic vial and diluted with 17.5 mL of 10%  $\text{HNO}_3$  to bring the total volume to 20 mL. The final solution-to-sample dilution factor for this procedure was ~4000 $\times$ .

Major (Si, Ti, Al, Fe, Mn, Mg, Ca, Na, K, and P) and trace (Sc, V, Cr, Ni, Sr, S, Y, Zr, Nb, and Ba) element concentrations of standards and samples were determined with the JY2000 Ultracore ICP-AES, which routinely measures wavelengths between ~100 and 800 nm. Specific analytical conditions for each sample run during Expedition 301 are provided in Table T10.

The JY2000 plasma was ignited at least 30 min before each sample run to allow the instrument to warm up and stabilize. After the warm-up period, a zero-order search was performed to check the mechanical zero of the diffraction grating. After the zero-order search, the mechanical step positions of emission lines were tuned by automatically searching with a 0.002 nm window across each emission peak using the BAS 148 standard (basalt standard created during ODP Leg 148, Hole 504B; Bach et al., 1996), or the BAS 206 (basalt interlaboratory standard created during ODP Leg 206; Shipboard Scientific Party, 2003a) prepared in 10%  $\text{HNO}_3$ . During the initial setup, an emission profile was selected for each peak, using standard BHVO-2, to determine peak-to-background intensities and to set the locations of background points for each element. The JY2000 software uses these background locations to calculate the net intensity for each emission line. The photomultiplier voltage was optimized by automatically adjusting the gain for each element using BHVO-2.

ICP-AES data presented in “[Hard rock geochemistry](#)” in “[Igneous and metamorphic petrology](#)” in the “[Site U1301](#)” chapter were acquired using either the

Gaussian or maximum mode of the Windows 5 JY2000 software. Gaussian mode fits a curve to points across a peak and integrates the area under the curve to determine element intensity. Gaussian mode was used for Si, Ti, Al, Fe, Ca, Na, K, Sc, V, Sr, Zr, and Nb, and maximum mode was used for elements with asymmetric emission peaks (Mn, Mg, P, Y, Cr, Ni, and Ba). Intensity is integrated using the maximum intensity detected. Each unknown sample was run at least twice, nonsequentially, within a given sample run.

A typical hard rock ICP-AES run (Table T11) during Expedition 301 included the following:

- A set of five certified rock standards (JA-1, JR-1, BIR-1, AII, and BOB-1) analyzed twice each throughout the sample run
- Up to seven unknown samples run in duplicate
- A drift-correcting sample, BCR-2, analyzed every fourth sample position and at the beginning and end of each run
- Blank solutions run near the beginning and end of each run
- A check standard (i.e., standard run as an unknown), typically BAS-148 or BAS-206, although Run 1 consisted primarily of check standards and also included standards JA-3, JGb-1, and JB-2
- A 10%  $\text{HNO}_3$  wash solution run for 90 s between each analysis.

Following each sample run, the raw intensities were transferred to a data file and all samples were corrected first for drift and then for the full procedural blank. The drift correction was applied to each element by linear interpolation between drift-monitoring solutions run approximately every fourth analysis. Following drift correction and blank subtraction, calibration curves were constructed based on five certified rock standards (JA-1, JR-1, BIR-1, AII, and BOB-1). Unknown concentrations were then calculated from the calibration line. Estimates of accuracy and precision for major and trace element analyses were based on replicate analyses of check standards (usually BAS-148 and BAS-206), the results of which are presented in Table T12. In general, run-to-run relative precision by ICP-AES was <3.5% for the major elements. Run-to-run relative precision for trace elements was generally <9%. Exceptions typically occurred when the element in question was near background values.

## Paleomagnetism

The goals of paleomagnetic studies during Expedition 301 were twofold: (1) to determine magnetic

polarities of cores for correlation with the geomagnetic polarity timescale (GPTS) and (2) to measure paleomagnetic directions for tectonic and polarity studies. Paleomagnetic studies during Expedition 301 were done using the shipboard pass-through cryogenic magnetometer to measure archive-half core sections and discrete samples from the working half of the core. Archive-half measurements were made for natural remanent magnetization (NRM) and remanent magnetization after alternating-field (AF) demagnetization. Whole-section measurements were made only on APC cores because of the internal rotation of core segments in most RCB cores. In effect, this limited archive-half core measurements to the sediment column. Discrete samples were studied from the APC and RCB cores. Such samples usually avoid core deformation that occurs at core edges and are therefore considered more reliable. In the RCB cores from igneous basement, these samples were the sole source of paleomagnetic information because the paleomagnetists did not wish to create spurious data by measuring highly fractured core pieces in the pass-through mode.

### Paleomagnetic instruments

A 2G Enterprises pass-through cryogenic direct-current superconducting quantum interference device (SQUID) rock magnetometer (model 760R) was used to make paleomagnetic measurements during Expedition 301. This pass-through cryogenic magnetometer is equipped with an in-line AF demagnetizer (2G model 2G600) that allows for demagnetization of samples up to 80 mT. The magnetometer and AF demagnetizer are interfaced with a PC-compatible computer that is used to archive and analyze the collected data. Sensor coils of the cryogenic magnetometer measure a width of a little more than 30 cm, although ~85% of the remanence is sensed from a 20 cm width of a core section. A background resolution limit is imposed on measurement of rock remanence by the magnetization of the core liner itself, which is  $\sim 3 \times 10^{-5}$  A/m. In almost all cases, Expedition 301 samples had magnetization intensities well above the magnetometer limit.

Magnetic susceptibility of core sections was measured with two devices. Whole-core sections were measured on the whole-core MST. This apparatus includes a Bartington model MS2 meter with an 80 mm internal diameter MS2C sensor loop (88 mm coil diameter) operating at a frequency of 565 Hz and an alternating field of 80 A/m (0.1 mT). The specified sensitivity for the MS2 susceptibility meter is  $10^{-5}$  SI per  $10 \text{ cm}^3$  volume or  $10^{-8}$  SI per 10 g mass. A second Bartington susceptibility meter is included on the AMST. This meter uses a 15 mm diameter

MS2F probe capable of making measurements of susceptibility at the core surface, giving a greater resolution than the loop sensor of the whole-core MST. The susceptibility sensitivity of the split-core meter is the same as the whole-core meter, and its specified horizontal resolution is 20 mm. Most of the probe sensitivity is within less than a diameter of the probe tip. Additional instruments in the paleomagnetic laboratory include a DTECH model D-2000 AF demagnetizer capable of demagnetization up to 200 mT and a Schonstedt thermal demagnetizer (model TSD-1) capable of demagnetization up to 700°C.

### Paleomagnetic measurements

Standard ODP paleomagnetic measurement conventions were used for Expedition 301 paleomagnetic studies. The x-axis is positive upward (downward) from the split face of the archive (working) half of the core. The positive y-axis is left facing upcore along the split surface of the archive half, whereas the positive z-axis is downcore (Fig. F10).

Each APC core archive half was routinely measured at 5 cm intervals using the shipboard pass-through cryogenic magnetometer. NRM was measured initially, followed by magnetization after progressive AF demagnetization at 10 mT steps from 10 to 40 mT. Demagnetization was accomplished using the in-line AF demagnetization coils built into the cryogenic magnetometer. Discrete samples were taken at intervals dictated by core recovery and scientific interest. Sediment samples were taken in  $7 \text{ cm}^3$  plastic cubes pressed into the core split face, whereas igneous samples were collected as either  $2.5 \text{ cm}$  cubes ( $16 \text{ cm}^3$  volume) cut with the rock saw or  $2.5 \text{ cm}$  diameter minicores ( $12 \text{ cm}^3$  volume) drilled perpendicular to the core split face. Samples were usually either AF demagnetized at 5 mT intervals from 0 to 70 mT or thermally demagnetized at 50°C steps from 0° to 700°C. Magnetic susceptibility measurements were made on APC cores with the MST and the AMST at 3 cm intervals. The quality of these results degraded in XCB and RCB sections when the core was undersized and/or disturbed. Nevertheless, the general downhole trends were useful for stratigraphic correlations. The MS2 meter measures relative susceptibilities that have not been corrected for the differences between core and coil diameters. Susceptibility values were stored in the Janus database as raw data in units of  $10^{-5}$  SI. The true SI volume of susceptibilities should be multiplied by a correction factor to account for the volume of material that passed through the coils.

### Geomagnetic polarity timescale

Magnetic polarity results were correlated to the polarity reversal sequence and absolute age using the

Berggren et al. (1995) geochronology (Fig. F11). This timescale incorporates the widely used calibration of age and polarity intervals derived by Cande and Kent (1995).

## Biogeochemistry

### Interstitial water samples

Shipboard IW samples were obtained from 20–40 cm long whole-round intervals cut on the catwalk, capped, and taken to the laboratory for immediate processing. Details on sampling resolution are described in the individual site chapters of this volume. When there were too many IW intervals to process immediately, the capped whole-round intervals were stored temporarily in the refrigerator.

Processing of sediment for IW sampling in the laboratory was carried out in a nitrogen-flushed glove-bag. After extrusion from the core liner, the outer layer of each whole-round interval was carefully scraped with a spatula to remove potential contamination from drill water (surface seawater). Remaining sediment was then placed into a titanium squeezer, modified after the standard stainless steel squeezer of Manheim and Sayles (1974). The piston was positioned on top of the squeezer, and the entire unit was removed from the glove bag and placed on the hydraulic press. Pressures of up to 76 MPa were applied in the squeezer, calculated based on the measured hydraulic press pressure and the ratio of the piston areas of the hydraulic press and the squeezer. Interstitial water was passed through a prewashed Whatman number 1 filter above a titanium screen, filtered through a 0.45  $\mu\text{m}$  Gelman polysulfone disposable filter, and subsequently extruded either into a 50 mL gas-tight glass syringe or into a precleaned (10% HCl) 50 mL plastic syringe. Both types of syringes were attached to the bottom of the squeezer assembly via a three-way plastic valve. The 50 mL glass syringe was used to collect the first fraction of IW for analyses of organic components. This procedure was implemented in order to prevent the release of organic contaminants from plastic syringes and the loss of ephemeral constituents during the squeezing process. After collection of IW, the syringe was removed to dispense aliquots for shipboard and shore-based analyses.

Samples were stored in acid-cleaned plastic vials pending shipboard analyses. Aliquots for future shore-based trace metal and elemental analyses were placed in triple acid-washed plastic vials and acidified with 4 mL of subboiled 6N HCl per liter of sample. Samples for organic and carbon isotopic analyses

were placed in precombusted glass vials with polytetrafluoroethylene-coated screw caps.

### Interstitial water analyses

Interstitial water samples were analyzed routinely according to standard shipboard procedures (Gieskes et al., 1991). The pH was determined by ion-selective electrode. Alkalinity was determined by Gran titration with a Metrohm autotitrator.

Dissolved total carbon (TC), total inorganic carbon (IC), and total organic carbon (TOC) were measured using a Shimadzu TOC analyzer TOC-5000. Aliquots of 0.5 to 1.0 mL of IW were diluted manually to 5 mL. Solutions were then injected with the Shimadzu ASI-5000A autosampler using volumes of 26  $\mu\text{L}$  and 33  $\mu\text{L}$  for TC and IC, respectively. The total carbon was combusted at 680°C in the TC combustion tube filled with Pt catalyst to become  $\text{CO}_2$ . For the inorganic carbon analysis, only the IC component of the sample was converted to  $\text{CO}_2$  into a reaction vessel containing a solution acidified with  $\text{H}_3\text{PO}_4$ . The  $\text{CO}_2$  was then detected by a nondispersive infrared gas analyzer. The amount of total organic carbon was calculated as the difference between total carbon and inorganic carbon.

Concentrations of sulfate and of the major cations calcium, magnesium, potassium, and sodium were determined by ion chromatography after manual dilution of IW samples (200 $\times$ ). The instrumental setup involved either a Dionex AS4 column for anion exchange or a Dionex CS12A column for cation exchange on a Dionex DX-120 ion chromatograph equipped with a Spectrophysics autosampler. Chloride analysis was carried out by potentiometric titration using silver nitrate and a Mettler Toledo DL25 titrator equipped with a silver ring electrode (Mettler/Toledo ME 89599) and 2M  $\text{KNO}_3$  electrode filling solution. All quantifications were based on comparison with International Association of the Physical Sciences of the Ocean (IAPSO) standard seawater.

Dissolved phosphate and ammonium concentrations were determined by spectrophotometric methods using a Milton Roy Spectronic 301 spectrophotometer. In order to account for the limited volume of IW samples, these analyses were carried out on samples that had already been titrated for alkalinity and were thus acidified, degassed, and in a pH range appropriate for colorimetric determination of phosphate by the phosphomolybdate blue method.

Selected major, minor, and trace elements were analyzed using the JY2000 ICP-AES. Concentrations of Ba, B, Fe, Li, Mn, Si, and Sr were determined following the procedures outlined by Murray et al. (2000).

For these analyses, the shipboard “Master” ICP standard (Murray et al., 2000; modified by M. Delaney) was expanded so that Si concentrations could be determined. In preparation for analysis by ICP-AES, aliquots of IW were acidified with nitric acid and diluted tenfold with nanopure water for minor elements. Analytical blanks were prepared identically by analyzing deionized water, which was acidified to matrix match the samples.

### Gas analyses

Concentrations of the light hydrocarbon gases (methane, ethane, propane, and propene) were monitored for safety and pollution prevention. Sampling of headspace gases followed the standard procedures described by Kvenvolden and McDonald (1986). Upon core retrieval, a 3 mL sediment sample was collected with a syringe or borer tool from a freshly exposed end of a core section. After withdrawing the syringe, the plunger was advanced slightly to extrude a small amount of sediment. This excess was shaved off with a flat spatula flush with the end of the syringe barrel to provide an accurate determination of the sediment volume within the syringe. The sample was then extruded into a 20 mL glass serum vial and sealed immediately with a septum and metal crimp cap. For consolidated or lithified samples, chips of material were placed in a vial and sealed. Prior to gas analysis, vials were heated to 60°C for 20 min.

For gas chromatographic analyses, a 5 mL subsample of headspace gas was extracted from the vial using a standard gas syringe. Concentrations of methane, ethane, ethene, propane, and propene were analyzed using a Hewlett Packard 6890 Plus gas chromatograph (GC) equipped with a 25  $\mu$ L sample loop, an 8 ft  $\times$   $\frac{1}{8}$  inch stainless steel column packed with HayeSep R (80–100 mesh), and a flame ionization detector. The carrier gas was helium, and the GC oven was programmed from 100°C (5 min hold) to 140°C (4.5 min hold) at a rate of 50°C/min. Data were collected using a Hewlett-Packard 3365 chromatography data processing program. Chromatographic responses were calibrated using commercial standards (analyzed gases from Scott Specialty Gas Co.) and the results reported in parts per million by volume (ppmv [ $\mu$ L/L]).

The concentration of methane in interstitial water was derived from the headspace concentration by the following equation:

$$CH_4 = (\chi_M \times P_{atm} \times V_H) / (R \times T \times \phi \times V_S), \quad (1)$$

where

- $V_H$  = volume of the sample vial headspace,
- $V_S$  = volume of the whole sediment sample,

- $\chi_M$  = molar fraction of methane in the headspace gas (obtained from GC analysis),
- $P_{atm}$  = pressure in the vial headspace (assumed to be the measured atmospheric pressure when the vials were sealed),
- $R$  = the universal gas constant,
- $T$  = temperature of the vial headspace in degrees Kelvin, and
- $\phi$  = sediment porosity (determined either from moisture and density measurements on adjacent samples or from porosity estimates derived from gamma ray attenuation [GRA] data representative of the sampled interval).

Quantities of methane that remain undetected because of dissolution in the aqueous phase are minimal (e.g., Duan et al., 1992) and are not accounted for. The internal volume of the employed headspace vials was measured beforehand and was determined to be 21 mL. This volume was taken as constant in calculations of gas concentrations.

### Sediments

Sediment samples were analyzed according to the standard methodology employed during previous ODP legs. IC concentration was determined by titration using a Coulometrics 5011 CO<sub>2</sub> coulometer. Approximately 10 mg ( $\pm 10\%$ ) of freeze-dried, ground sediment was weighed using a gimballed Cahn C-31 microbalance and then reacted with 2N HCl to release CO<sub>2</sub>. Purified air used as the carrier gas was passed through a KOH solution to remove CO<sub>2</sub>. Sample gas was then scrubbed of SO<sub>2</sub> through a 3% AgNO<sub>3</sub> solution before being transferred into a coulometric (cathode) cell filled with a monoethanolamine (ME) proprietary solution used as the colorimetric solution. In this cell, the CO<sub>2</sub> was quantitatively absorbed, where it reacted with the ME solution to form a titratable acid, causing the blue color to fade. A photodetector monitored the color change as percent transmittance (%T). As %T increased, a titration current was automatically activated to generate a base from an adjacent anode cell at a rate proportional to %T. The endpoint of the titration was determined when %T returned to the original setpoint of 29. Calcium carbonate, expressed as weight percent, was calculated from the IC content, assuming that all evolved CO<sub>2</sub> was derived from dissolution of CaCO<sub>3</sub>, by the following equation:

$$CaCO_3 \text{ (wt\%)} = 8.33 \times IC \text{ (wt\%)}. \quad (2)$$

No correction was made for the presence of other carbonate minerals.

TC, nitrogen, and sulfur concentrations were determined using a Carlo Erba 1500 CHNS elemental analyzer. Approximately 10 mg of freeze-dried, ground

sediment was weighed again, using the Cahn C-31 microbalance, and combusted at 1000°C in a stream of oxygen. Nitrogen oxides were reduced to nitrogen, and the mixture of carbon dioxide, nitrogen, and sulfur dioxide was separated by gas chromatography and detected by thermal conductivity detector (TCD). All measurements were calibrated by comparison to a pure sulfanilamide standard. The amount of TOC was calculated as the difference between TC and IC (determined from coulometry).

In addition to the TOC concentration, elemental analysis yields the C/N atomic ratio, which can be used to help identify sources of organic matter (fresh marine C/N = 6–8; degraded marine C/N = 8–20; terrestrial C/N = 20). Rock-Eval pyrolysis analysis was not carried out because data are generally unreliable for samples containing <0.5 wt% TOC.

## Microbiology

During Expedition 301, we collected samples from both sediments and basaltic crust. Samples were taken for cultivation assays, polymerase chain reaction (PCR)-based molecular phylogenetic studies, activity measurements, and contamination tests. Prior to Expedition 301, the microbiota of deep subsurface sediments and deep subsurface basalts had been investigated in only a few studies (Cowen et al., 2003; Fisk, et al., 1998; D'Hondt et al., 2002, 2004; Inagaki et al., 2003, 2005; Parkes et al., 1994, 2000). The eastern flank of the Juan de Fuca Ridge is of great interest to microbiologists because of the flow of hydrothermal fluids through basement rocks. Delivery of electron acceptors such as sulfate by hydrothermal fluid flow, combined with potential release of electron donors such as reduced metals and perhaps hydrogen (H<sub>2</sub>) from the basalt, may support high microbial activity and biomass tens to hundreds of meters below the top of basement. The moderately hot to very hot temperatures (65° to >100°C) may further promote microbial growth. Moreover, transport of sulfate and heat to the comparatively organic rich sediment column may foster high microbial biomass and activity in sediments near basement. Transport of sulfate into sediments from both the overlying water column and underlying basaltic basement creates two sulfate–methane transition zones, thereby enabling us to examine changes in community composition and activity of sulfate reducers, methanogens, and poorly understood anaerobic methane oxidizers along thermal and geochemical gradients at a single site.

## Core handling and sampling

### Sediment for cultivation and molecular biological analyses

Whole-round samples taken on the catwalk for microbiological analysis were handled aseptically to minimize contamination. Cores were visually inspected prior to sampling of whole rounds for signs of disturbance such as gas voids, cracks, or drilling disturbance. Core sections suitable for microbiological and molecular biological analyses were quickly transported to the adjacent core laboratory, where they were divided into smaller whole rounds, each used for different analyses. These analyses included cultivation assays, bacterial counts, contamination tests, and molecular biological surveys (all discussed below). To maximize comparability of microbiological and molecular biological information with geochemical and lithologic data, microbiological sampling was coordinated with other shipboard studies.

To prevent oxidation of anaerobic sediments, subsamples used for cultivation experiments were immediately subjected to anaerobic handling techniques. Subsamples used for molecular biological analyses were placed rapidly into sterile bags and frozen at –80°C. Core liners are not sterile, meaning the outer surfaces of cores are contaminated during drilling (Smith et al., 2000) and core cutting may introduce contaminants. Because of this, subsampling for cultivation and later molecular biological analyses was restricted to sediments at or near the center of the whole-round samples (Fig. F12B).

### Rock for cultivation and molecular biological analyses

RCB basalt cores were handled aseptically to minimize contamination. Samples were obtained from all representative lithologies and units. Suitable rock samples were chosen with preference for large, intact pieces. From every sampling depth, rocks were chosen for cultivation assays, bacterial counts, contamination tests, and molecular biological surveys (all discussed below).

Most subsurface microbes are sensitive to oxygen exposure. Therefore, rock samples for cultivation experiments were transferred as quickly as possible to anaerobic conditions. In some cases, this involved collection of rock pieces directly on the catwalk and immediate transfer to vials containing anaerobic saline solution (3% NaCl) flushed with N<sub>2</sub>, followed by slurry preparation. In other cases, rocks were transferred to an anaerobic glove box (97.5% N<sub>2</sub>, 2.5% H<sub>2</sub>)

within minutes of core arrival, cracked with a hammer and chisel, crushed with a mortar and pestle, and further processed in the glove box. A third approach was to wash and flame rock surfaces in the laboratory to remove microbial contaminants (as described in “[Contamination tests with perfluorocarbon tracer](#)”), crack the rock with a hammer and chisel, and then immediately transfer some of the resulting rock fragments to an anaerobic glovebox for crushing and further processing. Rocks used in molecular biological analyses were placed rapidly into sterile bags and frozen at  $-80^{\circ}\text{C}$ .

### Rock for bioreactor experiments

Samples of basement material were collected to conduct bioreactor experiments. All samples were handled aseptically to minimize contamination. These experiments are a follow-up to previous molecular biological studies by Cowen et al. (2003) in which relatives of nitrate- and sulfate-reducing microorganisms had been detected in a BioColumn deployed on the Circulation Obviation Retrofit Kit (CORK) in ODP Hole 1026B. We will conduct experiments onshore to measure microbial activity and examine the possibility of microbially mediated nitrate and/or sulfate reduction in the basaltic oceanic crust.

We collected 5 cm whole-round samples on the catwalk and, based on size and shape, placed them into  $\text{N}_2$ -flushed polyethylene terephthalate (PET) bags. Samples were placed in the anaerobic glove box and rinsed twice in sterile anaerobic artificial seawater to remove contaminants. Wash water was saved for analysis. Cleaned samples were transferred to sterile PET bags and submerged in artificial seawater, sealed, and refrigerated.

### Water sampling

As part of the drilling process, huge amounts of surface seawater are injected into boreholes. This is the major source of contaminating microorganisms to cores collected for microbiological analyses. As a check on contamination (apart from the tracer tests discussed later), we inspected the microbial composition of drilling fluid. Water samples were collected and handled using sterile equipment. Samples of seawater were collected directly from the injection pipe into sterile bottles with screw caps. Microorganisms present in fluids were extracted by filtration using a vacuum pump, first through 5  $\mu\text{m}$  pore polycarbonate filters and then through 0.2  $\mu\text{m}$  pore polycarbonate filters. Using a scalpel, filters were divided into smaller pieces and frozen separately in small cryotubes at  $-80^{\circ}\text{C}$ . Tubes were brought back to the labo-

ratory on shore for deoxyribonucleic acid (DNA) extraction and analysis.

### Scale on CORK sampling

Mineral deposits growing on the Leg 168 CORK body recovered from Hole 1026B were sampled. Because the basement fluids at this site are overpressured and the CORK was unsealed, the hole has produced basement fluids for several years (Cowen et al., 2003; Fisher et al., 2003). The flow of  $65^{\circ}\text{C}$  basement fluid has prevented the intrusion of cold seawater from above. As a result, there is a strong biogeochemical interface at the seafloor, where warm, anoxic basement water meets cold, oxygenated seawater.

Using sterile spatulas, we scraped off mineral deposits and biofilms from where they coated the outside of the CORK body. Where necessary, we used a hammer and chisel to break off pieces of these materials. Samples used for cultivation assays were transferred immediately to an anaerobic glove box for further processing. Samples used for molecular biological analyses were placed rapidly into sterile bags and frozen at  $-80^{\circ}\text{C}$ . No contamination tests could be performed on these samples, but they were exposed extensively to ordinary seawater during formation and as the CORK body was retrieved from the seafloor.

### Storage conditions

All sediment cores used for molecular biological analyses were capped, placed in sterile plastic bags, and stored at  $-80^{\circ}\text{C}$ . Some of the sediment samples for ribonucleic acid (RNA) analyses were frozen immediately with liquid nitrogen and stored at  $-80^{\circ}\text{C}$ . The slurry samples for cultivation were stored either at  $4^{\circ}\text{C}$  or room temperature. They were kept at the same conditions until they were removed from the ship in Balboa, Panama (following the next drilling expedition), and then shipped under the same conditions to their respective laboratories.

### Total cell counts

The most direct method for quantifying the extent of the deep microbial biosphere is by total bacterial cell counts using nucleic acid dyes to distinguish cells from organic matter. These counts have been performed on sediments from a wide range of locations during previous ODP legs (Parkes et al., 1994). A common trend across many sampling locations is an exponential decrease of cell numbers with depth. Despite this reduction, cell densities of  $10^4$ – $10^5$  cells/ $\text{cm}^3$  have been detected consistently even in the deepest sediments. Total cell counts also can reveal sediment layers of increased cell density, which of-

ten coincide with geo- and physicochemical conditions conducive to bacterial growth (Parkes et al., 2000).

During Expedition 301, we performed total cell counts on one sample per sediment core. In geochemical or biogeochemical transition zones (e.g., the sulfate–methane transition zone or in bottom sediments that were near the hydrothermally active, basaltic basement), counts were performed at one sample per section to gain a higher-resolution view of microbial distribution. We counted total bacterial numbers under an epifluorescence microscope using acridine orange as a fluorochrome dye (Fry, 1988; Shipboard Scientific Party, 2003a).

We also tried total cell counts on basaltic basement cores using this method. However, strong interference from autofluorescent rock flour makes it difficult to achieve reliable results.

### Contamination tests with perfluorocarbon tracer

The assessment of contamination with microbes from drilling fluid (surface seawater and sepiolite mud) is critical during sample collection for microbiological or molecular biological analyses. Certainty that microbes isolated or DNA sequences extracted from IODP cores are part of the autochthonous microbiota, and not contaminants, is obligatory to draw any conclusions about microbial diversity and metabolism in the subsurface. To quantify sample contamination with drilling fluid, perfluorocarbon tracer (PFT) was injected into the fluid to produce a constant concentration of 1 mg/L.

Concentrations of PFT in sediment cores were monitored with a gas chromatograph with an electron capture detector, flushed with N<sub>2</sub> gas, and followed the settings outlined in Smith et al. (2000). To check for intrusion of drilling fluid from the outside of cores to the inside, we took six 2 cm<sup>3</sup> samples of sediment from each whole-round sample using cut-off 3 mL syringes. Two samples were from the outer part near the core liner, two from halfway between the outside and the center, and two from the center of every whole-round sample. We generally expected the PFT content of sediment to decline with increasing distance from the core liner, although APC coring can also operate cleanly enough to prevent any (measurable) sample contamination with drilling fluid.

Each sample was placed in a 10 mL vacuum-seal tube. We used these tubes instead of the 20 mL GC vials used by Smith et al. (2000) because we found that the GC vials' septa leaked after they had been

punctured. This became especially problematic with samples where measurements had to be repeated—for instance, when the rubber septum of the GC leaked and required replacement, or when pieces of septum got stuck in syringes during injection of sample into the GC, thereby preventing full sample injection. Since sufficient overpressure to push off rubber caps of vacuum-seal tubes could develop during incubation, the rubber cap of each tube was secured by wrapping electric tape around it several times. The secured tube with sample was then incubated at an oven temperature of 75°C for ~10 min. Using a disposable, preheated 1 mL syringe, 0.5 mL of headspace gas was injected into a GC. We found this technique to be more practical for making replicate analyses than repeated use of the same gas-tight syringe (e.g., Smith et al., 2000). We found that reusing the same gas-tight syringe required thorough and repeated flushing with methanol and incubation in the oven, with needle and plunger separated from syringes, for ≥30 min to remove all PFT residue. Even though disposable syringes were not gas tight, loss between transfer from storage tube to GC was minimal. Subsamples for PFT measurement were taken adjacent to all subsamples used for microbiological and molecular biological analyses.

Contamination of basalt samples and the effectiveness of decontamination treatments were examined in small pieces of rock from the exterior and interior. Rock pieces had been removed using a hammer and chisel and placed rapidly into 10 mL vacuum-seal tubes. To remove PFT, and hence microbial contaminants, from rock surfaces, each rock sample underwent a series of cleaning treatments. Removal of PFT from rock surfaces was essential to measure contamination in the interior. To prevent cross contamination, all surfaces and tools used were washed twice with ethanol and flamed between treatments. To evaluate the success of cleaning treatments, we took samples at each step. First, pieces of the untreated rock exterior were removed. The rock was washed twice by placement into a sterile bag containing sterile saline solution (deionized water; 3% NaCl) followed by vigorous shaking. For further PFT removal, the rock was flamed thoroughly using a propane torch until the exterior was completely dry. Finally, rocks were cracked open and subsamples taken from the rock interior. Where possible, only pieces that had not been in contact with the outside of the rock sample were analyzed. In cases where we could not obtain pieces that had not been in contact with the rock exterior, we chose pieces that appeared to have the lowest contact to the outside relative to their volume. Incubations and injections followed the same method as for sediment. The absence of PFT in the



untreated exterior of rocks was interpreted to indicate failure of the PFT delivery system because the RCB system used in basalt drilling should have led to contact of drilling fluid with essentially all samples. Greatly reduced PFT values on rock surfaces after cleanup treatments indicated successful removal. Zero to very low PFT concentrations in rock interiors were interpreted to indicate minimal contamination.

### Cultivation

Based on culture-independent molecular analyses using subseafloor sediment cores, most microbial communities in deep sediments appear to be composed of previously unidentified, yet-to-be-cultured microorganisms (Marchesi et al., 2001; Reed et al., 2002; Inagaki et al., 2003, 2005; Kormas et al., 2003; Newberry et al., 2004). There are, however, examples of successful microbial isolations from deep subsurface environments. For instance, *Desulfovibrio profundus* was isolated from the deep sediment of the Japan Sea at a depth of 500 mbsf (ODP Leg 128, Site 798B) (Bale et al., 1997). *Methanoculleus submarinus* was isolated from deep methane hydrate-bearing sediments in the Nankai Trough (Mikucki et al., 2003). In an attempt to increase knowledge of physiology of subseafloor microorganisms and to better understand the role of these microbes in the biogeochemical cycles of their environment, we tried to enrich for various types of microorganisms using a wide range of media and culture conditions (Tables T13, T14, T15, T16, T17, T18, T19, T20, T21, T22). We prepared (1) culture media without organic carbon substrates to select for chemolithoautotrophic microbes and (2) media with organic carbon compounds to select for chemohetero- and chemoorganoautotrophic microorganisms.

### Slurry preparation

Slurries were prepared in 200 mL flasks closed by rubber stoppers that allowed aseptic flushing with N<sub>2</sub>. Nitrogen gas was supplied with stainless steel tubes equipped with gas filters. Side arms could be closed by sterile stopcocks. Flasks contained 50 mL of sterilized artificial seawater that had been autoclaved and cooled under N<sub>2</sub>. Slurries were prepared by aseptically adding sediment contents from 50 mL syringes under an N<sub>2</sub> counterflow. Slurries were homogenized by repeated shaking and vortexing. Subsamples of this “master slurry” were used for cell counts, cultivation, and fluorescence in situ hybridization (FISH) analyses.

### Most probable number

Using classical cultivation techniques such as the most probable number (MPN) cultivation method,

various physiological types of microorganisms have been enriched and their numbers have been determined from marine sediments (e.g., Parkes et al., 2000; D'Hondt et al., 2004; Inagaki et al., 2005; Inagaki and Neilson, in press). For MPN counts, a series of tenfold dilutions is prepared from initial slurry and incubated (e.g., in 96 well microtiter plates) (Fig. F13). A sufficient number of dilutions are performed until a concentration is reached where no growth is detected and cells are presumably absent. Based on the number of dilutions necessary for no growth to occur, it is possible to estimate cell concentrations of the initial slurry and, hence, the environmental sample. MPN population counts obtained from the sediment column of the Peru margin (ODP Leg 201) ranged from 0 to 10<sup>5</sup> cells/cm<sup>3</sup>, showing a general decrease with depth. In general, <0.6% of total cell numbers in deep sediments are detected by MPN. Therefore, MPN counts only yield limited quantitative information about deep subsurface microbiology. However, isolation of microorganisms via high dilutions is an effective tool to select for phylotypes that are numerically abundant in the initial sample. Fast growing, opportunistic cells that are numerically insignificant in the environment, but cope best with culture conditions and therefore dominate many enrichments, can be eliminated.

### Gradient cultures

To examine the response of microbial communities from undisturbed sediment samples to low substrate concentrations, gradient cultures were inoculated with nonhomogenized sediment samples (Fig. F14). A mixture of monomers (4 mM each; 0.5 mL) was placed on the bottom of a glass tube and fixed with 0.5 mL of agar (4% in marine salt medium [MM]; 60°C). After the agar had solidified, another 2.5 mL of the same agar was added as a spacer and allowed to solidify. A 2 mL sediment sample in 5 mL MM was placed on top and the tube was gassed with N<sub>2</sub>, closed by a rubber stopper, and cooled on ice.

### Molecular biological surveys

Culture-independent molecular biological surveys are becoming an indispensable and powerful approach to investigate microbial diversity in the environment. Several kinds of molecular biological analyses will be performed in postcruise investigations and used for comparison with results from culture experiments. The most commonly used approach to obtain DNA sequences of genes uses PCR, an enzymatic reaction that produces replica of DNA. This reaction is repeated until target DNA has reached high enough concentrations to be cloned and sequenced. Molecular techniques using PCR al-

low rapid, sensitive, and extensive surveys of present (or past) marine subsurface microbial communities (Marchesi et al., 2001; Inagaki et al., 2001, 2003, 2005; Reed et al., 2002; Kormas et al., 2003). Numerous molecular approaches rely on PCR. Following, we list techniques that we will use as part of our postcruise work.

### **FISH**

FISH direct count (FISH-DC) and catalyzed reporter deposition-FISH (CARD-FISH) will be performed to estimate total microbial biomass as well as specific biomass of targeted phylogenetic groups. In general, CARD-FISH shows a higher sensitivity than the commonly used FISH technique. It is based on the use of horseradish peroxidase-labeled oligonucleotide probes and tyramide signal amplification (Bobbrow et al., 1989). This novel technique was introduced into microbial ecology for the identification of bacterial cells in marine plankton and benthos by Pernthaler et al. (2002). The signal amplification is essential to detect metabolically active cells with low numbers of ribosomes, as is typical for deep subsurface microorganisms.

### **Terminal restriction fragment length polymorphism**

Terminal restriction fragment length polymorphism allows identification of PCR products based on length variations after digestion with restriction endonucleases. It is used as a fingerprinting technique for nucleic acids of mixed microbial communities (Inagaki et al., 2001).

### **Gel electrophoresis**

Denaturing gradient gel electrophoresis and temperature gradient gel electrophoresis are gel electrophoretic methods that separate mixed PCR products in denaturing polyacrylamide gradients and are based on melting domain structure of the DNA double strand (Muyzer and Smalla, 1998). Bands appearing on the gel can be extracted and sequenced for phylogenetic identification of dominant members of the microbial community.

### **Real-time PCR**

Real-time PCR, a modification of classical PCR, is essentially a fluorogenic assay used to quantify the number of target genes, and hence cells, in a given environmental sample (Suzuki et al., 2000; Takai and Horikoshi, 2000).

### **Copy DNA PCR**

Copy DNA (cDNA)-PCR of reverse-transcribed RNA is a technique by which the 16S ribosomal RNA mole-

cule, or the unstable messenger RNA copy of a gene, is reverse-transcribed to its respective cDNA (Inagaki et al., 2002). Because prokaryotic DNA is likely to be preserved in anoxic sediments for geological time-scales (Inagaki et al., 2004; Inagaki and Neilson, in press), we try to distinguish metabolically active from inactive, buried cells by RNA-based molecular techniques. The cDNA is then used for qualitative and real-time PCR (Wilson et al., 1999). Using qualitative PCR, we can identify phylotypes of metabolically active cells, whereas with real-time PCR we cannot only identify phylotypes of active cells but also quantify metabolic activity of those phylotypes.

### **Gene sequencing**

Gene sequencing is used to obtain the primary information (base sequence) of the gene itself and is essential for phylogenetic analysis and identification. Genes that we will analyze include 16S ribosomal DNA, based on which sequence libraries of microbial diversity will be established and compared downhole. Furthermore, genes encoding key enzymes of different metabolic pathways will be PCR-amplified, sequenced, and analyzed with respect to their composition and distribution along environmental gradients. We will examine functional genes involved in sulfate reduction (dissimilatory sulfite reductase, adenosine-S'-phosphosulfate [APS] reductase), methanogenesis (methyl coenzyme-M reductase), acetogenesis (formyl tetrahydrofolate synthase), complex organic compound degradation (benzoyl-CoA reductase; group I/II dehalogenase), the Calvin-Benson-Bassham cycle (ribulose bisphosphate carboxylase I/II/III[?]), the acetyl-CoA pathway (carbon monoxide dehydrogenase), the reverse citric acid cycle (ATP synthase), and other processes.

## **Physical properties**

This section outlines the procedures used to measure physical properties during Expedition 301. A comprehensive discussion of all methodologies and calculations used in the *JOIDES Resolution* physical properties laboratory can be found in *ODP Technical Note 26* (Blum, 1997).

Shipboard measurements of physical properties are used to characterize lithologic units, correlate cored material with downhole logging data, and interpret seismic reflection profiles. After the cores equilibrated to ambient room temperature, physical properties were measured on whole-round sections, undisturbed parts of split cores, and discrete samples.

The suite of whole-core analyses performed on recovered cores varied according to the type of coring method used. For sediment core recovered by APC,

the core was cut into 1.5 m sections and whole-round samples were collected for geochemical and microbiological analyses. Remaining APC sections were set aside to equilibrate to laboratory temperature (>6 h) and passed through the MST. The MST has a GRA bulk densitometer, a *P*-wave logger (PWL), a magnetic susceptibility (MS) meter, and an NGR sensor. During Expedition 301, only the GRA, MS, and NGR were used for the entire interval of sediment coring. The PWL was used on the first four cores but then generated unreliable data. It was not repaired in time for use during the rest of the expedition. Thermal conductivity measurements were performed before the sediment sections were split. Moisture and density (MAD) properties (bulk density, grain density, water content, and porosity) and *P*-wave velocity were measured on split sections. Shear strength measurements were generally made once per section, depending on lithology and recovery.

Hard rock basement was cored using the RCB system. Due to poor core recovery, the MST was only used to measure magnetic susceptibility. Measurements of thermal conductivity, *P*-wave velocity, and MAD properties were made approximately once per section. Additional samples were collected when there was a visible change in lithology or texture.

### Multisensor track measurements

Measurement of wet bulk density by the GRA system is based on the principle that the attenuation (mainly by Compton scattering) of a collimated beam of gamma rays produced by a  $^{137}\text{Ce}$  source passing through a known volume of sediment is related to material density (Evans, 1965). Calibration of the GRA system was completed using seawater/aluminum density standards. The minimum integration time for a statistically significant GRA measurement is 1 s, and routine Expedition 301 GRA measurements used a 3 s integration time. The measurement width of the GRA sensor is ~5 mm, with sample spacing generally set at 2.5 cm. A freshwater control standard was run with each section to measure instrument drift. GRA bulk density data are of highest quality when determined on APC cores in which the liner is completely filled with sediment. Occasionally, we recovered sandy intervals in which the core liner was incompletely filled. These intervals yielded poor-quality data. No corrections were made to the archived data to correct for partially filled core liners. Basement cores were not subjected to GRA measurements.

Whole-core MS was measured with the MST using a Bartington MS2 meter coupled to a MS2C sensor coil with a diameter of 8.8 cm operating at 565 Hz. The measurement resolution of the MS2C sensor is 4 cm,

with a minimum statistically significant count time of 1 s. On sediment cores, MST magnetic susceptibility was routinely measured every 2.5 cm with a 1 s sampling interval. On hard rock cores, MS was measured every centimeter with a 1 s measurement period. Magnetic susceptibility data were archived as raw instrument units (SI) and not corrected for changes in volume, although a correction was made for instrument drift.

Transverse *P*-wave velocity was measured on the MST with the PWL for sediment Cores 301-U1301C-1H to 4H, at which time the PWL stopped working. The PWL transmits a 500 kHz compressional wave pulse through the core every 1 ms. The transmitting and receiving transducers are aligned perpendicular to the core axis, and a pair of displacement transducers monitors the separation between the compressional wave transducers. Variations in the outer diameter of the liner do not degrade the accuracy of the velocities, but the unconsolidated sediment or rock core must completely fill the liner for the PWL to provide acoustic coupling. When it was operational, measurements were made every 2.5 cm with 50 data acquisitions per site (1 s). Calibration of the displacement transducer and measurement of electronic delay within the PWL circuitry were conducted using a series of acrylic blocks of known thickness and *P*-wave traveltime. Repeated measurements of *P*-wave velocity through a core liner filled with distilled water were used to check calibration validity. The use of the PWL on basement cores was prevented by poor acoustic coupling between the sample and the core liner.

NGR emissions of sediments are a function of the random and discrete decay of radioactive isotopes, predominantly those of uranium, thorium, and potassium, and are measured through scintillation detectors arranged at 90° to each other and perpendicular to the core. The installation and operating principles of the NGR system are discussed in Hoppie et al. (1994). Data from 256 energy channels were collected and archived. For presentation purposes, counts were summed over the range of 200–3000 keV, so as to be comparable with data collected during previous ODP legs. The measurement width of the NGR is ~15 cm, with a statistically significant count time of at least 5 s, depending on lithology. The sample spacing of the NGR measurements was set at 15 cm, and integration time was 20 s.

### Thermal conductivity

Thermal conductivity was measured with the TK04 (Teka, Berlin, Germany) system, using the needle-probe method (Von Herzen and Maxwell, 1959). The needle probe contains a heater wire and calibrated

thermistor. It is assumed to be a perfect conductor because it is much more conductive than unconsolidated sediments. With this assumption, the temperature of the probe has a linear relationship with the natural logarithm of the time after the initiation of heating:

$$T(t) = (q/4\pi k) \ln(t) + C, \quad (3)$$

where

- $T$  = temperature;
- $q$  = heat input per unit length per unit time;
- $k$  = thermal conductivity;
- $t$  = time after the initiation of the heat; and
- $C$  = a constant.

Thermal conductivity was measured on unconsolidated sediment and rock samples using the TK04 system as described by Blum (1997). These measurements are used, along with in situ temperature measurements, to estimate heat flow. The system uses a single-needle probe heated continuously in full-space mode for soft sediments (Von Herzen and Maxwell, 1959) and in half-space configuration for hard rock samples (Vacquier, 1985). A small amount of thermal joint compound was used to ensure good contact between the needle and hard rock half cores. A self-test, including a drift study, was conducted at the beginning of each cycle. Once the samples were thermally equilibrated, the heater circuit was closed and the temperature rise in the probes was recorded. Thermal conductivities were calculated from the rate of temperature rise while the heater current was flowing. In full-space mode (sediment cores), temperatures measured during the first 150 s of the heating cycle were fitted to the equation shown above. In half-space mode, the heating cycle was adjusted to 80 s. For full-core soft-sediment sections, a hole was drilled in the outer core liner and a 2 mm diameter temperature probe was inserted into the working half of the core section. For hard rock samples, a half-space needle probe was attached to ~6 cm long split-core pieces. The face of the split core was sanded and/or polished to ensure complete thermal coupling of the probe to the sample. The core pieces were resaturated in seawater under vacuum for a minimum of 2 h and allowed to equilibrate thermally in a water bath for at least 20 min. The thermal conductivity measurement for each sample was the average of three repeated measurements for the full-space method and three to six repeated measurements for the half-space method. Individual measurements were evaluated and deleted (not archived) if the reported value was based on poor statistics and/or if the value was highly inconsistent with other values from the same sample. Thermal conductivity measurements were made once per section for

sediment and one or two per core for hard rock samples. In order to check instrumental drift, thermal conductivity of two standard materials (ceramic and a water/gelatin mixture) was measured during coring operations. For basalt samples (Hole U1301B), we based the drift calculations on the macor standard because its properties are closest to the basalt core samples. Measured values of the standard showed no significant trend but suggested a small bias tending to measure values slightly higher than the known macor conductivity (mean measured value =  $1.67 \pm 0.01$  W/m·K) (Fig. F15A). Because the measured value of the standard was within the uncertainty of the published value ( $1.61 \pm 0.08$  W/m·K), we did not apply a correction to the sample data. The gelatin and water standard ( $0.62 \pm 0.06$  W/m·K, 24°C) was used for measuring thermal conductivities in sediments. To prevent convection, 18% gelatin was added to the water. Measured values of the water/gelatin mixture showed no significant trend but suggested a small bias tending to measure slightly low (mean value =  $0.58 \pm 0.00$  W/m·K) (Fig. F15B). No correction was applied to the samples because the calibration standard was below the thermal conductivity of the samples and it was not possible to determine a correction.

### Moisture and density properties

Samples of ~10 cm<sup>3</sup> for sediments and hard rock were collected at a frequency of one per section (depending on core recovery and lithology) to determine MAD properties.

Samples were taken from undisturbed parts of the core where possible. Wet sediment mass was measured immediately after the samples were collected. Dry mass and volume were measured after samples were heated in an oven at  $105^\circ \pm 5^\circ\text{C}$  for 24 h and allowed to cool in a desiccator. Hard rock samples were resaturated in seawater for 24 h, and then moisture content and density were measured using the same procedure as for the sediment sections.

Sample mass was determined to a precision of 0.01 g using two Scientech 202 electronic balances and a computer averaging system to compensate for the ship's motion. Sample volumes were determined using a Quantachrome helium-displacement pycnometer with a precision of 0.02 cm<sup>3</sup>. Volume measurements were repeated five times. All cells were calibrated after three sample runs to check for instrument drift and systematic error. A purge time of 3–5 min was used before each run. The procedures for the determination of these properties comply with the American Society for Testing and Materials designation (D) 2216 (ASTM, 1990).

### Mass and volume calculation

Wet mass ( $M_{\text{wet}}$ ), dry mass ( $M_{\text{dry}}$ ), and dry volume ( $V_{\text{dry}}$ ) are measured in the laboratory. Salt precipitated in sediment pores during the drying process is included in the dry mass and dry volume values. The mass of the evaporated water ( $M_{\text{water}}$ ) and the salt ( $M_{\text{salt}}$ ) in the sample are given by

$$M_{\text{water}} = M_{\text{wet}} - M_{\text{dry}} \quad (4)$$

and

$$M_{\text{salt}} = M_{\text{water}} [s/(1-s)], \quad (5)$$

where  $s$  = assumed saltwater salinity (0.035) corresponding to a pore water density ( $\rho_{\text{pw}}$ ) of 1.024 g/cm<sup>3</sup> and a salt density ( $\rho_{\text{salt}}$ ) of 2.2 g/cm<sup>3</sup>. The corrected mass of pore water ( $M_{\text{pw}}$ ), volume of pore water ( $V_{\text{pw}}$ ), mass of solids excluding salt ( $M_{\text{solid}}$ ), volume of salt ( $V_{\text{salt}}$ ), volume of solids excluding salt ( $V_{\text{solid}}$ ), and wet volume ( $V_{\text{wet}}$ ) are, respectively,

$$M_{\text{pw}} = M_{\text{water}} + M_{\text{salt}} = M_{\text{water}}/(1-s), \quad (6)$$

$$V_{\text{pw}} = M_{\text{pw}}/\rho_{\text{pw}} \quad (7)$$

$$M_{\text{solid}} = M_{\text{dry}} - M_{\text{salt}} \quad (8)$$

$$V_{\text{salt}} = M_{\text{salt}}/\rho_{\text{salt}} \quad (9)$$

$$V_{\text{solid}} = V_{\text{dry}} - V_{\text{salt}} = V_{\text{dry}} - M_{\text{salt}}/\rho_{\text{salt}} \quad (10)$$

and

$$V_{\text{wet}} = V_{\text{solid}} + V_{\text{pw}} \quad (11)$$

### Calculation of bulk properties

For all sediment samples, water content ( $w$ ) is expressed as the ratio of the mass of pore water to the wet sediment (total) mass:

$$w = M_{\text{pw}}/M_{\text{wet}} \quad (12)$$

Wet bulk density ( $\rho_{\text{wet}}$ ), dry bulk density ( $\rho_{\text{dry}}$ ), sediment grain (solid) density ( $\rho_{\text{solid}}$ ), and porosity ( $\phi$ ) are calculated from, respectively,

$$\rho_{\text{wet}} = M_{\text{wet}}/V_{\text{wet}} \quad (13)$$

$$\rho_{\text{dry}} = M_{\text{solid}}/V_{\text{wet}} \quad (14)$$

$$\rho_{\text{solid}} = M_{\text{solid}}/V_{\text{solid}} \quad (15)$$

and

$$\phi = V_{\text{pw}}/V_{\text{wet}} \quad (16)$$

### Velocity

For sediment sections, velocity determinations in the x-, y-, and z-directions were made using the Hamilton frame PWS3 contact probe system. Using this system, *P*-wave velocities were generally measured at a frequency of once per section on all cores except where changes in lithology required extra measurements. Hard rock samples were taken every section where there was sufficient oriented core. Sample preparation included cutting cubes with flat and parallel sides, followed by sanding and polishing

the cubes to ensure good contact between sample and transducer, placing the samples in an ultrasonic bath to remove the polishing grit, and, finally, resaturating the samples under vacuum in a seawater bath for at least 2 h. The compressional wave velocity calculation is based on the accurate measurement of the delay time of a 500 kHz square wave signal traveling between a pair of piezoelectric transducers. The transducer pair for PWS3 is adjusted to the thickness of the half core or discrete sample. The separation between the fixed lower PWS3 transducer and the movable upper transducer is measured by a linear voltage displacement transducer. Deionized water was added to the contact between the transducers and sample to improve acoustic coupling. The core temperature was recorded at the time velocity was measured; however, the velocity data stored in the Janus database are uncorrected for in situ temperature and pressure. These corrections can be made using the relationships outlined in Wyllie et al. (1956), Wilson (1960), and Mackenzie (1981).

### Shear strength

Sediment shear strength, or shear resistance, is an important aspect of slope stability. However, shear strength values measured at sea provide information only on the relative strength profile. For clay-rich marine sediments, the stress-strain behavior is greatly dependent upon the stress history of the sample. The stress history can be estimated in a semiquantitative way by the ratio of measured shear strength ( $s_u$ ) to in situ overburden stress,  $\sigma_{ov}$ :

$$h = s_u/\sigma_{ov} \quad (17)$$

For normally consolidated, fine-grained, cohesive soils,  $h$  has a value of ~0.25. Larger values indicate overconsolidation; smaller values indicate underconsolidation. Marine sediments are typically overconsolidated in the uppermost few to several meters and lightly or strongly underconsolidated in the next 100–200 m and deeper.

Direct shear and triaxial tests are the most common laboratory shear strength tests. Additional special tests are for direct simple shear, ring shear, plain strain, and true triaxial test. These tests allow independent control and measurement of at least the principal stresses,  $\sigma_1$  and  $\sigma_3$ , and changes in void ratio and pore pressure. The results can be analyzed by a  $\sigma$ - $\tau$  diagram (Mohr circle), a  $p$ - $q$  diagram (stress path), or other methods (e.g., Lambe and Whitman, 1979; Holtz and Kovacs, 1981).

IODP provides two rapid and simple tests that can be applied at sea, the vane shear test and the penetrometer test. These tests should be used only as a guide because they provide rough estimates of sediment

properties (e.g., Lambe and Whitman, 1979). Particularly, the influence of pore pressure changes during the undrained experiment cannot be estimated. More sophisticated tests must be performed in a shore-based laboratory.

Undrained shear strength is determined using a vane shear instrument that is inserted into soft sediment and rotated until the sediment fails. The torque,  $T$ , required to shear the sediment along the vertical and horizontal edges of the vane is a relatively direct measure of the shear strength. It must be normalized to the vane constant,  $K$ , which is a function of the vane size and geometry:

$$\tau_f \sim s_u = T/K, \quad (18)$$

where  $\tau_f$  is shear strength and  $s_u$  is a common notation for the vane shear strength (e.g., Lambe and Whitman, 1979). Shear strength has the units of pascals (= Newtons per square meter [N/m<sup>2</sup>]), torque has the units of Newton-meters (N·m), and  $K$  has the units of cubic meters (m<sup>3</sup>). The handheld Torvane instrument used during Expedition 301 returns a measure of shear strength from calibrated springs.

The penetrometer is a flat-footed, cylindrical probe that is pushed 6.4 mm deep below the split-core surface. The resulting resistance is the unconfined compressive strength of  $2s_u$ . The mechanical scale is in units of kilogram per square centimeter (kg/cm<sup>2</sup>), which are converted to units of kilopascals by

$$2\tau_f \text{ (kPa)} = 98.1 \times 2\tau_f \text{ (kg/cm}^2\text{)}. \quad (19)$$

The maximum  $\tau_f$  that can be measured with the pocket penetrometer is 220 kPa.

## Thermal experiments

The Expedition 301 downhole measurements program included several thermal tools. These tools are used to determine heat flow within sediments and to assess the thermal state of the borehole. Measurements within sediments should provide an indication of predrilling thermal conditions because the temperature tools penetrate ahead of the bit into undisturbed material. In contrast, measurements in boreholes can be strongly influenced by drilling operations, particularly if made soon after drilling. Borehole thermal data in basement are potentially useful, nevertheless, because they can indicate formation intervals that are likely to be hydrogeologically active. Data collected postdrilling from CORK observatories will be more useful for determining predisturbance thermal conditions in basement.

Estimation of heat flow also requires determination of formation thermal conductivity. Methods used during Expedition 301 for measuring thermal con-

ductivity are described in “[Thermal conductivity](#)” in “Physical Properties.”

## Thermal tools

The APC temperature (APCT) coring shoe allows collection of temperature data without a separate tool run because the sensor and data logger are incorporated into the APC coring system. Details regarding operation and interpretation of this instrument are given in Shipboard Scientific Party (1992b).

The Davis-Villinger Temperature Probe (DVTP) requires a dedicated tool run on the coring line but can be run in sediments that are too lithified to provide good APCT tool data. A description of DVTP operation and data interpretation is provided in Davis et al. (1997).

## Packer experiments

A drill string packer was used during Expedition 301 to isolate and test the hydrological properties of basement sections at Site U1301. In summary, the method involves (1) activating inflatable elements of the packer to isolate the formation to be tested; (2) using the rig pumps to pump seawater into the isolated formation in a controlled fashion, either as short (<1 min) pressure impulses for “slug tests” or at a constant rate for “injection tests” lasting tens of minutes; and (3) recording the pressure response in the isolated zone and at the rig floor. The pressure records can be interpreted to estimate average or “bulk” permeability of the isolated zone close to the borehole. In greater detail, the tools and methods employed were similar to those developed and applied during ODP, especially as described for Leg 139 (Shipboard Scientific Party, 1992b) and Leg 168 (Appendix of Becker and Fisher, 2000).

## Wireline logging

The wireline logging program planned for Expedition 301 was specifically designed for assessing basement alteration, fine-scale lithostratigraphy, and fracture distribution; crustal layering, seismic velocity, and velocity anisotropy; and vertical and near-hole permeability distribution. Individual logging tools are joined together into tool strings to make several measurements during each logging run. The tool strings are lowered to the bottom of the borehole on a wireline, and data are logged as the tool string is pulled back up the hole. Repeat runs are made to improve coverage and confirm the accuracy of logging data.

## Logging tools and tool strings

During Expedition 301, the following logging strings were deployed (Fig. F16; Table T23):

- The triple combination (triple combo) string, which consists of the Hostile Environment Gamma Ray Sonde (HNGS), the Accelerator Porosity Sonde (APS), the Hostile Environment Litho-Density Sonde (HLDS), and the SlimXtreme Array Induction Tool (QAIT);
- The Formation MicroScanner (FMS)-sonic tool string, which consists of the Dipole Sonic Imager (DSI), the Scintillation Gamma Ray Tool (SGT); the General Purpose Inclinator Tool (GPIT), and the FMS;
- The Ultrasonic Borehole Imager (UBI) tool string, consisting of the SGT, the GPIT, and the UBI; and
- The Well Seismic Tool (WST).

## Principles and uses of the logging tools

The properties measured by each tool, sampling intervals, and vertical resolutions are summarized in Table T23. Explanations of tool name acronyms and their measurement units are summarized in Table T24. More detailed descriptions of individual logging tools and their geological applications can be found in Ellis (1987), Goldberg (1997), Rider (1996), Schlumberger (1989, 1994), Serra (1984, 1986, 1989), and the Lamont-Doherty Earth Observatory–Borehole Research Group (LDEO-BRG) Wireline Logging Services Guide (2001).

### SlimXtreme Array Induction Tool

Expedition 301 marks the first deployment in scientific ocean drilling of the QAIT, which is the slim and high-pressure/high-temperature version in the series of Schlumberger array induction tools. The QAIT features an outside diameter of 3 inches, is rated for operations in environments up to 260°C (500°F), and is pressure rated to 30,000 psi. The QAIT's cartridge and sonde weigh 500 lb. This sonde contains eight mutually balanced induction arrays, with spacings ranging from several inches to several feet. A single transmitter operates at one unique frequency (26.3 kHz). Thus, signal components are measured for each array at one frequency, providing 16 raw conductivity measurements acquired at 3 inch depth intervals.

As with other induction tools, primary calibration is done with a set of test loops. The QAIT continuously autocalibrates the tool while logging to minimize sensitivity changes with temperature. The 16-array conductivity measurements are corrected for borehole diameter and combined using functions that

are weighted in both the radial and depth directions to produce a set of five logs. The logs have closely matched vertical resolution and median depths of investigation of 10, 20, 30, 60, and 90 inches from the center of the borehole.

Response functions are used to radially deconvolve the set of matched vertical resolution logs to produce a detailed record of the radial conductivity. This data can, in turn, be transformed into a number of computed color-coded images and discrete value log curves.

The QAIT provides the following list of major measurements:

- Five basic log resistivity curves with a median radial depth of investigation of 10, 20, 30, 60, and 90 inches;
- The basic log set with a 1, 2, and 4 ft vertical resolution;
- Flushed zone resistivity ( $R_{xo}$ ), which can be used for determining water saturation ( $S_w$ ) if porosity is known;
- Model-independent resistivity and two-dimensional quantitative imaging of formation ( $R_{wa}$  images);
- Model-dependent water saturation ( $S_w$ );
- Analog spontaneous potential log or a measure of the natural difference in electrical potential, in millivolts, between an electrode in the borehole and a fixed reference electrode on the surface; and
- Volume of mud filtrate estimation.

## Logging data flow and processing

Data for each wireline logging run were recorded, stored digitally, and monitored in real time using the Schlumberger multitask, acquisition, and imaging system (MAXIS) 500 system located in the new Off-shore Service Unit-F-model Modular Configuration MAXIS Electrical Capstan Capable (OSU-FMEC) winch unit. The OSU-FMEC is a full backup system to the main MAXIS 500 system commonly used during logging operations. During Expedition 301, the OSU-FMEC unit was used as the primary acquisition system because we were using new winch and heave compensator units that were at the same location (Fig. F17). Training and supervision of winch operators with the new system took place during deployments of the logging tools and the CORK remotely operated vehicle platforms.

The new heave compensation system is one of a kind and compensates via a hydraulic pump, which controls the motion of the wireline drum. The data are processed in the acquisition system and correlated

with the compensated depth. The compensated distance measured in the winch control is applied to the acquisition system, and the measured depth is then corrected. This system also uses data from surface three-axis accelerometers to correct for tool motion at the drum. Ultrasonic transducers measure the radius of the drum to calculate tangential velocity and to get an estimate of the tool speed downhole.

After logging was completed in each hole, data were transferred to the shipboard downhole measurements laboratory for preliminary processing and interpretation. FMS image data were interpreted using Schlumberger's Geoframe (version 4.0.4.1) software package. Logging data were also transmitted to IODP-USIO Science Services, LDEO, using a satellite high-speed data link for processing soon after each hole was logged. Data processing at LDEO consists of (1) depth-shifting all logs relative to a common datum (i.e., in mbsf), (2) corrections specific to individual tools, and (3) quality control and rejection of unrealistic or spurious values. Once processed at LDEO, logging data were transmitted back to the ship, providing near-real time data processing. Processed data were then replotted on board (see **"Wireline logging"** in the "Site U1301" chapter). Postcruise-processed data in ASCII format are available directly from the IODP-USIO Science Services LDEO Web site at [iodp.ldeo.columbia.edu/DATA/IODP/index.html](http://iodp.ldeo.columbia.edu/DATA/IODP/index.html). A summary of "logging highlights" is posted on the LDEO Web site at the end of each expedition.

### Wireline logging data quality

Logging data quality may be seriously degraded by changes in the hole diameter and in sections where the borehole diameter greatly decreases or is washed out. Deep-investigation measurements such as resistivity and sonic velocity are least sensitive to borehole conditions. Nuclear measurements (density and neutron porosity) are more sensitive because of their shallower depth of investigation and the effect of drilling fluid volume on neutron and gamma ray attenuation. Corrections can be applied to the original data in order to reduce these effects. HNGS and SGT data provide a depth correlation between logging runs. Logs from different tool strings may, however, still have depth mismatches caused by either cable stretch or ship heave during recording. FMS, DSI, and UBI data acquired during Expedition 301 were seriously degraded because of poor performance by the new wireline heave compensation software system (see **"Wireline logging"** in the "Site U1301" chapter).

## References

- ASTM, 1990. Standard method for laboratory determination of water (moisture) content of soil and rock. In *Annual Book of ASTM Standards for Soil and Rock* (Vol. 04.08): Philadelphia (Am. Soc. Testing and Mater.), D2216-90 (revision of D2216-63, D2216-80).
- Bach, W., Erzinger, J., Alt, J.C., and Teagle, D.A.H., 1996. Chemistry of the lower sheeted dike complex, Hole 504B (Leg 148): influence of magmatic differentiation and hydrothermal alteration. In Alt, J.C., Kinoshita, H., Stokking, L.B., and Michael, P.J. (Eds.), *Proc. ODP, Sci. Results*, 148: College Station, TX (Ocean Drilling Program), 39–55.
- Bale, S.J., Goodman, K., Rochelle, P.A., Marchesi, J.R., Fry, J.C., Weightman, A.J., and Parkes, R.J., 1997. *Desulfovibrio profundus* sp. nov., a novel barophilic sulfate-reducing bacterium from deep sediment layers in the Japan Sea. *Int. J. Syst. Bacteriol.*, 47:515–521.
- Becker, K., and Fisher, A.T., 2000. Permeability of upper oceanic basement on the eastern flank of the Juan de Fuca Ridge determined with drill-string packer experiments. *J. Geophys. Res.*, 105:897–912. doi:10.1029/1999JB900250
- Berggren, W.A., Kent, D.V., Swisher, C.C., III, and Aubry, M.-P., 1995. A revised Cenozoic geochronology and chronostratigraphy. In Berggren, W.A., Kent, D.V., Aubry, M.-P., and Hardenbol, J. (Eds.), *Geochronology, Time Scales and Global Stratigraphic Correlation*. Spec. Publ.—SEPM (Soc. Sediment. Geol.), 54:129–212.
- Blum, P., 1997. Physical properties handbook: a guide to the shipboard measurement of physical properties of deep-sea cores. *ODP Tech. Note*, 26 [Online]. Available from World Wide Web: <<http://www-odp.tamu.edu/publications/tnotes/tn26/INDEX.HTM>>.
- Bobrow, M.N., Harris, T.D., Shaughnessy, K.J., and Litt, G.J., 1989. Catalyzed reporter deposition, a novel method of signal amplification application to immunoassays. *J. Immunol. Methods*, 125:279–285. doi:10.1016/0022-1759(89)90104-X
- Cande, S.C., and Kent, D.V., 1995. Revised calibration of the geomagnetic polarity timescale for the Late Cretaceous and Cenozoic. *J. Geophys. Res.*, 100:6093–6095. doi:10.1029/94JB03098
- Cowen, J.P., Giovannoni, S.J., Kenig, F., Johnson, H.P., Butterfield, D., Rappé, M.S., Hutnak, M., and Lam, P., 2003. Fluids from aging ocean crust that support microbial life. *Science*, 299:120–123. doi:10.1126/science.1075653
- D'Hondt, S., Jørgensen, B.B., Miller, D.J., Blake, R., Cragg, B.A., Dickens, G.R., Ferdelman, T., Hinrichs, K.-U., Holm, N.G., Mitterer, R., Spivack, A., Bekins, B., Ford, K., Gettemy, G., Skilbeck, C.G., Aiello, I.W., Cypionka, H., Guerin, G., House, C., Inagaki, F., Meister, P., Naehr, T., Niitsuma, S., Parkes, R.J., Schippers, A., Smith, D.C., Teske, A., Wiegel, J., Padilla, C.N., Acosta, J.L.S., Wang, G., and Rutherford, S.D., 2004. Distribution of metabolic activities in deep seafloor sediments. *Science*, 306(5705):2216–2221. doi:10.1126/science.1101155



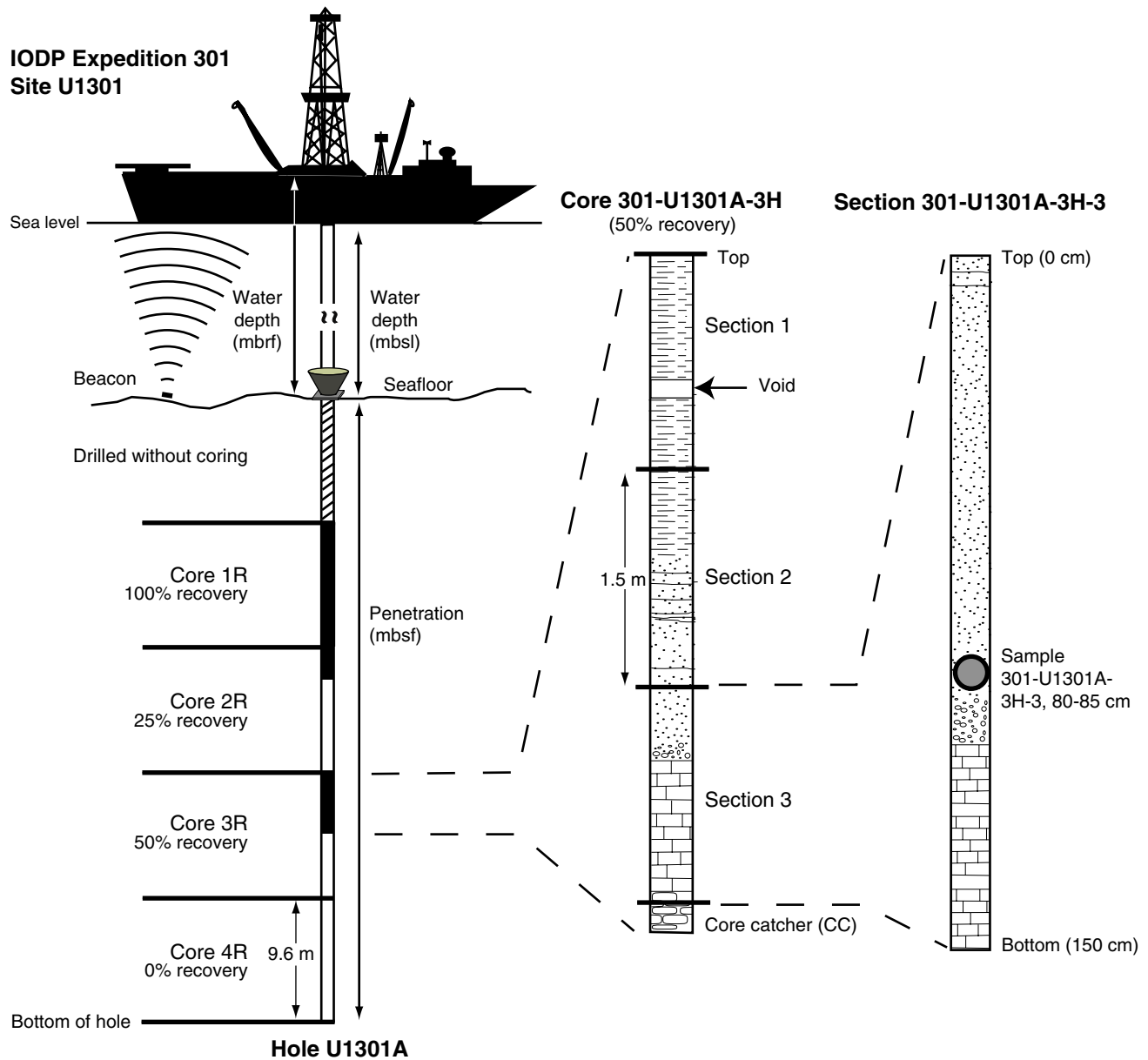
- D'Hondt, S., Rutherford, S., and Spivack, A.J., 2002. Metabolic activity of subsurface life in deep-sea sediments. *Science*, 295:2067–2070. doi:10.1126/science.1064878
- Davis, E.E., Villinger, H., MacDonald, R.D., Meldrum, R.D., and Grigel, J., 1997. A robust rapid-response probe for measuring bottom-hole temperatures in deep-ocean boreholes. *Mar. Geophys. Res.*, 19:267–281. doi:10.1023/A:1004292930361
- Droser, M.L., and Bottjer, D.J., 1986. A semiquantitative field classification of ichnofabric. *J. Sediment. Petrol.*, 56:558–559.
- Duan, Z., Møller, N., Greenberg, J., and Weare, J.H., 1992. The prediction of methane solubility in natural waters to high ionic strengths from 0 to 250°C and from 0 to 1600 bar. *Geochim. Cosmochim. Acta*, 56:1451–1460. doi:10.1016/0016-7037(92)90215-5
- Ellis, D.V., 1987. *Well Logging for Earth Scientists*: New York (Elsevier).
- Evans, H.B., 1965. GRAPE—a device for continuous determination of material density and porosity. *Trans. SPWLA 6th Ann. Logging Symp.*: Dallas, 2:B1–B25.
- Fisher, A.T., Davis, E.E., Hutnak, M., Spiess, V., Zühlsdorff, L., Cherkaoui, A., Christiansen, L., Edwards, K.M., MacDonald, R., Villinger, H., Mottl, M.J., Wheat, C.G., and Becker, K., 2003. Hydrothermal recharge and discharge across 50 km guided by seamounts on a young ridge flank. *Nature (London, U. K.)*, 421:618–621. doi:10.1038/nature01352
- Fisk, M.R., Giovannoni, S.J., and Thorseth, I.H., 1998. Alteration of oceanic volcanic glass: textural evidence of microbial activity. *Science*, 281:978–980. doi:10.1126/science.281.5379.978
- Fry, J.C., 1988. Determination of biomass. In Austin, B. (Ed.), *Methods in Aquatic Bacteriology*: Chichester (Wiley), 27–72.
- Gieskes, J.M., Gamo, T., and Brumsack, H., 1991. Chemical methods for interstitial water analysis aboard JOIDES Resolution. *ODP Tech. Note*, 15 [Online]. Available from World Wide Web: <[http://www-odp.tamu.edu/publications/tnotes/tn15/f\\_chem1.htm](http://www-odp.tamu.edu/publications/tnotes/tn15/f_chem1.htm)>.
- Goldberg, D., 1997. The role of downhole measurements in marine geology and geophysics. *Rev. Geophys.*, 35:315–342. doi:10.1029/97RG00221
- Holtz, R.D., and Kovacs, W.D., 1981. *An Introduction to Geotechnical Engineering*: Englewood Cliffs, NJ (Prentice-Hall).
- Hoppie, B.W., Blum, P., and the Shipboard Scientific Party, 1994. Natural gamma-ray measurements on ODP cores: introduction to procedures with examples from Leg 150. In Mountain, G.S., Miller, K.G., Blum, P., et al., *Proc. ODP, Init. Repts.*, 150: College Station, TX (Ocean Drilling Program), 51–59.
- Inagaki, F., Takai, K., Komatsu, T., Kanamatsu, T., Fujioka, K., and Horikoshi, K., 2001. Archaeology of Archaea: geomicrobiological record of Pleistocene thermal events concealed in a deep-sea seafloor environment. *Extremophiles*, 5:385–392. doi:10.1007/s007920100211
- Inagaki, F., Sakihama, Y., Inoue, A., Kato, C., and Horikoshi, K., 2002. Molecular phylogenetic analyses of reverse-transcribed bacterial rRNA obtained from deep-sea cold seep sediments. *Environ. Microbiol.*, 4:277–286. doi:10.1046/j.1462-2920.2002.00294.x
- Inagaki, F., Suzuki, M., Takai, K., Oida, H., Sakamoto, T., Aoki, K., Nealson, K.H., and Horikoshi, K., 2003. Microbial communities associated with geological horizons in coastal seafloor sediments from the sea of Okhotsk. *Appl. Environ. Microbiol.*, 69:7224–7235. doi:10.1128/AEM.69.12.7224-7235.2003
- Inagaki, F., Okada, H., Tsapin, A.I., and Nealson, K.H., 2005. Microbial Survival: the paleome: a sedimentary genetic record of past microbial communities. *Astrobiology*, 5(2):141–153. doi:10.1089/ast.2005.5.141
- Keene, J.B., 1975. Cherts and porcellanites from the North Pacific DSDP, Leg 32. In Larson, R.L., Moberly, R., et al. *Init. Repts. DSDP*, 32: Washington (U.S. Govt. Printing Office), 429–507.
- Kormas, K.A., Smith, D.C., Edgcomb, V., and Teske, A., 2003. Molecular analysis of deep subsurface microbial communities in Nankai Trough sediments (ODP Leg 190, Site 1176). *FEMS Microbiol. Ecol.*, 45:115–125. doi:10.1016/S0168-6496(03)00128-4
- Kvenvolden, K.A., and McDonald, T.J., 1986. Organic geochemistry on the JOIDES Resolution—an assay. *ODP Tech. Note*, 6.
- Lambe, T.W., and Whitman, R.V., 1979. *Soil Mechanics* (SI ver.): New York (Wiley).
- Lamont-Doherty Earth Observatory–Borehole Research Group, 2001. *Wireline Logging Services Guide* [Online]. Available from World Wide Web: <<http://www.ldeo.columbia.edu/BRG/ODP/LOGGING/>>.
- Mackenzie, K.V., 1981. Nine-term equation for sound speed in the oceans. *J. Acoust. Soc. Am.*, 70:807–812.
- Manheim, F.T., and Sayles, F.L., 1974. Composition and origin of interstitial waters of marine sediments, based on deep sea drill cores. In Goldberg, E.D. (Ed.), *The Sea* (Vol. 5): *Marine Chemistry: The Sedimentary Cycle*: New York (Wiley), 527–568.
- Marchesi, J.R., Weightman, A.J., Cragg, B.A., Parkes, R.J., and Fry, J.C., 2001. Methanogen and bacterial diversity and distribution in deep gas hydrate sediments from the Cascadia margin as revealed by 16S rRNA molecular analysis. *FEMS Microbiol. Ecol.*, 34:221–228. doi:10.1016/S0168-6496(00)00099-4
- Mazzullo, J.M., Meyer, A., and Kidd, R.B., 1988. New sediment classification scheme for the Ocean Drilling Program. In Mazzullo, J.M., and Graham, A.G. (Eds.), *Handbook for shipboard sedimentologists. ODP Tech. Note*, 8:45–67.
- Mikucki, J.A., Liu, Y., Delwiche, M., Colwell, F.S., and Boone, D.R., 2003. Isolation of a methanogen from deep marine sediments that contain methane hydrates, and description of *Methanoculleus submarinus* sp. nov. *Appl. Environ. Microbiol.*, 69:3311–3316.
- Murray, R.W., Miller, D.J., and Kryc, K.A., 2000. Analysis of major and trace elements in rocks, sediments, and interstitial waters by inductively coupled plasma–atomic emission spectrometry (ICP–AES). *ODP Tech. Note*, 29 [Online]. Available from World Wide Web: <<http://www-odp.tamu.edu/publications/tnotes/tn29/INDEX.HTM>>.

- Muyzer, G., and Smalla, K., 1998. Application of denaturing gradient gel electrophoresis (DGGE) and temperature gradient electrophoresis (TGGE) in microbial ecology. *Antonie van Leeuwenhoek*, 73:127–141. doi:10.1023/A:1000669317571
- Newberry, C.J., Webster, G., Cragg, B.A., Parkes, R.J., Weightman, A.J., and Fry, J.C., 2004. Diversity of prokaryotes and methanogenesis in deep subsurface sediments from the Nankai Trough, Ocean Drilling Program Leg 190. *Environ. Microbiol.*, 6:274–287. doi:10.1111/j.1462-2920.2004.00568.x
- Parkes, R.J., Cragg, B.A., Bale, S.J., Getliff, J.M., Goodman, K., Rochelle, P.A., Fry, J.C., Weightman, A.J., and Harvey, S.M., 1994. Deep bacterial biosphere in Pacific Ocean sediments. *Nature (London, U. K.)*, 371:410–413. doi:10.1038/371410a0
- Parkes, R.J., Cragg, B.A., and Wellsbury, P., 2000. Recent studies on bacterial populations and processes in marine sediments: a review. *Hydrogeol. Rev.*, 8:11–28.
- Passchier, C.W., and Trouw, R.A.J., 1996. *Microtectonics*: Berlin (Springer-Verlag).
- Pernthaler, A., Pernthaler, J., and Amman, R., 2002. Fluorescence in situ hybridization and catalyzed reporter deposition for the identification of marine bacteria. *Appl. Environ. Microbiol.* 68:3094–3101. doi:10.1128/AEM.68.6.3094-3101.2002
- Ramsay, J.G., and Huber, M.I., 1987. *The Techniques of Modern Structural Geology (Vol. 2): Folds and Fractures*: New York (Acad. Press).
- Reed, D.W., Fujita, Y., Delwiche, M.E., Blackwelder, D.B., Sheridan, P.P., Uchida, T., and Colwell, F.S. 2002. Microbial communities from methane hydrate-bearing deep marine sediments in a forearc basin. *Appl. Environ. Microbiol.*, 68:3759–3770. doi:10.1128/AEM.68.8.3759-3770.2002
- Rider, M.H., 1996. *The Geological Interpretation of Well Logs (2nd ed.)*: Caithness (Whittles Publishing).
- Rock-Color Chart Committee, 1991. *Rock Color Charts*. Geol. Soc. Am.
- Schlumberger, 1989. *Log Interpretation Principles/Applications*: Houston (Schlumberger Educ. Services), SMP-7017.
- Schlumberger, 1994. *Log Interpretation Charts*: Sugarland, TX (Schlumberger Wireline and Testing), SMP-7006.
- Serra, O., 1984. *Fundamentals of Well-Log Interpretation (Vol. 1): The Acquisition of Logging Data*: Dev. Pet. Sci., 15A: Amsterdam (Elsevier).
- Serra, O., 1986. *Fundamentals of Well-Log Interpretation (Vol. 2): The Interpretation of Logging Data*: Dev. Pet. Sci., 15B: Amsterdam (Elsevier).
- Serra, O., 1989. *Formation MicroScanner Image Interpretation*: Houston (Schlumberger Educ. Services), SMP-7028.
- Shipboard Scientific Party, 1989. Introduction and explanatory notes. In Robinson, P.T., Von Herzen, R., et al., *Proc. ODP, Init. Repts.*, 118: College Station, TX (Ocean Drilling Program), 3–24.
- Shipboard Scientific Party, 1991. Explanatory notes. In Taira, A., Hill, I., Firth, J.V., et al., *Proc. ODP, Init. Repts.*, 131: College Station, TX (Ocean Drilling Program), 25–60.
- Shipboard Scientific Party, 1992a. Explanatory notes. In Behrmann, J.H., Lewis, S.D., Musgrave, R.J., et al., *Proc. ODP, Init. Repts.*, 141: College Station, TX (Ocean Drilling Program), 37–71.
- Shipboard Scientific Party, 1992b. Explanatory notes. In Davis, E.E., Mottl, M.J., Fisher, A.T., et al., *Proc. ODP, Init. Repts.*, 139: College Station, TX (Ocean Drilling Program), 55–97.
- Shipboard Scientific Party, 1992c. Explanatory notes. In Dick, H.J.B., Erzinger, J., Stokking, L.B., et al., *Proc. ODP, Init. Repts.*, 140: College Station, TX (Ocean Drilling Program), 5–33.
- Shipboard Scientific Party, 1992d. Explanatory notes. In Parson, L., Hawkins, J., Allan, J., et al., *Proc. ODP, Init. Repts.*, 135: College Station, TX (Ocean Drilling Program), 49–79.
- Shipboard Scientific Party, 1993a. Explanatory notes. In Alt, J.C., Kinoshita, H., Stokking, L.B., et al., *Proc. ODP, Init. Repts.*, 148: College Station, TX (Ocean Drilling Program), 5–24.
- Shipboard Scientific Party, 1993b. Explanatory notes. In Gillis, K., Mével, C., Allan, J., et al., *Proc. ODP, Init. Repts.*, 147: College Station, TX (Ocean Drilling Program), 15–42.
- Shipboard Scientific Party, 1995. Explanatory notes. In Cannat, M., Karson, J.A., Miller, D.J., et al., *Proc. ODP, Init. Repts.*, 153: College Station, TX (Ocean Drilling Program), 15–42.
- Shipboard Scientific Party, 1999. Explanatory notes. In Dick, H.J.B., Natland, J.H., Miller, D.J., et al., *Proc. ODP, Init. Repts.*, 176, 1–42 [CD-ROM]. Available from: Ocean Drilling Program, Texas A&M University, College Station, TX 77845-9547, U.S.A.
- Shipboard Scientific Party, 2003a. Explanatory notes. In D'Hondt, S.L., Jørgensen, B.B., Miller, D.J., et al., *Proc. ODP, Init. Repts.*, 201, 1–103 [CD-ROM]. Available from: Ocean Drilling Program, Texas A&M University, College Station TX 77845-9547, USA.
- Shipboard Scientific Party, 2003b. Explanatory notes. In Wilson, D.S., Teagle, D.A.H., Acton, G.D., *Proc. ODP, Init. Repts.*, 206 [Online]. Available from World Wide Web: <[http://www-odp.tamu.edu/publications/206\\_IR/chap\\_02/chap\\_02.htm](http://www-odp.tamu.edu/publications/206_IR/chap_02/chap_02.htm)>.
- Smith, D.C., Spivack, A.J., Fisk, M.R., Haveman, S.A., Staudigel, H., and ODP Leg 185 Shipboard Scientific Party, 2000. Methods for quantifying potential microbial contamination during deep ocean coring. *ODP Tech. Note*, 28 [Online]. Available from World Wide Web: <<http://www-odp.tamu.edu/publications/tnotes/tn28/INDEX.HTM>>.
- Suzuki, M.T., Taylor, L.T., and DeLong, E.F., 2000. Quantitative analysis of small-subunit rRNA genes in mixed microbial populations via 5'-nuclease assays. *Appl. Environ. Microbiol.*, 66:4605–4614. doi:10.1128/AEM.66.11.4605-4614.2000
- Takai, K., and Horikoshi, K., 2000. Rapid detection and quantification of members of the archaeal community by quantitative PCR using fluorogenic probes. *Appl.*

- Environ. Microbiol.*, 66:5066–5072. doi:10.1128/AEM.66.11.5066-5072.2000
- Twiss, R.J., and Moores, E.M., 1992. *Structural Geology*: New York (Freeman).
- Vacquier, V., 1985. The measurement of thermal conductivity of solids with a transient linear heat source on the plane surface of a poorly conducting body. *Earth Planet. Sci. Lett.*, 74:275–279. doi:10.1016/0012-821X(85)90027-5
- Von Herzen, R.P., and Maxwell, A.E., 1959. The measurement of thermal conductivity of deep-sea sediments by a needle-probe method. *J. Geophys. Res.*, 64:1557–1563.
- Wentworth, C.K., 1922. A scale of grade and class terms of clastic sediments. *J. Geol.*, 30:377–392.
- Wilson, M.S., Bakermans, C., and Madson, E.L., 1999. In situ, real-time catabolic gene expression: extraction and characterization of naphthalene dioxygenase mRNA transcripts from groundwater. *Appl. Environ. Microbiol.*, 65:80–87.
- Wilson, W.D., 1960. Speed of sound in seawater as a function of temperature, pressure and salinity. *J. Acoust. Soc. Am.*, 32:641–644.
- Wyllie, M.R.J., Gregory, A.R., and Gardner, L.W., 1956. Elastic wave velocities in heterogeneous and porous media. *Geophysics*, 21:41–70. doi:10.1190/1.1438217

**Publication:** 31 October 2005  
**MS 301-105**

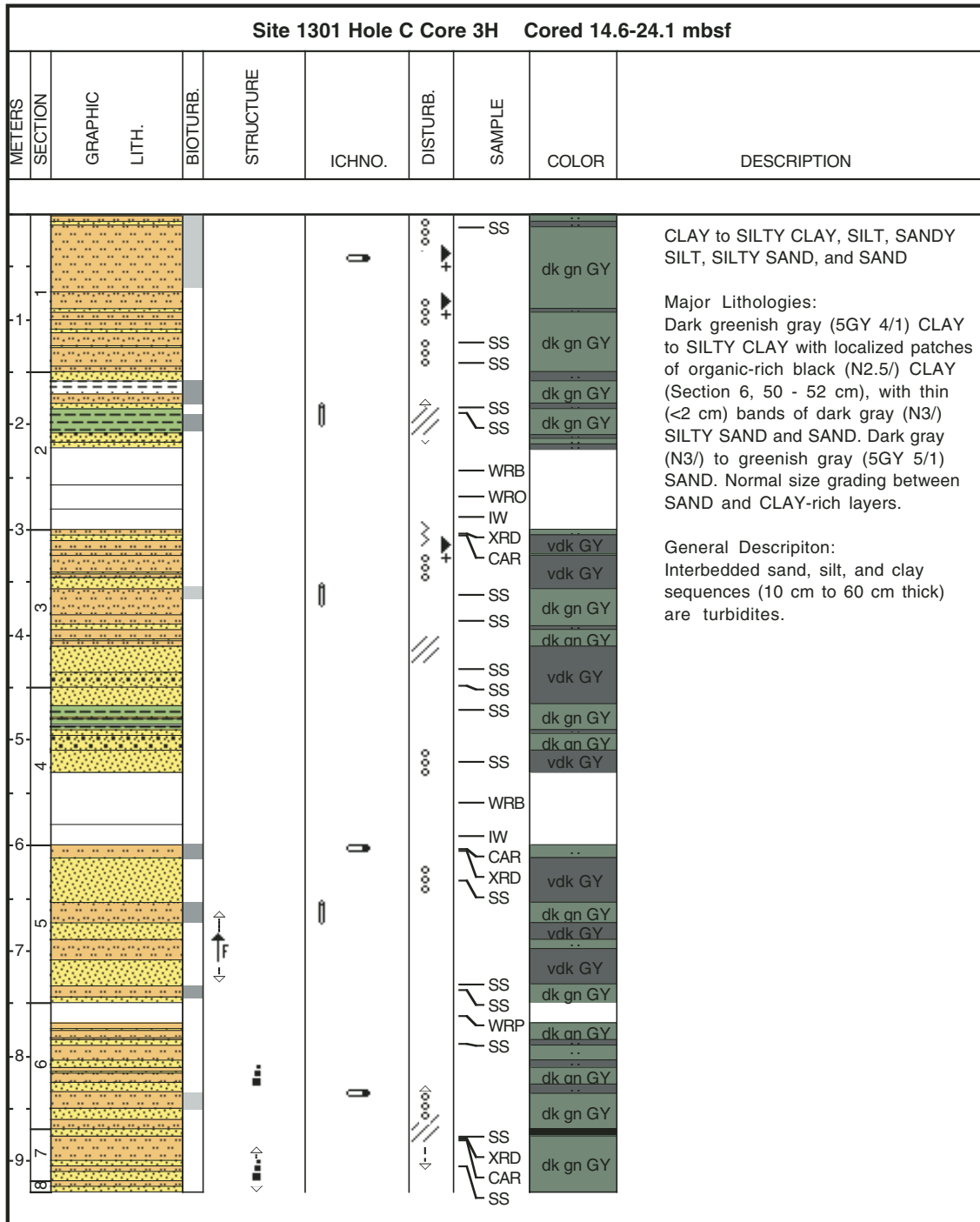
**Figure F1.** Schematic illustration of core, section, and sample numbering. mbrf = meters below rig floor, mbsl = meters below sea level, mbsf = meters below seafloor.



**Figure F2.** Grain-size divisions for sedimentary rocks (adapted from Wentworth, 1922) (Shipboard Scientific Party, 2003b; fig. F5).

Millimeters (mm)	Micrometers ( $\mu\text{m}$ )	Phi ( $\phi$ )	Wentworth size class	Rock type
4096		-12.0	Boulder	Conglomerate/ Breccia
256		-8.0	Cobble	
64		-6.0	Pebble	
4		-2.0	Granule	
2.00		-1.0		
			Very coarse sand	Sandstone
1.00		0.0	Coarse sand	
1/2	0.50	1.0	Medium sand	
1/4	0.25	2.0	Fine sand	
1/8	0.125	3.0	Very fine sand	
1/16	0.0625	4.0		Siltstone
1/32	0.031	5.0	Coarse silt	
1/64	0.0156	6.0	Medium silt	
1/128	0.0078	7.0	Fine silt	
1/256	0.0039	8.0	Very fine silt	Claystone
	0.00006	14.0	Clay	



**Figure F3.** Example of a computer-generated visual core description barrel sheet. Graphic lith. = graphic lithology, Bioturb. = bioturbation, Ichno. = ichnofossils, Disturb. = core disturbance, SS = smear slide, WRB = microbiology (whole-round), WRO = organic chemistry (whole-round), IW = pore water from whole-round samples, XRD = X-ray diffraction, CAR = carbonate analysis, WRP = physical property (whole-round) analyses, dk = dark, vdk = very dark, gn = greenish, GY = gray.









**Figure F4.** Key to symbols used in the graphic lithology column log on the computer-generated core description forms and to symbols used for contacts, physical structures, lithologic accessories, ichnofossils, fossils, core disturbance, and bioturbation on the computer-generated core description forms.

**Graphic lithology**

Siliciclastic sediments

 Gravel	 Clayey sand	 Silt or siltstone
 Clay	 Clay or claystone	 Silty clay
 Silty sand	 Sand or sandstone	 Breccia
 Sand	 Sandy silt	





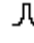


**Physical structures**

 - Graded bedding	 - Microfault (normal)	 - Pebbles/Granules/Sand
 - Fining upward	 - Column not wide enough to show second symbol	 - Breccia


**Ichnofossils**

 - <i>Planolites</i>	 - <i>Skolithos</i>
---	--

**Core disturbance**

 - Disturbed	 - Deformed	 - Biscuit
 - Soupy	 - Flow-in	 - Fractured
 - Breccia		

**Bioturbation**

 Abundant	 Rare
 Common	 Barren
 Moderate	

**Figure F5.** Example of VCD. PP = physical property analysis, TC = thermal conductivity, TSB = thin section, MB = microbiological analysis, PM = paleomagnetic analysis, ICP = hard rock geochemical analysis by ICP-AES, XRD = X-ray diffraction analysis. Tr = trace. Shaded boxes with red sample codes (e.g., MBNU) in the graphic representation column show the locations of whole-round samples removed on the core receiving table for microbiology studies. Sample codes and locations are recorded in the Janus database. For other definitions, see Figure F6.

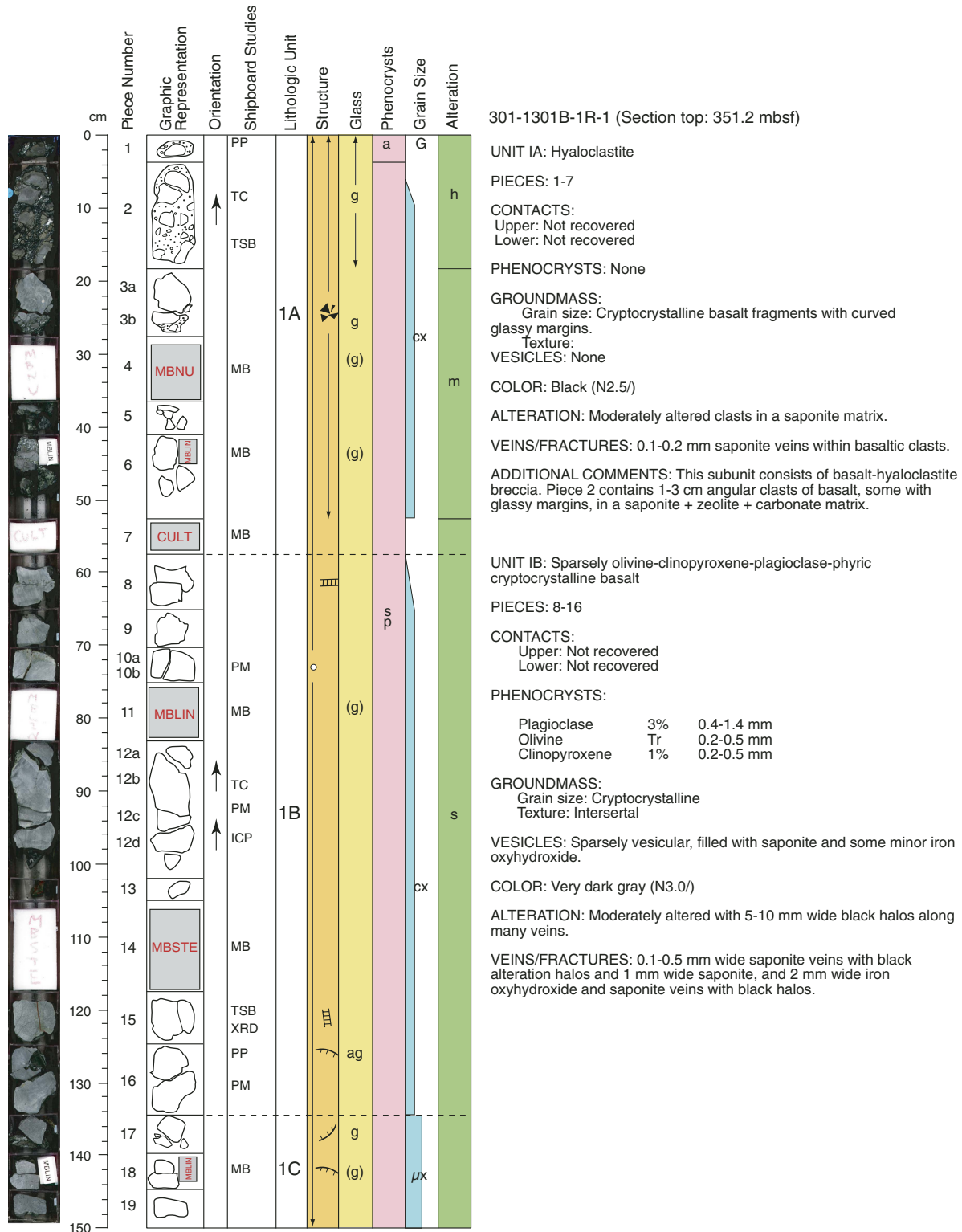




Figure F6. Key for VCD sheets.

Expedition 301 Igneous texture/structure definitions and abbreviations

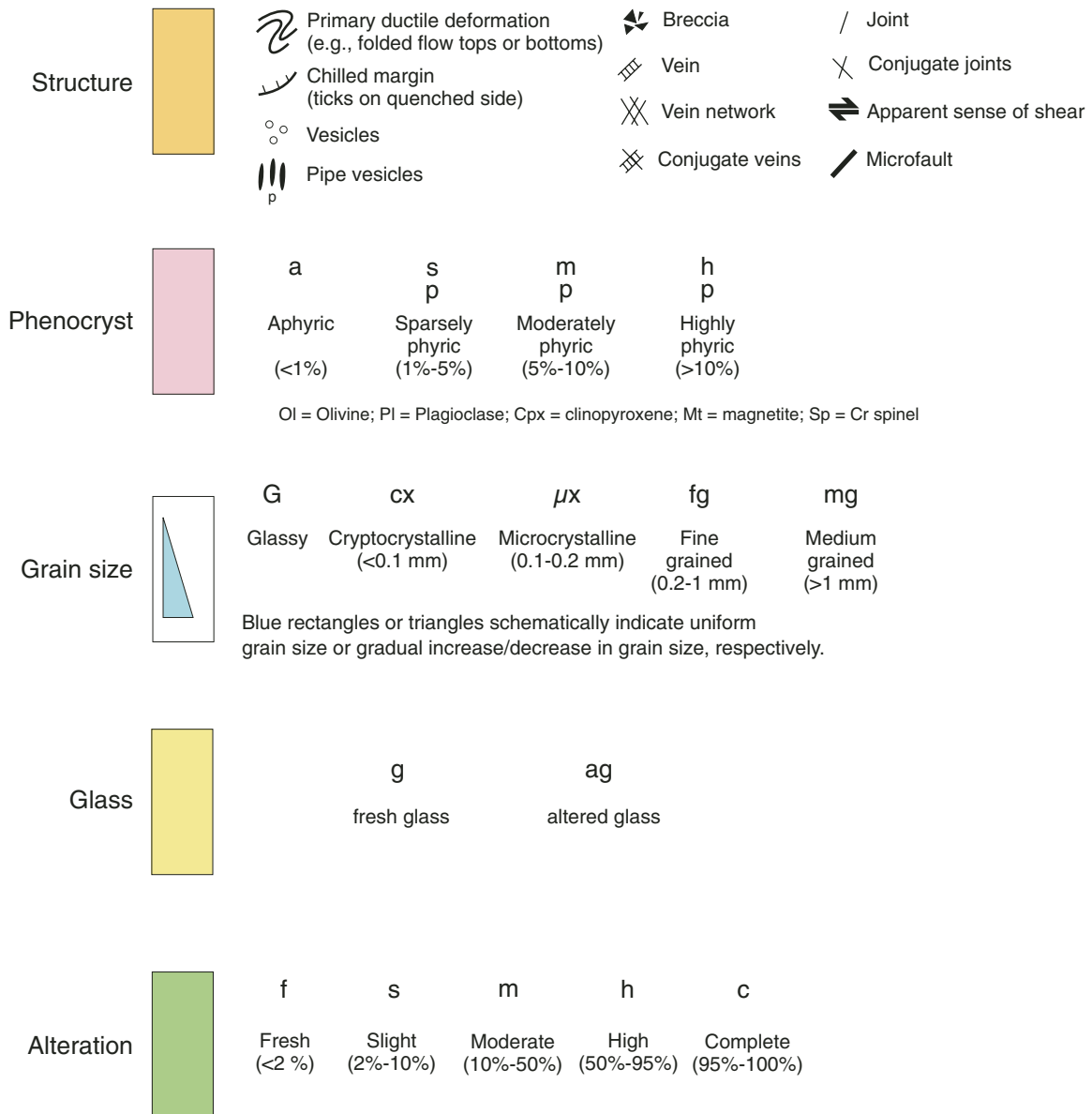
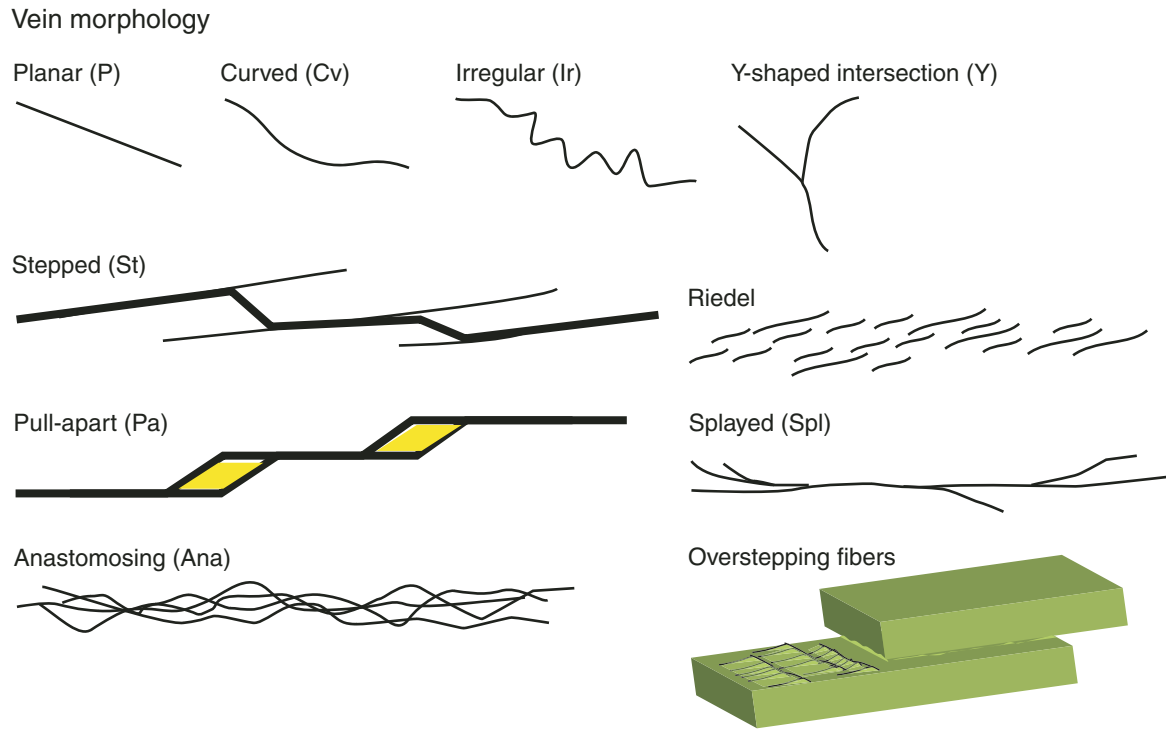


Figure F7. Example of structural description form.

### Structural Description

Leg.	Hole	Core	section	Sample No.							
301	1301b	36	1	⑦ ⑫ ⑱ ⑳							
<p>sketch</p> <div style="display: flex; justify-content: space-around;"> <div style="width: 45%;"> <p>⑦</p> <p>⑫</p> </div> <div style="width: 45%;"> <p>⑱</p> <p>⑳</p> </div> </div>											
pillow	vein no.	core length	orientation on core**		width	vein type		mineral	halo		
			strike	plane dip	(mm)				width(mm)	type	
	7-1	11	208	85	side	P	side	SP	6		
	7-2		320	73	0.2	stop	P	Fe. sp	6-8		
	12-1	9	277	77	side	P	side	SP	10		⊕
	12-2		329	32	>0.1	P	stop	Fe. sp	No		
	12-3		340	20	0.2	P		Fe. sp	?		
	18-1	14	346	83	0.3	P		Fe. sp	14		green Halo
Ⓚ	20-1		215	43	0.1	P	stop	Fe sp	No		
	20-2	10	196	82	side	P	side	Fe <sup>Fe</sup> SP	9		

Figure F8. Vein morphology examples.



**Figure F9.** Orientation conventions. Sketch of the archive half of the core showing the conventions used for measuring orientation of structural features during Expedition 301.

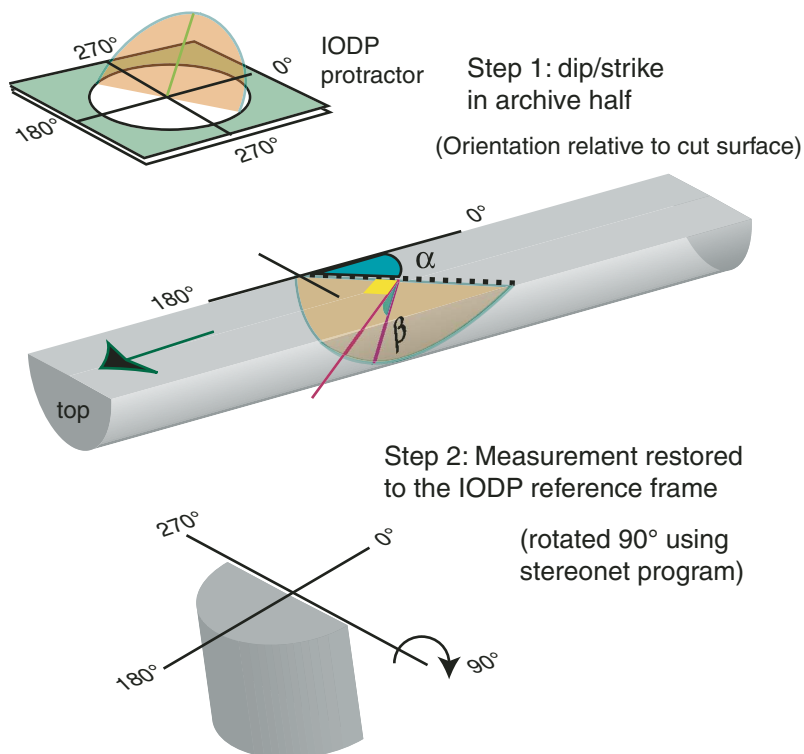


**Figure F10.** Coordinate systems for IODP cores and discrete paleomagnetic samples. **A.** The magnetic coordinates of archive- (bottom) and working-half (top) core sections. **B.** Orientation of discrete samples. Note that the double line is on the bottom of the working half (and defines the +x axis).

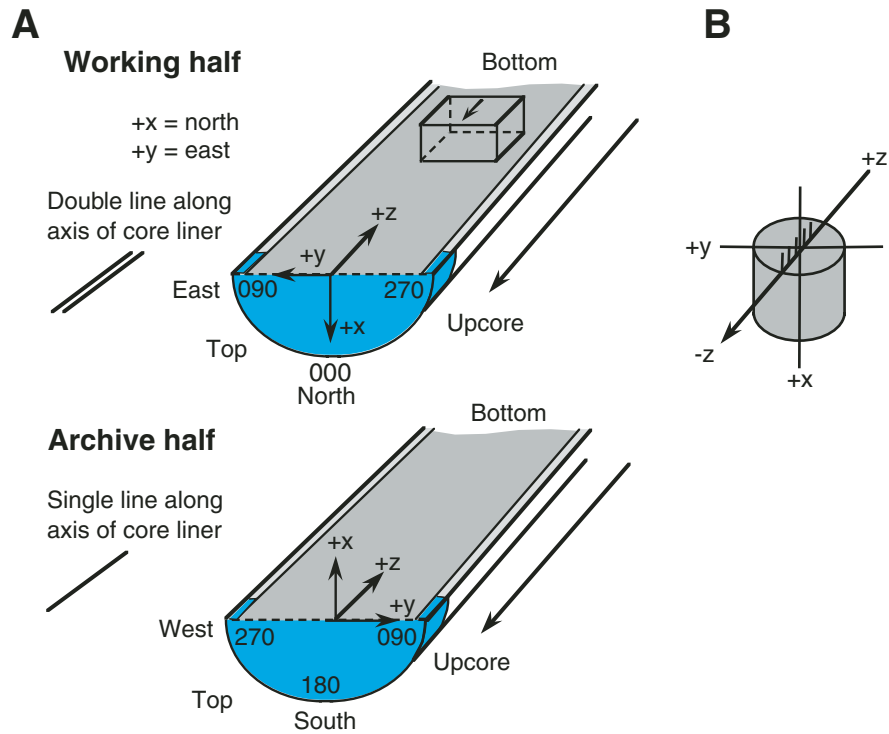


**Figure F11.** Miocene to Holocene geomagnetic polarity timescale (GPTS). In the polarity column, black = normal polarity and white = reversed polarity. Absolute ages, geologic periods, and magnetic chron terminology are shown at left. The figure is based on the Berggren et al. (1995) and Cande and Kent (1995) GPTS.

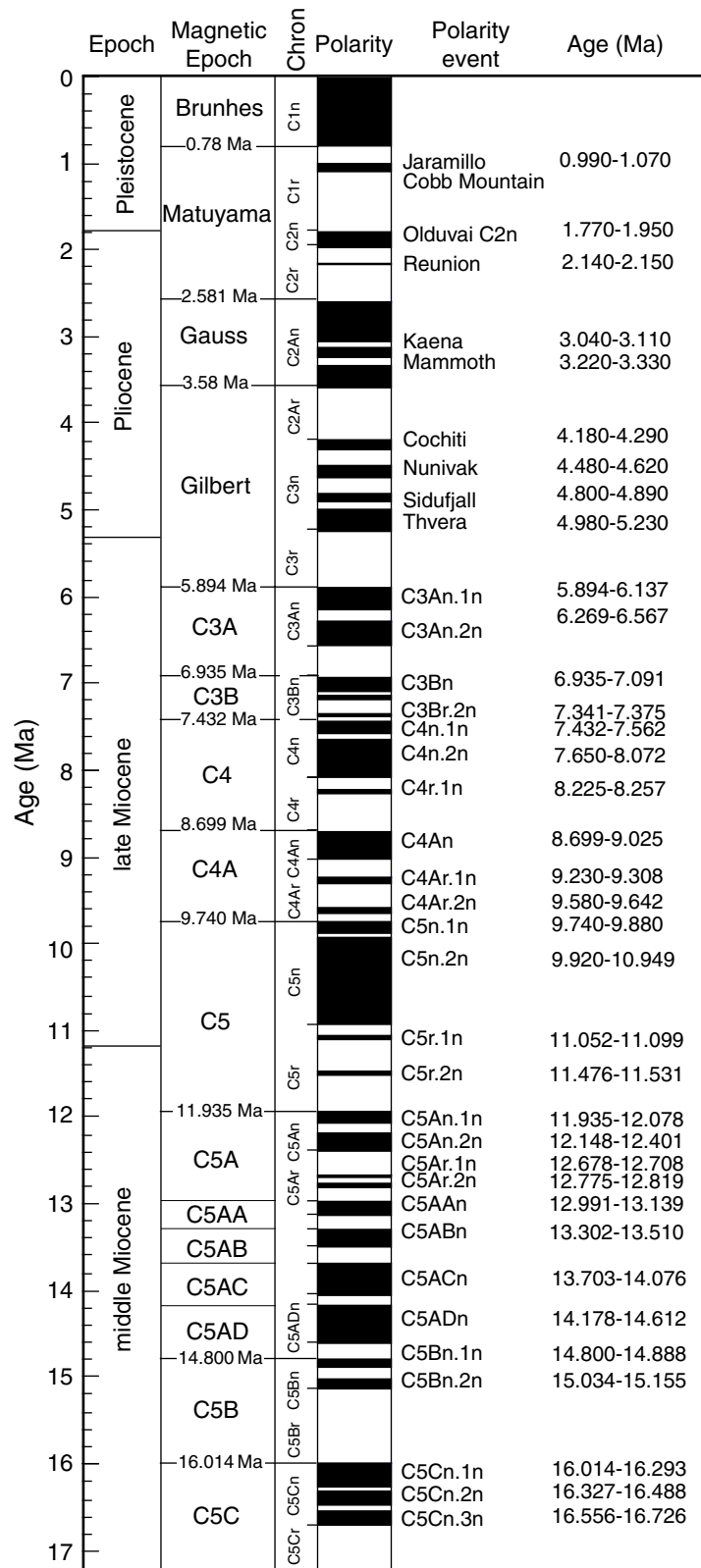


**Figure F12.** Schematic figure of microbiology (MBIO) subsampling strategy. **A.** Whole-round core sampling scheme. **B.** Aseptic subsampling from the center of whole-round samples using a tip-cutting syringe. CT = cultivation, FISH = fluorescence in situ hybridization, RNA = ribonucleic acid, DNA = deoxyribonucleic acid, RT = room temperature, AODC = acridine orange direct count, FISH-DC = FISH direct count, CARD-FISH = catalyzed reporter deposition-FISH.

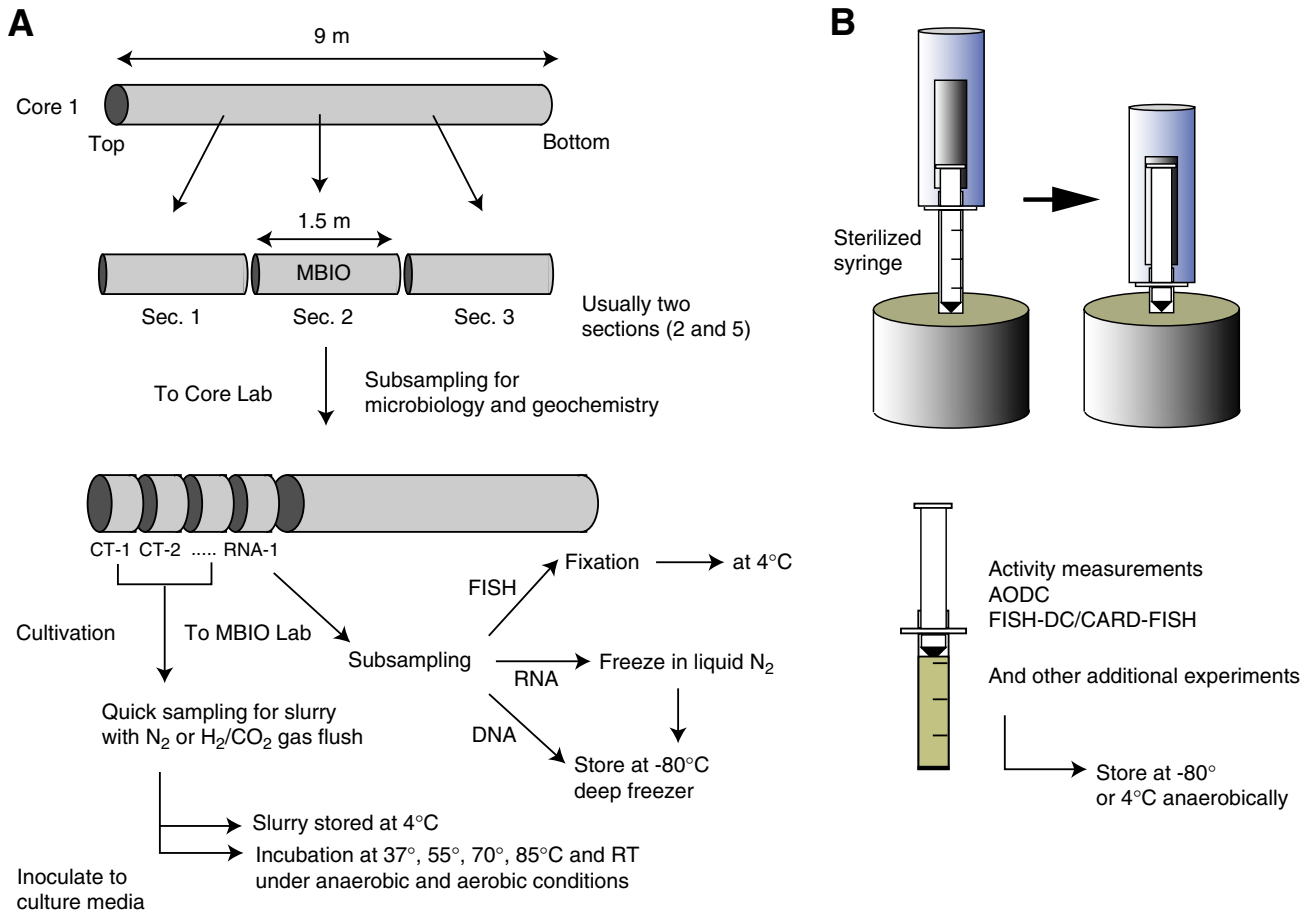


**Figure F13.** Most probable number counts with a microtiter plate. On a deep-well microtiter plate, four different slurry samples were diluted in triplicate down to  $1:10^6$ . For each sample, a row remained uninoculated as control. The wells were sealed with a capmat and the plate stored in an anaerobic bag with an oxygen-consuming catalyst and an oxygen indicator.

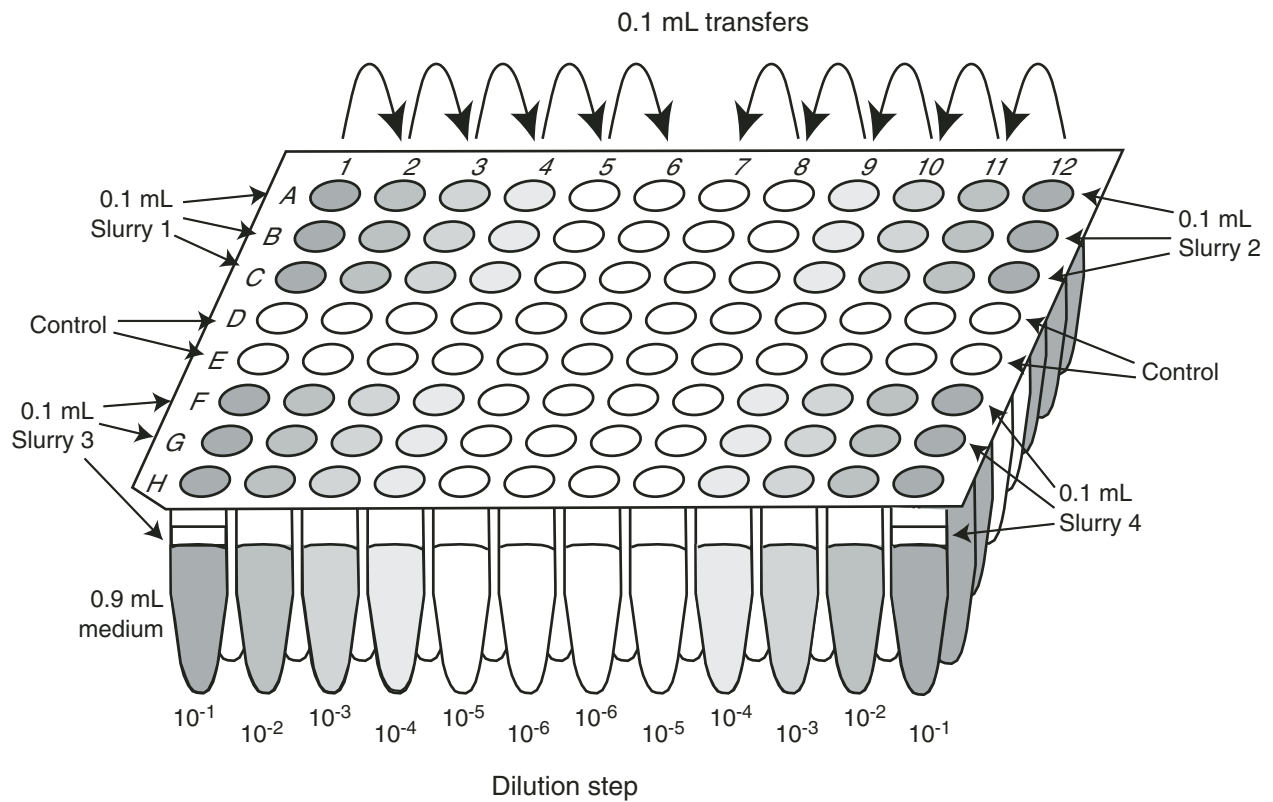




**Figure F14.** Gradient culture tubes were prepared by fixing 0.5 mL of a monomer medium on the bottom with agar. Substrate-free mineral medium with agar was then added as a spacer, a sediment piece was positioned, and the tube was filled with mineral medium and gassed with N<sub>2</sub> on ice. MM = marine salt medium.

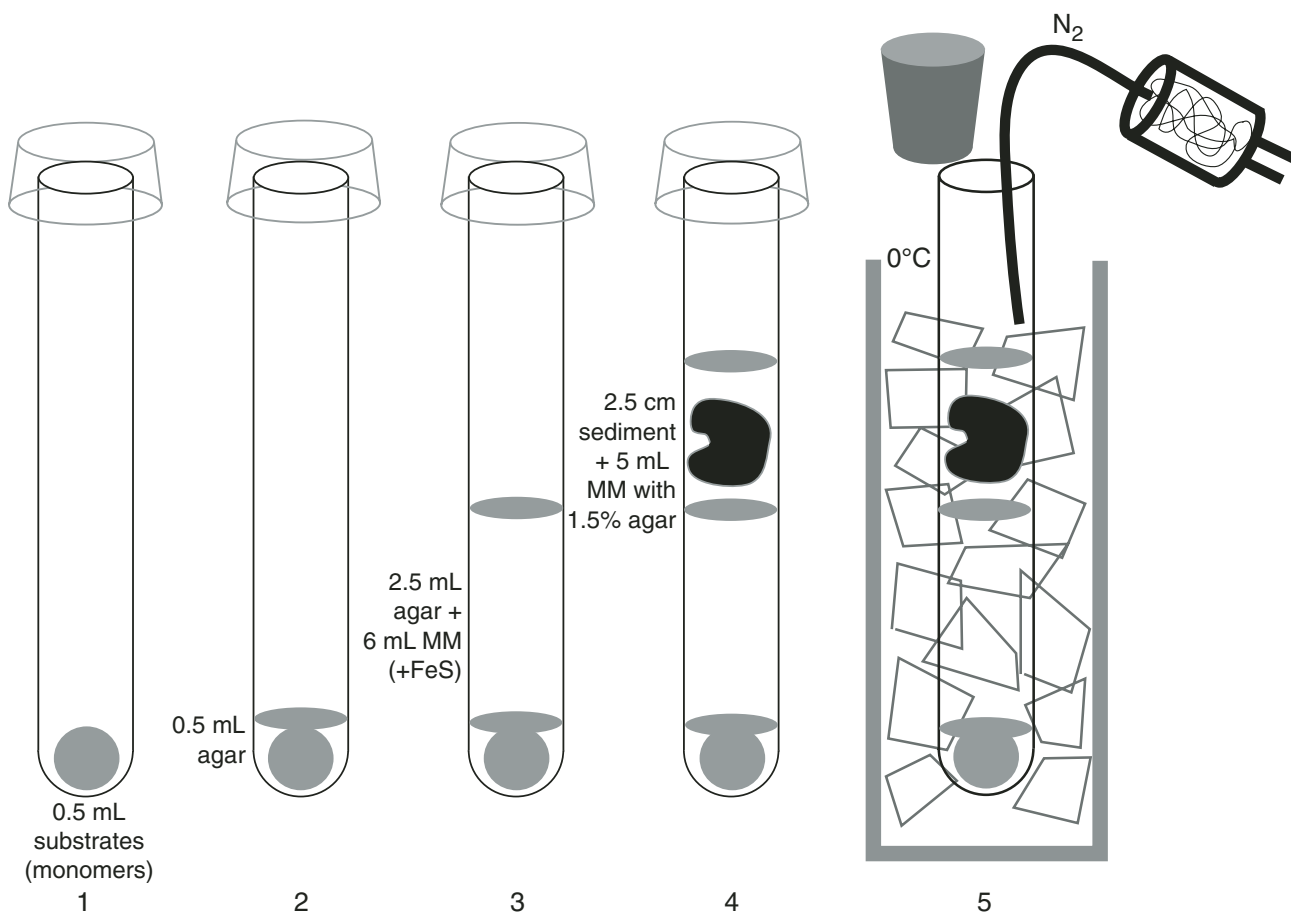


**Figure F15.** Summary of thermal conductivity measurements of standard materials made during Expedition 301. Neither (A) ceramic nor (B) gelatin showed significant drift during the course of coring operations. Corrections based on these standards were not applied to archived data for either basalt or sediment sections.

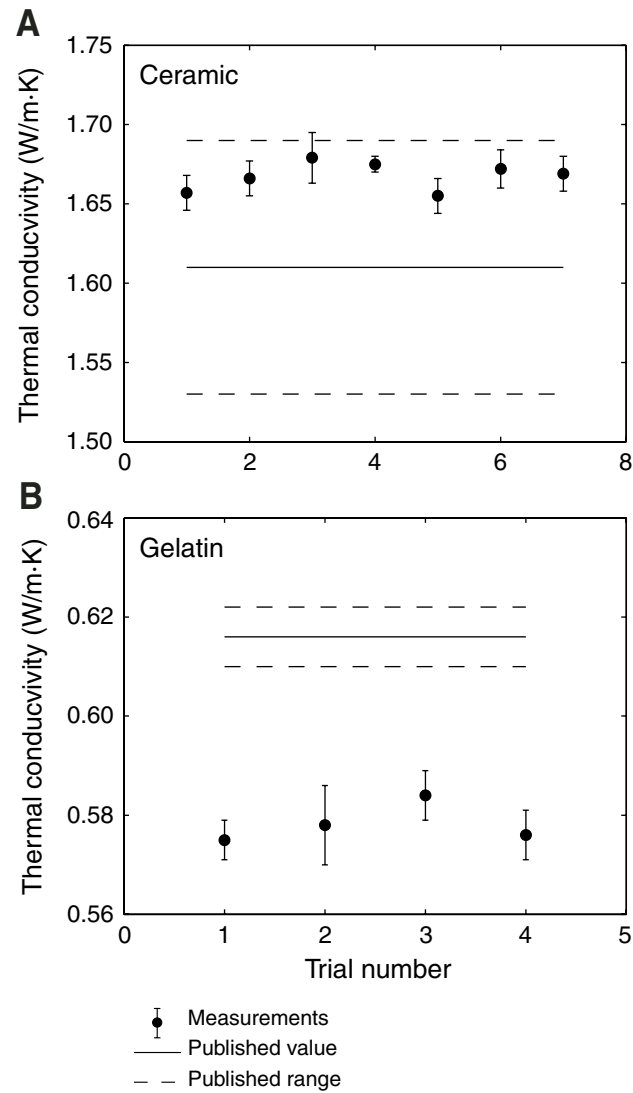


Figure F16. Configuration of the wireline logging tool strings that were used during IODP Expedition 301.

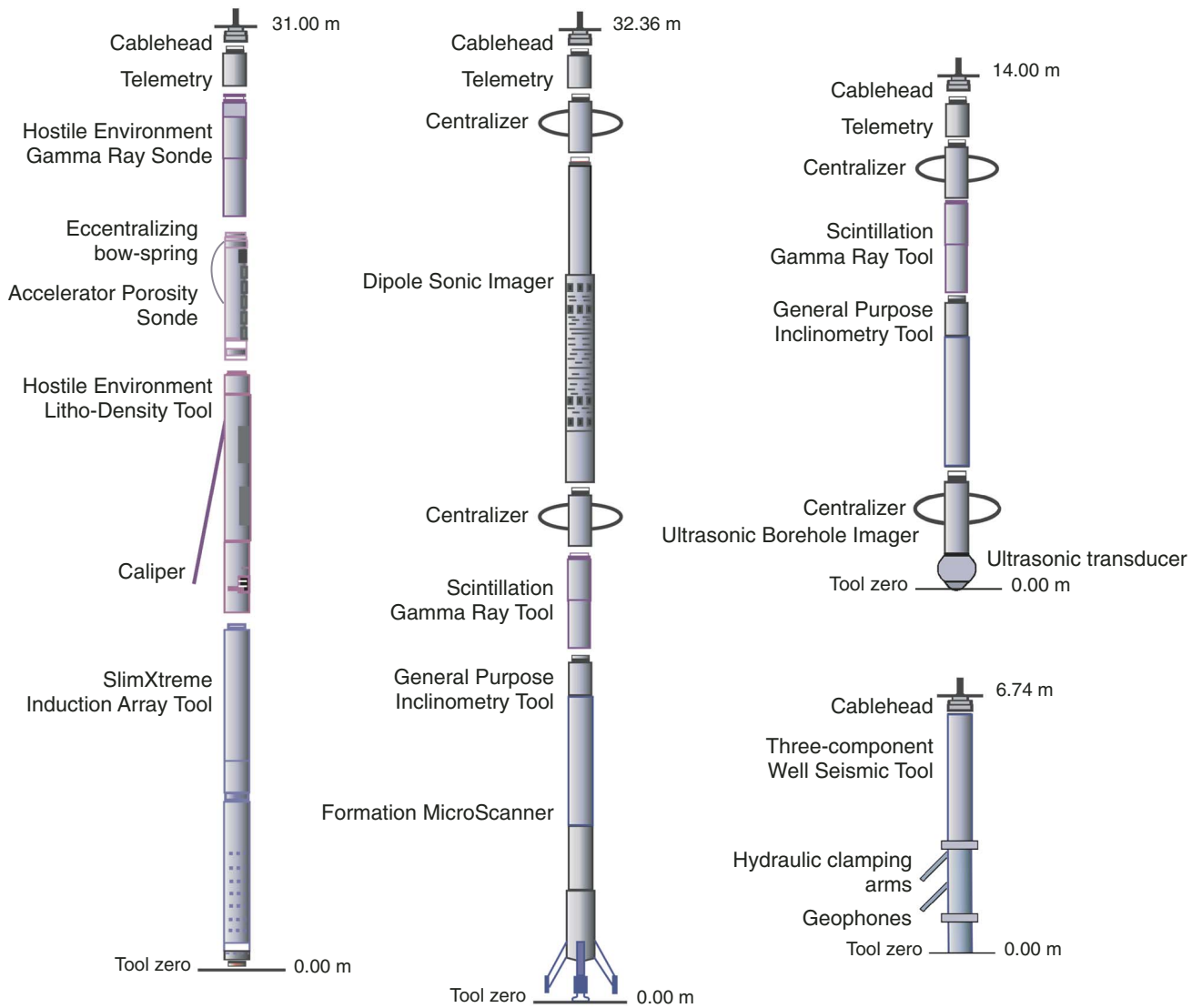
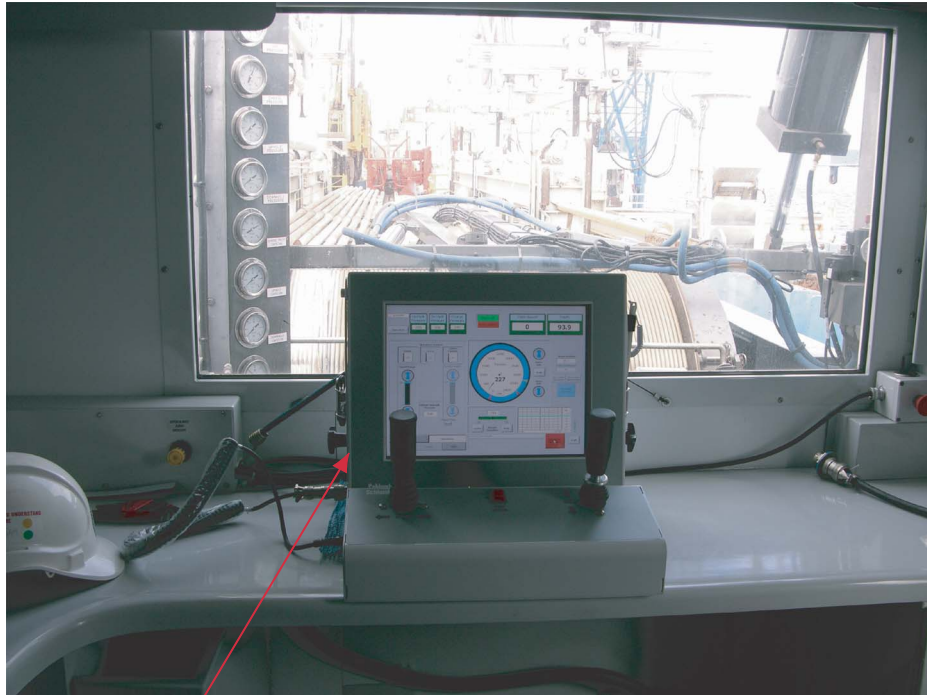


Figure F17. New winch unit and heave compensator.



Digital control panel

Old heave compensating system



New heave compensating system

Table T1. Abbreviations used in the “Color” column of the AppleCORE core description sheets.

Term	Acronym
Intensity	
Very light	vlt
Light	lt
Medium light	mlt
Moderate/Medium	med
Medium dark	mdk
Dark	dk
Very dark	vdk
Very pale	vpl
Pale	pl
Dusky	dsk
Very dusky	vds
Brilliant	bri
Vivid	viv
Strong	str
Deep	dp
Very deep	vdp
Color	
Black	BK
Blue	BL
Brown	BR
Cream	CR
Gray	CY
Green	GN
Orange	OR
Olive	OL
Pink	PK
Purple	PU
Red	RD
White	WH
Yellow	YE
Buff	BF
Modifier	
Bluish	bl
Brownish	br
Creamy	cr
Grayish	gy
Greenish	gn
Orange	or
Olive	ol
Pinkish	pk
Purplish	pu
Reddish	rd
Whitish	wh
Yellowish	ye
Mottled	mo
Spotty	sp

Table T2. Example of Hole U1301B piece log.

Curatorial data sheet/Piece length							Taken as MBIO sample	
Hole	Core	Piece	Subpieces	Top (cm)	Bottom (cm)	Length (cm)		
U1301B	1R-1	1		0	3	3		
		2		4	18	14		
		3	A-B	18	24	6		
		4		28	36	8	MBNU	
		5		37	39	2		
		6		41	49	8	MBLIN	
		7		52	56	4	CULT	
		8		57	63	6		
		9		65	70	5		
		10	A-B	70	74	4		
		11		75	83	8	MBLIN	
		12	A-D	83	85	2		
		13		102	103	1		
		14		105	117	12	MBSTE	
		15		117	123	6		
		16		124	134	10		
		17		134	138	4		
		18		140	144	4	MBLIN	
		19		144	147	3		
	2R-2	1R-2	1		0	3	3	
			2		4	6	2	
			3		7	12	5	
			4		14	18	4	
		2R-1	1		0	4.5	4.5	
			2		5	8.5	3.5	
			3		9	12	3	
			4		12	15	3	
			5		15.5	17.5	2	
			6	A-B	18.5	22.5	4	
			7	A-B	23	30	7	
			8	A-B	30.5	39.5	9	
			9	A-B	40	44	4	
			10	A-B	44.5	55	10.5	
		11	A-B	55	72	17		
		12	A-G	73	117.5	44.5		
		13		120.5	127	6.5		
		14	A-C	128	132	4		
		15		134	143.5	9.5		
	2R-2	1		0	9	9	MBNU	

Notes: Sample codes (e.g., MBNU, MBLIN, CULT, and MBSTE) of pieces removed as whole-round microbiology (MBIO) samples are noted in the right-hand column. A complete list of microbiology samples is available from the Janus database. Only a portion of this table appears here.

Table T3. Hole U1301B igneous unit and contacts log.

Unit	Subunit	Upper contact				Depth interval (mbsf)	Minimum thickness (m)	Lithology
		Core	Section	Piece	Type			
1	A	1R	1	1	NR	351.20–351.77	0.50	Basalt-hyaloclastite breccia
	B	1R	1	8	NR	351.77–352.54	0.52	Sparsely clinopyroxene-plagioclase phyric basalt
	C	1R	1	17	C	352.54–425.01	20.26	Sparsely to moderately clinopyroxene-plagioclase phyric pillow basalt
2	A	11R	1	12	C	425.01–431.53	3.91	Sparsely to moderately olivine-clinopyroxene-plagioclase phyric massive basalt
	B	13R	2	3	C	431.53–435.29	1.26	Sparsely to moderately olivine-clinopyroxene-plagioclase phyric basalt massive flow
3		14R	1	16	C	435.29–444.09	0.90	Moderately olivine-clinopyroxene-plagioclase phyric pillow basalt
4	A	15R	1	7	C	444.09–444.66	0.40	Sparsely to moderately clinopyroxene-plagioclase phyric basalt massive flow
	B	15R	1	12	NR	444.66–448.10	2.94	Sparsely to moderately clinopyroxene-plagioclase phyric basalt massive flow
	C	15R	4	1	C	448.10–449.73	1.47	Sparsely to moderately clinopyroxene-plagioclase phyric basalt massive flow
5		15R	5	3	C	449.73–471	2.09	Moderately olivine-clinopyroxene-plagioclase phyric pillow basalt
6		18R	1	1	C	471–475.77	4.39	Sparsely plagioclase phyric massive basalt
7	A	18R	4	4	C	475.77–491.78	4.72	Sparsely to moderately olivine-plagioclase phyric pillow basalt
	B	21R	2	5	C	491.78–511.78	11.00	Moderately to highly clinopyroxene-olivine-plagioclase phyric pillow basalt
	C	25R	2	7	NR	511.41–564.41	14.25	Aphyric and sparsely to moderately clinopyroxene-olivine-plagioclase phyric pillow basalt
8	A	35R	1	10	C	564.41–565.6	1.06	Basalt-hyaloclastite breccia
	B	35R	2	8	C	565.6–573.20	1.24	Sparsely to moderately clinopyroxene-olivine-plagioclase phyric basalt
	C	36R	1	15	C	573.20–582.8	2.91	Moderately to highly clinopyroxene-olivine-plagioclase phyric pillow basalt

Notes: NR = not recovered, C = chilled margin.



**Table T4.** Key to rock data used in the logs and thin section descriptions.

Code	Description	Size (mm)
Grain size:		
G	Glassy	
cx	Cryptocrystalline	< 0.1
μx	Microcrystalline	0.1–0.2
fg	Fine	0.2–1
mg	Medium	1–5
ND	Not determined	
Contact type:		
nr	Not recovered	
C	Chilled margin—lava surface	
I	Chilled margin—intrusive	
T	Tectonic	
GS	Gradational change in grain size	
Mineral name:		
ol	Olivine	
pl	Plagioclase	
cpx	Clinopyroxene	
opx	Orthopyroxene	
di	Diopside	
aug	Augite	
pig	Pigeonite	
hyp	Hypersthene	
sp	Spinel	
ox	Fe-Ti oxide	
py	Pyrite	
sap	Saponite	
cel	Celadonite	
CC	Calcium carbonate	
Feox	Iron oxyhydroxide	
zeo	Zeolite	
Contact form:		
P	Planar	
C	Curved	
I	Irregular	
S	Sheared	
Rock type:		
	Pillow basalt	
	Flow margins	
	Sheet flows	
	Massive flow	
	Dike	
	Breccia	
	Pillow breccia	
	Hyaloclastite	





Table T5. Example of thin section description.

Thin section:	301-U1301B-18R-4, 17–19 cm (Piece 1A)		TS #	33	Unit:	6	Observer:	MS, RC
Rock name:	Moderately olivine-clinopyroxene-plagioclase-phyric basalt							
Where sampled:	Vein							
Grain size:	Crypto to microcrystalline							
Texture:	Intersertal to intergranular, glomeroporphyritic							
Primary mineralogy	Percent present	Percent original	Size (mm)			Approx. comp.	Morphology	Comments
			Min.	Max.	Av.			
<b>Phenocrysts:</b>								
Plagioclase	5	5	1.1	3.8	1.8		Euhedral to subhedral	Stubby laths and in mono- and polyglomeroporphyritic clots. Pale green or brown glass inclusions in the cores of some crystals.
Clinopyroxene	2	2	0.5	1.2	0.8		Euhedral to anhedral	Occurs singly, but more frequently in glomeroporphyritic clots or associated with plagioclase laths.
Olivine	0	1	0.8	1.2	1		Euhedral to subhedral	Completely replaced by saponite.
<b>Groundmass:</b>								
Plagioclase	55	55		<1.1			Euhedral to subhedral	Laths.
Clinopyroxene	20	20		<0.5			Euhedral to anhedral	Occurs singly or attached to/intergrown with plagioclase.
Olivine	0	12		<0.8			Euhedral to subhedral	Completely replaced by saponite.
Opaque minerals	5	5						
Secondary mineralogy	Percent	Size (mm)			Replacing/filling	Comments		
		Min.	Max.	Av.				
Saponite	12				Olivine, mesostasis, vein, vesicles	Brown to brown-gray color.		
Carbonate	1				Vein			
Vesicles/cavities	Percent	Location	Size (mm)			Filling/morphology	Comments	
			Min.	Max.	Av.			
Vesicles	Tr	Even	0.1	0.3	0.2	Saponite		

Notes: Veins = 0.05–0.2 mm; anastomosing saponite and carbonate veins. These microveins cut through crystals, or “step” around them. Carbonate does not occur along the entire length of the vein. Carbonate forms a fibrous central vein fill suggesting it formed after the saponite. Approx. comp. = approximate composition, Min. = minimum, Max. = maximum, Av. = average, Tr = trace. Only a portion of this table appears here.



Table T6. Example of Expedition 301 alteration log.

Hole	Core	Section	Piece number	Interval (cm)		Length (cm)	Rock color/Alteration type (%)					Glass (%)		Vesicles		Comments
				Top	Base		Dark gray	Brown	Black halo	Light gray	Green halo	Glass	Altered	Vesicles (%)	Minerals	
1301B	1R	1	1	0	3	3	70		30			50	50	<1	Sap	
1301B	1R	1	2	4	18	14	70		30			50	50	<1	Sap	
1301B	1R	1	3	18	24	6	40		50	10		15	80			
1301B	1R	1	4	28	36	8								<1		MBNU
1301B	1R	1	5	37	39	2	30	2	68					<1		
1301B	1R	1	6	41	49	8	90		10			40	50			
1301B	1R	1	7	52	56	4										
1301B	1R	1	8	57	63	6	30		70							
1301B	1R	1	9	65	70	5	50		50					2	Sap, FeOx	
1301B	1R	1	10	70	74	4	60		40					3	Sap, FeOx	
1301B	1R	1	11	75	83	8			40							MBLIN
1301B	1R	1	12	83	85	2	60							3	Sap, FeOx	
1301B	1R	1	13	102	103	1										MBSTE
1301B	1R	1	14	105	117	12										
1301B	1R	1	15	117	123	6	80			20				3	Sap, FeOx	
1301B	1R	1	16	124	134	10	40		60			2	100	3	Sap, FeOx	
1301B	1R	1	17	134	138	4	100					20	95	3	Sap	
1301B	1R	1	18	140	144	4	40		60					3	Sap, FeOx	
1301B	1R	1	19	144	147	3	40		60					3	Sap, FeOx	
1301B	1R	2	1	0	3	3	50		50					3	Sap	
1301B	1R	2	2	4	6	2	50		50					3	Sap	
1301B	1R	2	3	7	12	5	50		50					3	Sap	
1301B	1R	2	4	14	18	4	40		60			5	90	3	Sap	
1301B	2R	1	1	0	5	5	69		25	6				3	Sap, FeOx	
1301B	2R	1	2	5	9	4	69		25	6				3	Sap, FeOx	
1301B	2R	1	3	9	12	3	69		25	6				3	Sap, FeOx	
1301B	2R	1	4	12	15	3	69		25	6				3	Sap, FeOx	
1301B	2R	1	5	16	18	2	69		25	6				3	Sap, FeOx	
1301B	2R	1	6	19	23	4	69		25	6				3	Sap, FeOx	
1301B	2R	1	7	23	30	7	69		25	6				3	Sap, FeOx	
1301B	2R	1	8	31	40	9	69		25	6				3	Sap, FeOx	
1301B	2R	1	9	40	44	4	69		25	6				3	Sap, FeOx	
1301B	2R	1	10	45	55	11	100					20	50	4	Sap	
1301B	2R	1	11	55	72	17	60		40			2.5	80	4	Sap, FeOx	
1301B	2R	1	12	73	118	45	80		20					5	Sap	
1301B	2R	1	13	121	127	7	20		80					5	Sap	
1301B	2R	1	14	128	132	4	20		80					5	Sap	
1301B	2R	1	15	134	144	10	40		60			10	50	3	Sap	

Note: sap = saponite, FeOx = iron oxides. Comments column includes sample codes (e.g., MBNU, MBLIN, and MBSTE) for pieces taken as whole-round microbiology samples, which were therefore not described. Only a portion of this table appears here.



Table T7. Example of Expedition 301 vein log.

Hole	Core	Section	Piece number	Interval (cm)		Width (mm)	Vein		Breccia, vein net, etc.		Secondary minerals in vein (%)					Halo		Second, outer, halo		Comments
				Top	Base		Vertical?	On side of piece?	Type	Secondary (%)	Dark green/black clay (sap)	Green/blue clay (cel)	CC	Py	FeOx	Zeo?	Width (mm)	Halo Type	Width (mm)	
1301B	1R	1	1	0	3				br	60	97				3					Altered glass
1301B	1R	1	2	4	17				br	60	97				3					Altered glass
1301B	1R	1	2	17	25	0.2					100						5	blk		
1301B	1R	1	2	18	22	0.1	v				100						2			
1301B	1R	1	2	18	19	0.1	v				100						2	brn		
1301B	1R	1	2	18	22	0.2	v				100									
1301B	1R	1	2	23	24	0.8	v				100						5	blk		
1301B	1R	1	3	23	27				br	30	97				3					Altered glass
1301B	1R	1	5	36	39				ru	5	98									
1301B	1R	1	6	41	49				br	30	80			20						
1301B	1R	1	8	60	60	0.1					100						10	mix		
1301B	1R	1	8	57	61	0.3					100						6	mix		
1301B	1R	1	8	60	61	0.3	v				100									
1301B	1R	1	9	65	65	0.1		s			100									
1301B	1R	1	9	65	69	0.3	v				100						3	blk		
1301B	1R	1	9	65	69	0.3					50						5	blk		
1301B	1R	1	10	70	74	0.2	v				50						4	blk		
1301B	1R	1	12	83	83	0.1					100									
1301B	1R	1	12	83	98	0.2	v	s			40						3	mix		
1301B	1R	1	12	82	97	1		s			90						6	mix		
1301B	1R	1	12	82	86	0.2					90						4	mix		
1301B	1R	1	12	82	84	0.1	v				100									
1301B	1R	1	12	86	90	0.1	v				95						2	mix		

Note: sap = saponite, cel = celadonite, CC = calcium carbonate, Py = pyrite, FeOx = iron oxides, Zeo = zeolite, v = vertical, s = on side of piece, br = breccia, ru = rubble, blk = black, brn = brown, mix = mixed. Only a portion of this table appears here.



Table T8. Example of Expedition 301 structural log.

Unit	Core, section	Vein number	Piece length (cm)	Number of veins	Ratio (number of veins/piece length)	Plane (°)	Dip (°)	Vein width (mm)	Vein morphology	Veins on side of piece	Mineral	Halo width (mm)		Margin	Orientation of chilled margin (°)	Dip of chilled margin (°)	Lineation (°)
												Min.	Max.				
301-U1301B-																	
1B	1R-1	10-1	15	2	0.13	288	32	0.2	P		fe	5.0					
1B	1R-1	10-2				137	46	0.2	I		sp	5.0					
1B	1R-1	15-1	5.5	5	0.91	177	87	2	P		fe red	8.0					
1B	1R-1	15-2				35	47	0.1	C		sp	0.0					
1B	1R-1	15-3				209	41	0.1	P		fe	2.0					
1B	1R-1	15-4				227	25	0.1	C		sp	0.0					
1B	1R-1	15-5				13	43	0.1	C		sp	0.0					
1B	1R-1	16-1	9	2	0.22	242	73	0.2	P		fe sp	10.0		P	321	76	
1B	1R-1	16-2				68	27	0.2	P		sp	2.0		P			
1C	2R-1	8-1	9.5	2	0.21	127	78	0.2	P		fe sp	7.0					
1C	2R-1	8-2				340	53	0.2	P stop		fe sp	10.0					
1C	2R-1	10-1	10.5	3	0.29	108	78	0.2	y		sp	0.0		P	006	73	
1C	2R-1	10-2				75	76	0.1	P stop		sp	0.0		P			
1C	2R-1	10-3				203	60	0.1	P stop		sp	0.0		P			
1C	2R-1	11-1	14	4	0.29	173	88	side		sd	fe sp	7.0		P	86	73	
1C	2R-1	11-2				332	70	0.2	P		fe sp	7.0		P			
1C	2R-1	11-3				20	78	0.2	y		fe sp	7.0		P			
1C	2R-1	11-4				241	51	0.2	P		fe	7.0		P			
1C	2R-1	12-1	46	7	0.15	89	76	side		sd	fe sp	0.0					
1C	2R-1	12-2				131	78	0.1	P		fe sp	5.0					
1C	2R-1	12-3				282	33	0.2	P		fe sp	0.0					
1C	2R-1	12-4				176	42	0.2	P		fe	6.0					
1C	2R-1	12-5				211	55	0.2	P		fe sp	5.0					
1C	2R-1	12-6				67	68	0.5	C		fe sp	2.0					
1C	2R-1	12-7				218	71	1	C		fe sp	3.0	7.0				
1C	2R-1	15-1	9.5	3	0.32	218	73	1.3	P		sp dg	7.0		P	302	70	
1C	2R-1	15-2				222	27	0.5	P		sp	*		P			
1C	2R-1	15-3				322	78	0.1	I		sp	2.0		P			
1C	2R-2	4-1	8	1	0.13	45	74	0.5	P		fe sp	2.0					
1C	2R-2	6-1	12	3	0.25	8	82	0.7	P		sp	0.0		P	251	80	

Note: Min. = minimum, Max. = maximum, P = planar, I = irregular, C = curved, stop = vein stopped in the rock, y = y-shaped intersection, sd = side surface is identified as half of vein, fe = iron oxide, sp = spinel, dg = dark green. Only a portion of this table appears here.

**Table T9.** Analyses of potential grinding contamination and background blank.

Element	Grinding error, Leg 206 N = 3	Background blank, Exp. 301 N = 4
Major element oxides (wt%):		
SiO <sub>2</sub>	0	BDL
Al <sub>2</sub> O <sub>3</sub>	BDL	BDL
TiO <sub>2</sub>	BDL	0.01
Fe <sub>2</sub> O <sub>3</sub>	BDL	0.14
MgO	BDL	0.20
MnO	BDL	BDL
CaO	BDL	0.08
Na <sub>2</sub> O	BDL	0.01
K <sub>2</sub> O	0.01	0.03
P <sub>2</sub> O <sub>5</sub>	BDL	0.13
Trace elements (ppm):		
Cr	4.3	BDL
Ni	3.9	44.45
V	BDL	7.61
Sc	BDL	0.08
Ba	BDL	0.23
Sr	BDL	BDL
Y	BDL	BDL
Zr	BDL	12.06
Nb	BDL	BDL

Notes: The grinding contamination test was conducted during Leg 206 (Shipboard Scientific Party, 2003); SiO<sub>2</sub> was subtracted from the grinding error because pure SiO<sub>2</sub> was used to determine grinding contamination. Because the same sample preparation techniques were used during Expedition 301, these data give an indication of the potential grinding contamination in our data. The background blank was determined from drift-corrected intensities. BDL = below detection limit. N = number of determinations.

**Table T10.** Analytical conditions for hard rock inductively coupled plasma–atomic emission spectroscopy runs.

Element	Wavelength (nm)	Integration time per calculation point (s)	Voltage (V)	Mode	Increment between points (nm)*	N
Al	396.15	1	570	Gauss	0.003	5
Ba	455.40	4	610	Max	0.003	1
Ca	393.37	1	390	Gauss	0.003	5
Cr	267.72	4	820	Max	0.003	1
Fe	259.94	1	570	Gauss	0.003	7
K	766.49	1	990	Gauss	0.003	5
Mg	285.21	4	640	Max	0.003	1
Mn	257.61	4	560	Max	0.003	1
Na	589.59	1	660	Gauss	0.003	5
Ni	231.60	4	930	Max	0.002	1
P	178.23	4	990	Max	0.003	1
Si	251.61	1	580	Gauss	0.003	5
Sr	407.77	1	700	Gauss	0.003	5
V	292.40	1	890	Gauss	0.003	7
Y	371.03	4	620	Max	0.003	1
Zr	343.82	1	640	Gauss	0.003	5
Ti	334.94	1	620	Gauss	0.003	5
Nb	316.34	1	550	Gauss	0.003	5
Sc	361.38	0.5	620	Gauss	0.002	5

Notes: Reported settings are stored in the software. Entrance and exit slits are the same for each element, 20/15 nm, respectively. \* = the interval between each of the calculation points in Gaussian (Gauss) mode or the calculation window that constitutes the single point in maximum (max) mode. N = number of calculation points.

**Table T11.** Example run sheet for a hard rock inductively coupled plasma–atomic emission spectroscopy run, Hole 1301B.

Analysis number	Cell ID	Hard rock sample	Analysis type
1		Drift 1	Drift
2	1	Std 3	Standard analysis
3		Drift 2	Drift
4	2	Unk 3	Sample analysis
5	3	CkStd 1	Check standard analysis
6		Drift 3	Drift
7	4	Unk 2	Sample analysis
8	5	Std 2	Standard analysis
9	6	Blank	Blank analysis
10		Drift 4	Drift
11	7	Unk 4	Sample analysis
12	8	Unk 1	Sample analysis
13	9	Std 4	Standard analysis
14	10	Unk 7	Sample analysis
15		Drift 5	Drift
16	11	Std 1	Standard analysis
17	12	CkStd 2	Check standard analysis
18	13	Unk 5	Sample analysis
19	14	Unk 6	Sample analysis
20		Drift 6	Drift
21	15	Std 5	Standard analysis
22	16	Unk 4	Sample analysis
23	17	Std 3	Standard analysis
24	18	Unk 3	Sample analysis
25		Drift 7	Drift
26	19	Unk 5	Sample analysis
27	20	CkStd 1	Check standard analysis
28	21	Std 5	Standard analysis
29	22	Unk 1	Sample analysis
30		Drift 8	Drift
31	23	Std 2	Standard analysis
32	24	Unk 7	Sample analysis
33	25	Std 1	Standard analysis
34	26	Blank	Blank analysis
35		Drift 9	Drift
36	27	Unk 2	Sample analysis
37	28	Std 4	Standard analysis
38	29	CkStd 2	Check standard analysis
39	30	Unk 6	Sample analysis
40		Drift 10	Drift

Notes: The run contained five certified standards (Std), seven unknown samples (Unk), two check standards (CkStd), and a full procedural blank (Blank). The drift monitor was typically analyzed more frequently at the beginning of each run. Cell ID = the position of each solution in the auto-sampler; the drift solution was kept in a 500 mL beaker. All analyses were run at least in duplicate, spaced randomly throughout the run.

Table T12. Precision and accuracy of inductively coupled plasma–atomic emission spectrometry analyses on the JY-2000, Expedition 301.

Run:	1	1	2	2	3	3	4	4	5	5	6	6	7	Average (N = 13)	Standard deviation	Precision (%)	Published value <sup>†</sup>
<b>BAS 148</b>																	
Major element oxides (wt%):																	
SiO <sub>2</sub>	49.59	49.76	49.63	48.37	49.82	49.07	48.68	49.16	50.29	49.55	48.52	48.07	49.77	49.25	0.67	1.4	49.31
Al <sub>2</sub> O <sub>3</sub>	15.52	15.71	15.29	15.25	15.27	15.61	15.47	15.45	15.23	15.23	15.70	15.66	15.59	15.46	0.19	1.2	15.59
TiO <sub>2</sub>	0.95	0.96	0.89	0.89	0.89	0.89	0.88	0.93	0.91	0.89	0.87	0.90	0.89	0.90	0.03	3.2	0.90
Fe <sub>2</sub> O <sub>3</sub>	9.89	9.60	9.64	9.44	9.74	9.87	9.72	9.93	9.77	9.67	9.96	10.05	9.80	9.78	0.17	1.7	9.96
MgO	8.40	8.02	8.42	8.66	8.72	8.58	8.81	8.93	8.49	8.52	8.77	8.24	8.53	8.54	0.24	2.9	8.61
MnO	0.18	0.17	0.17	0.17	0.15	0.15	0.19	0.20	0.19	0.20	0.19	0.18	0.18	0.18	0.02	9.4	0.17
CaO	12.50	13.06	12.80	12.69	13.05	12.69	12.21	12.49	12.44	12.64	12.73	13.05	12.72	12.70	0.26	2.0	12.80
Na <sub>2</sub> O	1.99	2.04	2.01	1.99	2.05	2.06	1.97	1.99	2.02	1.95	2.04	2.02	1.98	2.01	0.03	1.6	1.97
K <sub>2</sub> O	0.04	0.06	0.04	0.04	0.04	0.05	-0.02	0.01	0.04	0.06	0.04	0.04	0.04	0.04	0.01	30.5	0.02
P <sub>2</sub> O <sub>5</sub>	0.07	0.05	0.06	0.07	0.07	0.08	0.06	0.14	0.06	0.06	0.11	0.07	0.09	0.08	0.02	31.4	0.07
Total	99.13	99.42	98.95	97.58	99.80	99.04	97.95	99.22	99.43	98.76	98.93	98.29	99.59	98.94			99.40
Trace elements (ppm):																	
Cr	416	350	383	394	418	406	397	427	390	390	361	395	388	393	21.5	5	344
Ni	88	54	172	103	128	88	109	126	86	91	161	108	172	114	36.1	32	110
V	259	273	294	285	274	285	272	288	277	285	289	291	275	281	9.7	3	NR
Sc	44	43	43	42	42	43	43	60	36	39	42	50	44	44	5.6	13	NR
Ba	10	-7	12	12	12	12	-10	-9	11	22	14	29	12	15	6.1	42	NR
Sr	58	57	65	66	67	68	62	67	67	66	67	67	63	65	3.6	6	63
Y	24	23	28	28	29	27	29	32	29	26	26	24	31	27	2.8	10	28
Zr	48	42	45	48	48	45	43	37	48	48	47	49	49	46	3.4	7	48
Nb	0.5	0.4	2.8	2.8	2.8	2.8	2.6	2.8	2.7	2.6	2.7	2.9	2.3	2.4	0.9	36	1.50
<b>BAS 206</b>																	
Major element oxides (wt%):																	
SiO <sub>2</sub>	49.21	52.60	47.24	48.67	48.77	49.20	47.78	49.72	48.59	48.84	48.92	48.91	49.21	49.05	1.24	2.5	49.53
Al <sub>2</sub> O <sub>3</sub>	14.21	14.49	13.80	13.60	13.63	13.86	13.66	13.87	13.82	13.95	13.92	14.06	14.04	13.92	0.25	1.8	14.22
TiO <sub>2</sub>	2.08	2.21	2.04	2.07	2.11	2.11	2.06	2.23	2.02	2.04	2.00	2.09	2.06	2.09	0.07	3.3	2.04
Fe <sub>2</sub> O <sub>3</sub>	14.83	14.95	13.95	13.87	14.29	14.61	14.80	14.71	14.43	14.35	15.19	14.98	13.35	14.49	0.52	3.6	14.30
MgO	6.81	7.06	6.86	6.70	6.73	6.93	6.55	7.11	6.97	6.28	6.76	7.63	6.51	6.84	0.33	4.8	6.77
MnO	0.26	0.29	0.27	0.27	0.23	0.23	0.31	0.33	0.33	0.30	0.30	0.33	0.27	0.29	0.03	12.2	0.22
CaO	9.75	10.26	9.65	9.58	9.72	9.54	9.51	9.43	9.51	9.82	9.61	9.30	9.75	9.65	0.23	2.4	9.70
Na <sub>2</sub> O	2.85	3.00	2.72	2.66	2.72	2.68	2.75	2.75	2.70	2.70	2.78	2.68	2.67	2.74	0.09	3.4	2.78
K <sub>2</sub> O	0.17	0.22	0.17	0.18	0.16	0.17	0.13	0.17	0.16	0.17	0.17	0.18	0.18	0.17	0.02	12.1	0.18
P <sub>2</sub> O <sub>5</sub>	0.20	0.18	0.19	0.19	0.17	0.20	0.19	0.29	0.18	0.14	0.20	0.16	0.16	0.19	0.03	17.8	0.16
Total	100.37	105.27	96.89	97.80	98.52	99.51	97.74	100.61	98.69	98.58	99.85	100.31	98.21	99.41			99.90
Trace elements (ppm):																	
Cr	111	99	88	87	83	90	96	123	88	90	90	151	102	100	19.1	19.2	84
Ni	41	43	41	48	69	78	48	59	85	44	63	-15	107	60	21.1	34.9	54
V	444	476	463	464	468	457	444	457	453	431	439	455	452	454	12.3	2.7	461
Sc	46	51	47	46	46	47	49	55	45	42	49	61	50	49	5.0	10.2	47
Ba	35	38	52	53	52	53	34	32	55	64	60	63	49	49	11.1	22.5	50
Sr	97	101	109	106	107	109	107	107	109	109	108	106	106	106	3.6	3.3	112
Y	53	54	51	51	55	58	59	64	52	48	49	61	64	55	5.5	9.9	44
Zr	129	132	134	129	132	133	135	128	134	133	131	130	134	132	2.2	1.7	127
Nb	11.3	11.8	9.6	9.5	9.8	9.9	9.6	9.4	10.0	10.0	10.3	10.2	11.4	10.2	0.8	7.6	5.1

Notes: Standards analyzed as a check on precision and accuracy. Precision is calculated as the standard deviation of *N* analyses divided by the average value (values in bold were excluded from statistical calculations). For elements with near background concentrations, the analytical error is artificially high (i.e., the actual precision is much better than suggested by the numbers). † = Bach et al. (1996) and Shipboard Scientific Party (2003a). BAS 148 = basalt standard created during ODP Leg 148, Hole 504B (Bach et al., 1996), BAS 206 = basalt interlaboratory standard created during ODP Leg 206 (Shipboard Scientific Party, 2003a). NR = not recovered.

**Table T13.** Compositions of culture media and incubation temperatures for shipboard microbiological studies, Expedition 301. (See table notes. Continued on next page.)

Culture medium/Components	Concentration/ Amount	Basement saline	Gas phase			pH	Temperature (°C)
			Gas	Mix	Pressure		
Methanogen medium 1 (Me1):		MJ	H <sub>2</sub> /CO <sub>2</sub>	80/20	350 kPa	6.5	20, 37, 55, 70
Acetate	0.1%						
NaHCO <sub>3</sub>	0.1%						
Na <sub>2</sub> S·9H <sub>2</sub> O	0.05%						
Cysteine-HCl	0.05%						
Vitamin solution							
Resazurin	0.0001%						
Thermococcales (Tc):		MJ	N <sub>2</sub>		200 kPa	7.0	37, 55, 70, 85
Yeast extract	0.2%						
Tryptone	0.2%						
Glucose	0.02%						
S°	3%						
Resazurin	0.0001%						
Na <sub>2</sub> S·9H <sub>2</sub> O	0.05%						
Archaeoglobales (Ag):		MJ	H <sub>2</sub> /CO <sub>2</sub>	80/20	350 kPa	6.5	20, 37, 55, 85
Yeast extract	0.1%						
Acetate	0.1%						
NaHCO <sub>3</sub>	0.1%						
Na <sub>2</sub> SO <sub>4</sub>	0.2%						
Na <sub>2</sub> S·9H <sub>2</sub> O	0.05%						
Vitamin solution							
Resazurin	0.0001%						
Epsilon proteobacteria (Ep):		MJ	H <sub>2</sub> /CO <sub>2</sub>	80/20	350 kPa	6.5	20, 37, 55, 70
NaNO <sub>3</sub>	0.1%						
Na <sub>2</sub> S <sub>2</sub> O <sub>3</sub> ·5H <sub>2</sub> O	0.1%						
S°	3%						
NaHCO <sub>3</sub>	0.1%						
FeOOH	100 mM						
Oligotrophs (Og):		MJ-NP	Atmospheric air		100 kPa	7.0	20
Acetate	0.5 mM						
Casamino acid	0.005%						
Ascorbic acid	0.5 mM						
Glucose	2 mM						
(NH <sub>4</sub> ) <sub>3</sub> PO <sub>4</sub>	0.4 mM						
Agar	3%						
Fermenters (Fm):		MJ	N <sub>2</sub> /CO <sub>2</sub> /H <sub>2</sub>	90/5/5	100 kPa	7.0	20
Yeast extract	0.2%						
Tryptone	0.2%						
Glucose	0.02%						
S°	3%						
Resazurin	0.0001%						
Agar	3%						
Monomers (mono):		MM	N <sub>2</sub> /CO <sub>2</sub> /H <sub>2</sub>	90/5/5	100 kPa	7.2–7.4	Near in situ temperature
Amino acids mixture	0.01 M						
Short chain fatty acids	0.01 M						
Organic acid mixture	0.01 M						
n-alcohols	0.01 M						
Glycerol	0.01 M						
Glucose	0.01 M						
Ammonifex (Amfex):		S-1	H <sub>2</sub> /CO <sub>2</sub>	80/20	350 kPa	7.3	Near in situ temperature
NO <sub>3</sub> <sup>-</sup>	10 mM						
Methanogen medium 2 (Me2):							
1) Acetate or methanol	10 mM/0.4%	S-1	N <sub>2</sub> /CO <sub>2</sub> /H <sub>2</sub>	90/5/5	100 kPa	7.3	Near in situ temperature
2) No additional substrates			H <sub>2</sub> /CO <sub>2</sub>	80/20	350 kPa		
Sulfur (S°) reducers (S-red):							
S°	0.5%–1%	S-1	N <sub>2</sub> /CO <sub>2</sub>	80/20	100 kPa	7.3	Near in situ temperature
Substrates: acetate, PYG, or pectin							
Denitrifiers (Denit):							



Table T13 (continued).

Culture medium/Components	Concentration/ Amount	Basement saline	Gas phase			pH	Temperature (°C)
			Gas	Mix	Pressure		
CH <sub>3</sub> COONa·3H <sub>2</sub> O and Na <sub>2</sub> SO <sub>4</sub> + 1) NO <sub>3</sub> <sup>-</sup> + FeSO <sub>4</sub> or FeS 2) NO <sub>3</sub> <sup>-</sup> + Lactate (10 mM) Fumarate (10 mM) Formate (10 mM)	0.14 g/0.02 g 5 mM/10 mM 10 mM 10 mM 10 mM	S-2	N <sub>2</sub> /CO <sub>2</sub> /H <sub>2</sub> N <sub>2</sub> /CO <sub>2</sub> /H <sub>2</sub>	90/5/5 90/5/5	100 kPa 100 kPa	7.0	Near in situ temperature
Iron reducers (IR): CH <sub>3</sub> COONa·3H <sub>2</sub> O, C <sub>6</sub> H <sub>5</sub> O <sub>7</sub> Fe, and Na <sub>2</sub> SO <sub>4</sub> + 1) Acetate or lactate 2) No additional substrates	0.14 g/30mM/ 0.02 g 10 mM/10 mM	S-2	N <sub>2</sub> /CO <sub>2</sub> /H <sub>2</sub> N <sub>2</sub> /CO <sub>2</sub>	90/5/5 80/20	100 kPa 100 kPa	7.0	Near in situ temperature
Sulfate reducers (SR): 4 mL/L Na <sub>2</sub> S·9H <sub>2</sub> O and Na <sub>2</sub> SO <sub>4</sub> + 1) Lactate and/or acetate 2) No additional substrates	0.5 M/3.0 g 10 mM/10 mM	S-2	N <sub>2</sub> /CO <sub>2</sub> /H <sub>2</sub> N <sub>2</sub> /CO <sub>2</sub>	90/5/5 80/20	100 kPa 100 kPa	7.0	Near in situ temperature

Notes: Compositions of solutions are listed in the following tables: vitamin solution (see Table T14), MJ synthetic seawater (see Table T15); MJ-NP = MJ without nitrogen and phosphate sources; marine medium salts (MM) (see Table T16); S-1 (see Table T17); S-2 (see Table T18). Amino acids mixture = alanine, arginine, asparagine, asparagic acid, cystine, glutamine, glutamic acid, glycine, histidine, isoleucine, leucine, lysine, methionine, phenylalanine, proline, serine, threonine, tryptophane, tyrosine, and valine. Short-chain fatty acids (as sodium salts) = formate, acetate, propionate, butyrate, valerate, and capronate. Organic acid mixture = malate, fumarate, succinate, and lactate. n-alcohols = methanol, ethanol, propanol, and butanol. PYG = peptone (0.2%) + yeast extract (0.2%) + glucose (0.05%). See Table T19 for a description of the trace mineral solution added to culture media, Table T20 for a description of the trace element solution used in culture media, Table T21 for a description of the vitamin solution used in S-1 saline solutions and Table T22 for a description of the vitamin solution used in basement saline S-2 solutions.

**Table T14.** Vitamin solution used in Me1 and Ag cultivation media.

Component	Concentration (mg/L)
Biotin	2
Folic acid	2
Pyridoxin-HCl	10
Thiamine-HCl-2H <sub>2</sub> O	5
Riboflavin	5
Nicotinic acid	5
p-Aminobenzoic acid	5
Lipoic acid	5
D-Ca-pantothenate	5
Cyanocobalamine	0.1

**Table T15.** MJ solution used as the basis for cultivation media.

Component	Concentration (g/L)
NaCl	30
K <sub>2</sub> HPO <sub>4</sub>	0.14
CaCl <sub>2</sub> ·2H <sub>2</sub> O	0.7
NH <sub>4</sub> Cl	0.25
MgSO <sub>4</sub> ·7H <sub>2</sub> O	3.4
MgCl <sub>2</sub> ·6H <sub>2</sub> O	4.18
KCl	0.5
Fe(NH <sub>4</sub> ) <sub>2</sub> (SO <sub>4</sub> ) <sub>2</sub> ·6H <sub>2</sub> O	0.001
Trace mineral solution	10 mL/L

Notes: MJ = artificial seawater solution. See Table T19 for trace mineral solution.

**Table T16.** Marine medium salts used as a basis for cultivations.

Component	Concentration
NaCl	24.32 g/L
MgCl <sub>2</sub> ·6H <sub>2</sub> O	10 g/L
CaCl <sub>2</sub> ·2H <sub>2</sub> O	1.5 g/L
KCl	0.66 g/L
Na <sub>2</sub> SO <sub>4</sub>	4.0 g/L
KBr	0.84 mM
H <sub>2</sub> BO <sub>2</sub>	0.4 mM
SrCl <sub>2</sub>	0.15 mM
NH <sub>2</sub> PO <sub>4</sub>	0.4 mM
NaF	0.07 mM
Na <sub>2</sub> SeO <sub>3</sub>	10 <sup>-7</sup> mM
NaWO <sub>4</sub>	10 <sup>-7</sup> mM
Trace element solution	1 mL/L
Autoclave, cool under anerobic conditions, and then add from sterile stock solutions:	
NaHCO <sub>3</sub> (1M)	30 mL
Vitamin solution	2 mL
FeCl <sub>2</sub> (1M in 0.1M HCl)	0.5 mL
Na <sub>2</sub> S (1M)	1.2 mL

Note: Trace element solution is from Widdel et al., 1983. For oxic media, replace bicarbonate buffer with 2.38 g/L HEPES and cool under air atmosphere after autoclaving. HEPES = 4-(2-hydroxyethyl)-1-piperazineethanesulfonic acid.

**Table T17.** Basement saline S-1 solution used as a basis for cultivation media.

Component	Amount per liter
NaCl	22 g
K <sub>2</sub> HPO <sub>4</sub>	0.14 g
CaCl <sub>2</sub> ·2H <sub>2</sub> O	0.14 g
KCl	0.33 g
NH <sub>4</sub> Cl	0.5 g
MgCl <sub>2</sub> ·6H <sub>2</sub> O	6.2 g
CH <sub>3</sub> COONa·3H <sub>2</sub> O	0.2 g
Yeast extract	0.2 g
Cysteine-HCl (20%)	5 mL
Fe(NH <sub>4</sub> ) <sub>2</sub> (SO <sub>4</sub> ) <sub>2</sub> ·6H <sub>2</sub> O (0.2%)	5 mL
NaHCO <sub>3</sub> (1 M)	30 mL
Na <sub>2</sub> S·9H <sub>2</sub> O (0.5 M)	5 mL
Trace element solution	10 mL
Vitamin solution	10 mL
Resazurin (0.0001%)	0.0001%

Note: See Table T20 for trace element solution and Table T21 for vitamin solution.

**Table T18.** Basement saline S-2 solution used as the basis for culture media.

Component	Amount per liter
NaCl	20 g
KH <sub>2</sub> PO <sub>4</sub>	0.2 g
NH <sub>4</sub> Cl	0.25 g
MgCl <sub>2</sub> ·6H <sub>2</sub> O	3.0 g
KCl	0.5 g
CaCl <sub>2</sub> ·2H <sub>2</sub> O	0.15 g
Selenite-tungstate solution*	1.0 mL
NaHCO <sub>3</sub> (1M)	30 mL
Trace elements SL10*	1 mL
Vitamin solution	5 mL
Resazurin	0.0001%

Notes: \* = from Widdel et al., 1983. See Table T22 for vitamin solution.

**Table T19.** Trace mineral solution added to cultivation media.

Component	Concentration (g/L)
Nitritotriacetic acid	1.5
MgSO <sub>4</sub> ·7H <sub>2</sub> O	3
MnSO <sub>4</sub> ·2H <sub>2</sub> O	0.5
NaCl	1
CoSO <sub>4</sub> ·7H <sub>2</sub> O	0.18
FeSO <sub>4</sub> ·7H <sub>2</sub> O	0.1
CaCl <sub>2</sub> ·2H <sub>2</sub> O	0.1
ZnSO <sub>4</sub> ·2H <sub>2</sub> O	0.18
KAl(SO <sub>4</sub> ) <sub>2</sub> ·12H <sub>2</sub> O	0.02
CuSO <sub>4</sub> ·5H <sub>2</sub> O	0.01
H <sub>3</sub> BO <sub>3</sub>	0.01
Na <sub>2</sub> MoO <sub>4</sub> ·2H <sub>2</sub> O	0.01
NiCl <sub>2</sub> ·6H <sub>2</sub> O	0.075
Na <sub>2</sub> SeO <sub>3</sub> ·5H <sub>2</sub> O	0.053

**Table T20.** Trace element solution used in culture media.

Component	Concentration (g/L)
Nitrilotriacetic acid	1.5
Fe(NH <sub>4</sub> ) <sub>2</sub> (SO <sub>4</sub> ) <sub>2</sub> ·6H <sub>2</sub> O	0.2
Na <sub>2</sub> SeO <sub>3</sub>	0.2
CoCl <sub>2</sub> ·6H <sub>2</sub> O	0.1
MnSO <sub>4</sub> ·2H <sub>2</sub> O	0.1
Na <sub>2</sub> MoO <sub>4</sub> ·2H <sub>2</sub> O	0.1
Na <sub>2</sub> WO <sub>4</sub> ·2H <sub>2</sub> O	0.1
ZnSO <sub>4</sub> ·7H <sub>2</sub> O	0.1
AlCl <sub>3</sub> ·6H <sub>2</sub> O	0.04
NiCl <sub>2</sub> ·6H <sub>2</sub> O	0.025
H <sub>3</sub> BO <sub>3</sub>	0.01
CuSO <sub>4</sub> ·5H <sub>2</sub> O	0.01

**Table T21.** Vitamin solution used in S-1 saline solution.

Component	Concentration (mg/L)
p-Amonobenzoic acid	10
Nicotinic acid	10
D-Ca-pantothenate	10
Pyridoxine-HCl	10
Riboflavin	10
Thiamine-HCl	10
Biotin	5
Folic acid	5
Lipoic acid	5
Cyanocobalamine	5

**Table T22.** Vitamin solution used in enrichment media containing saline S-2 solution.

Component	Concentration (mg/L)
p-Aminobenzoic acid	8
Biotin	2
Nicotinic acid	20
D-Ca-pantothenate	10
Pyridoxamine-2HCl	30
Thiamine-HCl	20
Cyanocobalamine	10

Table T23. Measurements made by wireline tool strings.

Tool string	Tool	Measurement	Sampling interval	Approximate vertical resolution (cm)
Triple combination	HNGS	Spectral gamma ray/Total gamma ray	15 cm	51
	APS	Porosity	15 cm	5
	HLDT	Bulk density, photoelectric factor	15 cm	38
	QAIT	Resistivity, spontaneous potential	25.4–228.6 cm	30.5/61/121.9
Formation MicroScanner (FMS)-sonic combination	FMS	Microresistivity imaging	0.25 cm	0.5
	SGT	Total gamma ray	15 cm	46/NA
	DSI	Acoustic velocity	15 cm	107/120/61/61
	GPIT	Tool orientation	0.25 and 15 cm	NA
Ultrasonic Borehole Imager	UBI	Ultrasonic imaging	0.5–2.5 cm	0.5–1
	GPIT	Tool orientation	0.25 and 15 cm	NA
	SGT	Total gamma ray	15 cm	
Well Seismic Tool	WST	Sonic traveltime	1, 2, or 4 ms	NA

Notes: All tool and tool string names presented in this table are trademarks of Schlumberger. For the complete list of acronyms used in IODP and for additional information consult IODP Downhole Logging Tools at [iodp.ideo.columbia.edu/TOOLS\\_LABS/tools.html](http://iodp.ideo.columbia.edu/TOOLS_LABS/tools.html). See Table T24, for explanation of acronyms used to describe tool string and tools. NA = not applicable.

Table T24. Acronyms and units used for wireline logging tools.

Tool	Output	Tool name/Explanation of output	Unit
APS		Accelerator Porosity Sonde	
	FPLC	Far array porosity (limestone calibrated)	%
	APLC	Near array porosity (limestone calibrated)	%
	SIGF	Formation capture cross section ( $\Sigma_f$ )	Capture units
	STOF	Tool standoff (computed distance from borehole wall)	Inches
DSI		Dipole Sonic Imager	
	DTCO	Compressional wave delay time ( $\Delta t$ )	$\mu\text{s}/\text{ft}$
	DTSM	Shear wave delay time ( $\Delta t$ )	$\mu\text{s}/\text{ft}$
	DTST	Stoneley wave delay time ( $\Delta t$ )	$\mu\text{s}/\text{ft}$
FMS		Formation MicroScanner	
		Spatially oriented resistivity images of borehole wall	
GPIT		General Purpose Inclinerometer Tool	
	DEVI	Hole deviation	Degrees
	HAZI	Hole azimuth	Degrees
	RB	Relative bearing	Degrees
	P1ZA	Pad 1 azimuth	Degrees
	ANOR	Acceleration computer norm	$\text{m}/\text{sec}^2$
	FINC	Magnetic field inclination	Degrees
FNOR	Intensity of the total magnetic field	oers	
HLDS		Hostile Environment Litho-Density Sonde	
	RHOM	Bulk density	$\text{g}/\text{cm}^3$
	PEFL	Photoelectric effect	$\text{b}/\text{e}^-$
	LCAL	Caliper (measure of borehole diameter)	Inches
	DRH	Bulk density correction	$\text{g}/\text{cm}^3$
	DPO	Density porosity	%
HNGS		Hostile Environment Gamma Ray Sonde	
	HSGR	Standard (total) gamma ray	gAPI
	HCGR	Computed gamma ray (HSGR minus uranium contribution)	gAPI
	HFK	Potassium	wt%
	HTHO	Thorium	ppm
	HURA	Uranium	ppm
LEH-MT		Logging Equipment Head—Mud Temperature	
	SP	Spontaneous potential	mV
	CTEM	Temperature	Degrees
	DHF	Downhole force	N
QAIT		SlimXtreme Array Induction Tool	
	AIT10	Resistivity with a median radial depth of investigation of 10 inches	$\Omega\text{-m}$
	AIT20	Resistivity with a median radial depth of investigation of 20 inches	$\Omega\text{-m}$
	AIT30	Resistivity with a median radial depth of investigation of 30 inches	$\Omega\text{-m}$
	AIT60	Resistivity with a median radial depth of investigation of 60 inches	$\Omega\text{-m}$
	AIT90	Resistivity with a median radial depth of investigation of 90 inches	$\Omega\text{-m}$
SGT		Scintillation Gamma Ray Tool	
	GR	Total gamma ray	gAPI
	ECGR	Environmentally corrected total gamma ray	gAPI
	EHGR	High-resolution environmentally corrected total gamma ray	gAPI
UBI		Ultrasonic Borehole Imager	
	FTDE	Internal radius	Inches
	TTBK	Transit times	$\mu\text{s}$
	AWAV	Amplitude average	db

Notes: All tool and tool string names presented in this table are trademarks of Schlumberger. For the complete list of acronyms used in IODP and for additional information consult IODP Downhole Logging Tools at [iodp.ideo.columbia.edu/TOOLS\\_LABS/tools.html](http://iodp.ideo.columbia.edu/TOOLS_LABS/tools.html).